CREWES

Research Report 2009
Volume 21

In print…
Report Summaries

On the memory stick…
Complete Reports
Student Theses
Software

UNIVERSITY OF CALGARY

CREWES Project faculty, staff and students, September 2009

Left to Right:
Back Row: Joanna Cooper, Farshid Forouhideh, Kevin Bertram, Hassan Khaniani, Don Lawton, Roohollah Askari, Larry Lines, Taher Sodagar, Michael Lamoureux, John Bancroft, Peter Manning, Rolf Maier, Salman Bubshait, Hussain Hammad, Peter Gagliardi, A. Nassir Saeed, Peng Cheng, Zimin Zhang, Akshay Gulati, Kris Innanen, Rob Ferguson, Andrew Gorman, Arnim Haase.
Middle Row: Dave Henley, Kayla Bonham, Chad Hogan, Eric Gallant, Thais Guirigay, Lauren Ostridge, Diane Lespinasse, Virginia Vera, Ritesh K. Sharma, Marcus Wilson, Lilly Han, Abdallah A. Zaharani, Mahdi Al Mutlaq, Dali Zhang, Baolin Qiao, Han-Xing Lu, Abdolnaser Yousefzadeh.
Front Row: Kevin Hall, Gary Margrave (Director), Ben Wards, Carlos Montaña, Joe Wong, Laura Baird, Faranak Mahmoudian

CREWES in 2009

I've been with CREWES for 14 years now which is just one year less than I have worked in industry. Each of those 14 years has culminated in a frenzy of activity, with everyone associated with CREWES literally working day and night to bring a year's effort to completion. It is remarkable to see such commitment from so many. Some focus on their own research while others are more group oriented, but all are giving their best. On each of those 14 occasions I've reflected upon the unique structure of CREWES that creates an environment that inspires such dedicated effort, and upon the value of that effort. Occasionally I experienced short bursts of intensive effort in industry, perhaps associated with a land sale, but nothing with the sustained intensity and group involvement that CREWES achieves every year. Precisely what motivates this intensity and dedication is difficult to say, but the consortium model that requires dual University and Industry reporting is a strong driver. Through most of the year we are immersed in the University environment teaching, learning, and conducting research; but, always with awareness that at this time of year we must report to our sponsors with useful, innovative research presented by mature and skilled scientists. Remarkably, this effort builds to a successful climax each year with benefits for all involved. CREWES students and staff get the satisfaction of seeing a year's hard work polished and presented, our Sponsors receive useful reports and software, and the University gets to brag about our collaboration. I extend my personal thanks to all CREWES students, staff, and faculty for their efforts. As for the ultimate value of our efforts, I'll let you judge.

There were several significant events in the past year worth mentioning. With the departure last year of Rob Stewart, our former director, came the opportunity to hire a new faculty member into the Department of Geoscience. I'm very pleased with the results of the hiring process which brought Dr. Kris Innanen to our group and he is now an Associate Director of CREWES. Kris brings needed expertise in advanced seismic inversion techniques, which is a great technical skill boost for us and his work complements nicely the research activities of our other Associate Directors, Rob Ferguson, Don Lawton, Larry Lines and Dave Eaton. Another milestone was the successful approval of a new CRD grant from NSERC which means that your sponsor dollars are leveraged strongly by the Canadian government. We also saw eight students complete their research and eleven students join us, making the present size of our student contingent thirty six.

The research report which we deliver this year comes to you in the form of electronic documents and software on a memory stick, papers and posters presented at this meeting, and this abstract booklet. We have some 77 research reports this year, an increase of 7 over last year. We trust you will enjoy the oral presentations and invite you to take copies of the electronic slides. Of course, we cannot present all our reports orally in two days and so we have prepared many posters which are on display for the entire meeting. Finally, this booklet contains a colourful expanded abstract for each report and we hope that you will circulate it within your company.

I'm happy to say that all of our Sponsors stayed with us through the difficult economic year of 2009, and we were joined by Ecopetrol of Columbia. We thank you all for your continued and generous support!

Calgary, Alberta
November, 2009

Gary F. Margrave
Director of CREWES

Table of Contents

*Presenter

2009 CREWES Sponsors

BHP Billiton Petroleum

BP p.l..c.

CGGVeritas

Chevron Corporation

ConocoPhillips

Devon Canada Corporation

Ecopetrol S.A.

EnCana Corporation

Eni S.p.A.

Exxon Mobil Corporation

GDF Suez E&P Deutschland GmbH

Geophysical Exploration & Development Corp.

Husky Energy Inc.

ION Geophysical Corporation

Landmark Graphics Corporation

Marathon Oil Corporation

Nexen Inc.

Oil Search (PNG) Limited

Penn West Energy Trust

Petrobras

Saudi Aramco

Seismic Micro-Technology, Inc.

Sensor Geophysical Ltd.

Shell Canada Limited

Statoil ASA

Suncor Energy

Talisman Energy Inc.

WesternGeco

Natural Sciences and Engineering Research Council of Canada (NSERC)
- Collaborative Research and Development Grant

CREWES Personnel

DIRECTORS

Gary F. Margrave
Professor, Department of Geoscience, University of Calgary

B.Sc. Physics, 1975, University of Utah
M.Sc. Physics, 1977, University of Utah
Ph.D. Geophysics, 1981, University of Alberta

- Work Experience: Chevron Canada Resources, Chevron Geoscience Company

Don C. Lawton
Professor, Department of Geoscience, University of Calgary

B.Sc. (Hons. Class I) Geology, 1973, University of Auckland
Ph.D. Geophysics, 1979, University of Auckland

- Work Experience: New Zealand Steel Mining Ltd., Amoco Minerals (N.Z.) Ltd.

Robert J. Ferguson
Associate Professor, Department of Geoscience, University of Calgary

B.Sc. Geophysics, 1989, University of British Columbia
M.Sc. Geophysics, 1996, University of Calgary
Ph.D. Geophysics, 1999, University of Calgary

- Work Experience: Chevron Research, University of Texas at Austin

Laurence R. Lines
Professor, Department of Geoscience, University of Calgary

B.Sc. Physics, 1971, University of Alberta
M.Sc. Geophysics, 1973, University of Alberta
Ph.D. Geophysics, 1976, University of B.C.

- Work Experience: Amoco Production Research, Tulsa University, Memorial University of Newfoundland

Kristopher A. Innanen
Associate Professor, Department of Geoscience, University of Calgary

B.Sc. Physics and Earth Science, 1996, York University
M.Sc. Physics and Earth Science, 1998, York University
Ph.D. Geophysics, 2003, University of British Columbia

- Work Experience: University of Houston

David W. Eaton
Department Head, Professor, Department of Geoscience, University of Calgary

B.Sc. Geology and Physics, 1984, Queen’s University
M.Sc. Geophysics, 1988, University of Calgary
Ph.D. Geophysics, 1983, University of Calgary

- Work Experience: Arco Exploration and Production Research Centre, Geological Survey of Canada, University of Western Ontario

Robert R. Stewart
Cullen Chair in Exploration Geophysics, University of Houston
Adjunct Professor, Department of Geoscience, University of Calgary

B.Sc. Physics and Mathematics, 1978, University of Toronto
Ph.D. Geophysics, 1983, Massachusetts Institute of Technology

- Work Experience: Arco Exploration and Production Research Centre, Chevron Geoscience Company, Veritas Software Ltd., Gennix Technology Corp., University of Calgary.

ASSOCIATED FACULTY

John C. Bancroft
Adjunct Professor, Department of Geoscience, University of Calgary

B.Sc. Electrical Engineering, 1970, University of Calgary
M.Sc. Electrical Engineering, 1972, University of Calgary
Ph.D. Electrical Engineering, 1975, Brigham Young University

- Work Experience: Geo-X Systems Ltd., Veritas Software Ltd., Ulterra Geoscience Ltd.

Michael P. Lamoureux
Professor, Department of Mathematics and Statistics, University of Calgary
Adjunct Professor, Department of Geoscience, University of Calgary

B.Sc. Mathematics, 1982, University of Alberta
M.Sc. Mathematics, 1983, Stanford University
Ph.D. Mathematics, 1988, University of California, Berkley

- Work Experience: Farallon Computing, NSERC Canada

Brian H. Russell
Adjunct Professor, Department of Geoscience, University of Calgary

B.Sc. Physics, 1972, University of Saskatchewan
Honours Certificate in Geophysics, 1975, University of Saskatchewan
M.Sc., Geophysics, 1978, University of Durham
Ph.D., Geophysics, 2004, University of Calgary

- Work Experience: Chevron Geoscience Company, Teknica Resource Development, Veritas Software Ltd., Hampson-Russell Software Ltd.

RESEARCH and ADMINISTRATION STAFF

Laura A. Baird

BA, History, 1992, University of Calgary

- Work Experience: Tom Baker Cancer Centre, University of Calgary

Kevin L. Bertram

Electronics Technician Certificate, 2005, Southern Alberta Institute of Technology

- Work Experience: Aram Systems Ltd.

Malcolm B. Bertram

B.Sc. Geology, Auckland, New Zealand

- Work Experience: Allied Minerals NL (Western Australia), GSI (Western Australia), Western Geophysics (Western Australia), Auckland University, University of Calgary.

Michaela H. Bonham

B.Sc. Computer Science, 1978, University of Calgary
M.Sc. Computer Science, 1985, University of Calgary

- Work Experience: Datap Systems Ltd., University of Calgary, Willowglen Systems Ltd., Jade Simulations International, RADSS Technologies, MACI/Westgrid Projects, University of Calgary

Patrick F. Daley

B.Sc. Mathematics, 1974, University of Alberta
M.Sc. Physics 1976, University of Alberta
Ph.D. Geophysics, 1979, University of Alberta

- Work Experience: Independent contractor associated with research centres of major oil companies

Eric V. Gallant

Journeyman Interprovincial Ticket in Electrical Construction, 1976, Cape Breton Institute of Technology

- Work Experience: IBEW, University of Calgary

Arnim B. Haase

Diplom Ingenieur, 1966, Technische Hochschule Ilmenau, East Germany
M.Sc. Electrical Engineering, 1973, University of Calgary
Ph.D. Electrical Engineering, 1976, University of Calgary

- Work Experience: Sefel Geophysical Ltd., Philips New Zealand Ltd., Geo-X Systems Ltd.

Kevin W. Hall

B.Sc. Geophysics, 1992, University of Calgary
M.Sc. Geophysics, 1996, University of Calgary

- Work Experience: Lithoprobe Seismic Processing Facility, University of Calgary

David C. Henley

B.Sc. Physics, 1967, Colorado State University
M.Sc. Physics, 1968, University of Michigan

- Work Experience: Shell Oil Co., Shell Canada Ltd

Han-Xing Lu

B.Sc. (equivalent) Physics, 1967, Fu Dan University, Shanghai, China
M.Sc. Geophysics, 1982, Chinese Academy of Sciences and Institute of Geophysics

- Work Experience: Institute of Geophysics, Beijing, China, Memorial University of Newfoundland

Rolf Maier

B.Sc. Chemical Engineering, 1978, Technikum Winterthur, ZH, Switzerland
M.Sc. Physical Chemistry, 1984, University of Calgary
Ph.D. Physical Chemistry, 1988, University of Calgary

- Work Experience: Lithoprobe Seismic Processing Facility, University of Calgary

Peter M. Manning

B.Sc. Mathematics, 1961, University of British Columbia
Ph.D. Geophysics, 2007, University of Calgary

- Work Experience: Mobil Oil Canada

Joe Wong

B.Sc. Physics/Mathematics, 1971, Queen's University
M.Sc. Applied Geophysics, 1973, University of Toronto
Ph.D. Applied Geophysics, 1979, University of Toronto

- Work Experience: Ontario Ministry of the Environment, University of Toronto, JODEX Applied Geoscience Limited

GRADUATE STUDENTS

Abdallah A. Zaharani

B.Sc. Geophysics, 2000, King Fahd University of Petroleum and Minerals

- Work Experience: Saudi Aramco

Mahdi Al Mutlaq

B.Sc. Exploration Geophysics, 1998, Boise State University
M.Sc. Geophysics, 2007, King Fahd University of Petroleum and Minerals

- Work Experience: Saudi Aramco, South Rub Al-Khali Co.

Abdullah Al-Shuhail

B.Sc. (3rd honour) Geophysics, 2001, King Fahd University
M.Sc. Geophysics, 2006, University of Calgary

- Work Experience: Saudi Aramco

Paul Anderson

B.Sc. Geophysics, 1998, University of Calgary

- Work Experience: Apache Canada Ltd.

Joaquin Aristimuno

M.Sc. Geophysics, Universidad Simon Bolivar

- Work Experience: National Oil Company (Venezuela), Schlumberger Mexico, Shell Canada, Imperial Oil – Esso.

Roohollah Askari

B.Sc. Applied Physics, 2002, University of Hormozgan
M.Sc. Geophysics, 2005, University of Tehran

- Work Experience: Institute for Advanced Studies in Basic Sciences, Zanjan, Iran

Salman Bubshait

B.Sc. Geophysical Engineering, 2005, Colorado School of Mines

- Work Experience: Saudi Aramco

Peng Cheng

B.Sc. Applied Geophysics, 2001, Jilin University, China
M.Sc. Electrical Engineering, 2005, Peking University

- Work Experience: VIA Technologies (China) Inc.

Joanna Cooper

B.Sc. Geophysics, B.Sc. Geology, 2006, University of Calgary

Farshid Forouhideh

B.Eng. Civil Engineering, Azad University, Central Tehran Campus, Iran
B.Sc. Geophysics, University of Western Ontario

Saul Guevara

B.Eng. Civil Engineering, 1984, National University of Colombia
M.Sc. Geophysics, 2001, University of Calgary

- Work Experience: Ecopetrol ICP

Thais Guirigay

B.Sc. Geophysics, 1994, Universidad Simon Bolivar
M.Sc. Geology, 2001, Colorado School of Mines

- Work Experience: National Oil Company (Venezuela), Geotrace (Houston)

Akshay Gulati

B. Eng. Civil Engineering, 2006, Nagpur University

- Work Experience: Indian Institute of Technology in Mumbai

Hussain Hammad

B.Sc. Geoscience / Mathematics, 2005, University of Tulsa

- Work Experience: Saudi Aramco

Lejia (Lilly) Han

B.Sc. Applied Geophysics, 1989, Chengdu University of Technology
B.Sc. Computer Science, 2000, McGill University

- Work Experience: Daqing Oilfield Company, Liaohe Oilfield Company

Chad Hogan

B.Sc. Physics/Math, 2000, University of Victoria

- Work Experience: Inphinity Interactive Inc.

Zaiming Jiang

B. Eng., Geology, 1992, Northeast Institute of Technology
M. Eng., Communications & Electronics, 1998, Northeastern University

- Work Experience: Neusoft Group Shenyang Business Software Company

Hassan Khaniani

B.Sc. Petroleum Exploration Engineering, 2002, Petroleum University of Technology, Iran
M.Sc Petroleum Exploration, 2004, University of Calgary
M.Sc. 2005, Petroleum University of Technology, Iran

Diane Lespinasse

B.Sc. Geophysical Engineering, Universidad Simon Bolivar, Venezuela

Faranak Mahmoudian

B.Sc. Applied Physics, 2000, Khage Nassir Toosi University
M.Sc. Geophysics, Tehran University
M.Sc. Geophysics, University of Calgary

- Work Experience: Shell Canada

Vanja Milicevic

B.Sc. Applied and Pure Mathematics, 2007, University of Calgary

Carlos Montaña

B.Sc. Mechanical Engineering, 1995, Universidad Industrial de Santander

- Work History: Geophysical Exploration and Development Corporation

Lauren Ostridge

B.Sc. Geology and Biology, 2006, Acadia University

Agnieszka Pawlak

B.Sc. Applied Mathematics, 2007, University of Calgary

Baolin Qiao

B.Sc. Geology and Ore Surveying, 1992, Northeastern University, China
M.Sc., 1999, Geology and Ore Surveying, Northeastern University, China

- Work Experience: China Geological Survey Centre, Shenyang Institute of Aeronautical Engineering

A.-Nassir Saeed

B.Sc. Geology, 1991, University of Salahaddin
M.Sc. 1998, University of Science Malaysia

- Work Experience: National Building Company (Libya), University of Sciences and National University of Malaysia

Ritesh Kumar Sharma

B.Sc. 2004, Choudhary Charan Singh University Meerut, India
M.Sc. Applied Geophysics, 2007, Indian Institute of Technology Roorkee, India

- Work Experience: Vedanta Group

Ghada Sindi

B.Sc. Mathematics, 1997, King Abdul Aziz University
M.Sc. Mathematics, 2000, King Abdul Aziz University

- Work Experience: Saudi Aramco

Taher Sodagar

B.Sc. Geophysics, 1994, King AbdulAziz University
M.Sc. Geology (Geophysics), 2002, University of New Orleans

- Work Experience: Saudi Aramco

Todor Todorov

B.Sc. Exploration Geophysics, 1994, University of Mining and Geology, Bulgaria
M.Sc. Geophysics, 2000, University of Calgary

- Work Experience: Hampson-Russell Software Ltd., Microtech Computer Systems Ltd., Hampson-Russell Software, Petro-Canada Resources

Virginia Vera

B.Sc. Geophysical Engineering, 2008, Universidad Simon Bolivar

Ben Wards

B.Sc. Hons. Applied and Pure Mathematics, 2003, University of Calgary
M.Sc. Applied and Pure Mathematics, 2005, University of Alberta

Marcus Wilson

B.Sc. Pure and Applied Mathematics, 2006, University of Calgary

Abdolnaser Yousefzadeh

B.Sc. 1997, Shahid Bahonar University
M.Sc. Geophysics, 2001, Institute of Geophysics, University of Tehran
M.Sc. Geophysics, University of Alberta

- Work Experience: National Iranian Oil Company

Zimin Zhang

B.Sc. Geophysics, 1998, Changchun University of Science and Technology, China
M.Sc. Geophysics, 2005, China University of Petroleum

- Work Experience: China National Petroleum Corporation

Student Theses

The following theses are included with the CREWES 2009 Research Report:

M.Sc.	Alejandro Alcudia	Microphone and geophone data analysis for noise characterization and seismic signal enhancement
M.Sc.	Matt Allen	Exploring a Maya Pyramid Ruin using Seismic and Radar Tomography
M.Sc.	Hong Feng	Hydrocarbon indicators derived from AVO analysis
Ph.D.	Yongwang Ma	Seismic depth migration using the Gabor imaging theories
M.Sc.	Jason McCrank	Seismic Detection and Characterization of a CO_2 Flood in Ardley Coals, Alberta, Canada
M.Sc.	Maria F. Quijada	Estimating elastic properties of sandstone reservoirs using well logs and seismic inversion
M.Sc.	Gabriela Suarez	Full-wave Seismic Analysis: Source Comparisons, Land Streamer Tests, and Converted-wave Processing
M.Sc.	Roxana M. Varga	Using multicomponent seismic data to delineate hydrocarbon reservoirs: 2D-3C Willesden Green, Alberta and 3D-3C Manitou Lake, Saskatchewan

Acoustic impedance inversion of vintage seismic data over a proposed CO_2 sequestration site in the Lake Wabamun Area, Alberta

Abdullah Alshuhail*, Don Lawton and Helen Isaac

SUMMARY

Seismic inversion of vintage seismic data in the Lake Wabamun area has revealed contrasts in acoustic impedance caused by lateral changes in lithology and/or porosity of the Nisku Formation. This interpretation is constrained by well control and supported by seismic modelling, which suggests that changes in Nisku thickness over the range encountered in the study area has an insignificant effect on acoustic impedance. If so, then acoustic impedance mapping may provide one approach in pursuing favourable sites for CO2 injection in addition to the conventional time structure, amplitude maps and other seismic attributes. Our analysis revealed favourable low-impedance, high-porosity locations that could be potential injection sites.

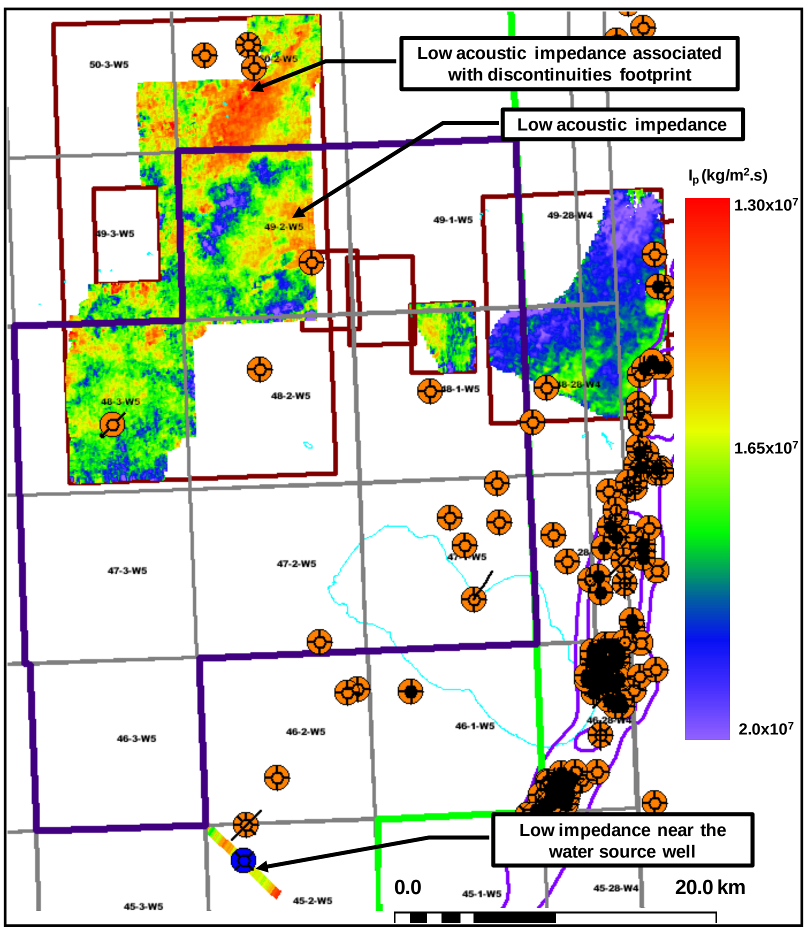

Estimated Acoustic impedance (I_p) map of the Nisku Formation using bandlimited inversion.

Choosing between the two Apollonius solutions when locating a microseismic event

John C. Bancroft

SUMMARY

The location and clock-time of a microseismic event can be computed analytically using the first arrival clock-times at four known receiver locations, assuming the velocity is known. The process is based on the Apollonius method that produces two solutions, either being possible for the same receiver geometry. The difficulty in choosing the correct solution is presented along with a method for identifying the best solution.

The following figures use 2D visualization to illustrate the two Apollonius solutions. In (a) and (b), the second solution (magenta) provides the correct solution while in (c) and (d) the first solution (cyan) is correct. In (d) the two solutions are in a similar location. The correct solution was identified by the polarity of the source clock-time.

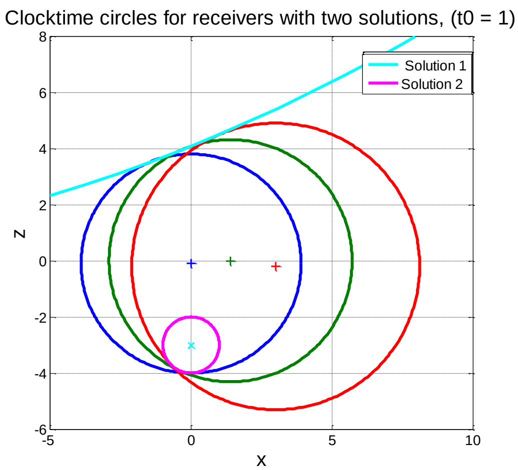

a)

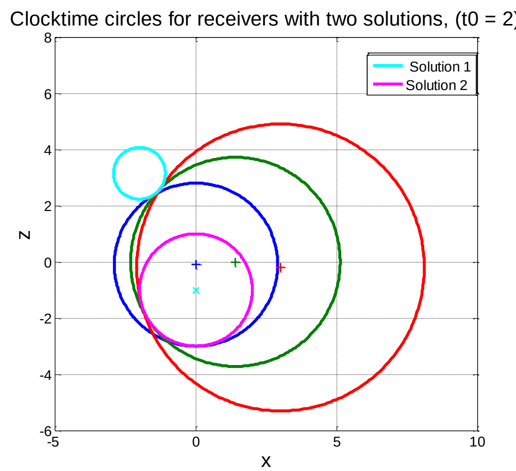

b)

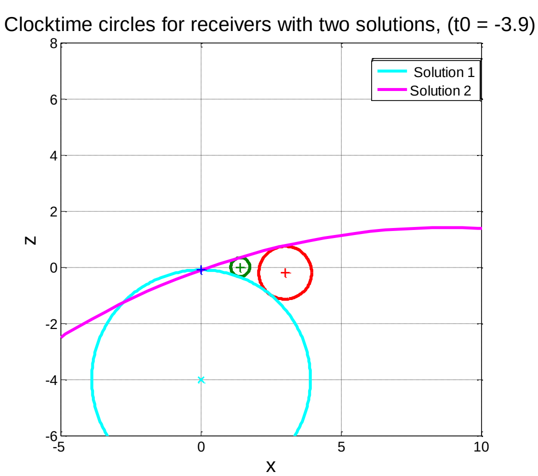

c)

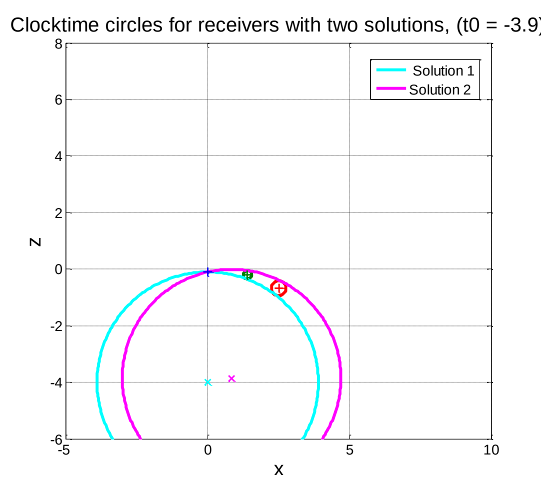

d)

Comments on diffraction modelling

John C. Bancroft

SUMMARY

Seismic data can be modelled by spreading energy along a diffraction shape. The energy spread along the diffraction should be a wavelet that is high cut filtered. However, single time samples are often used to reduce the computer runtime, but will introduce aliasing artifacts. Additional filtering techniques are often required to reduce these artifacts.

Diffraction modelling is used to illustrate the differences in the amplitudes of diffractions produced from a scatterpoint or from the termination of a reflector. This type of modelling introduces a phase shift to the data that require correction for accurate modelling. Aliasing artifacts may be produced, especially from horizontal reflectors. These problems are illustrated, discussed, and evaluated.

The following figure shows in (a) a diffraction with very high frequencies, and in (b) its aliased FK transform. In (c), a horizontal event was modelled with the diffraction in (a) and many aliased horizontal events are visible below the horizontal reflection.

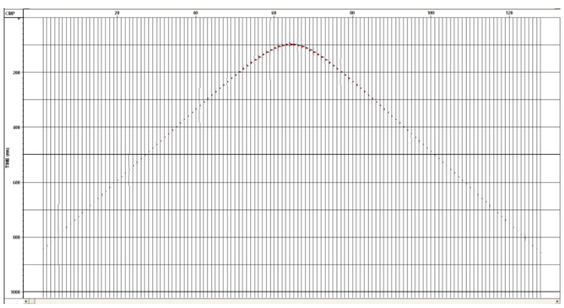

a)

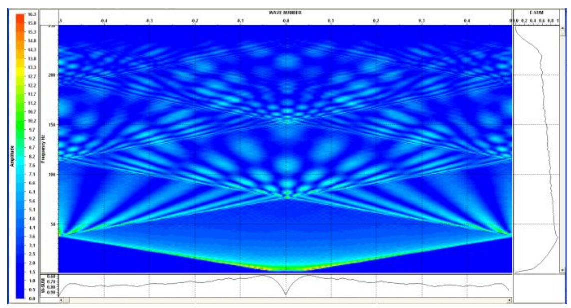

b)

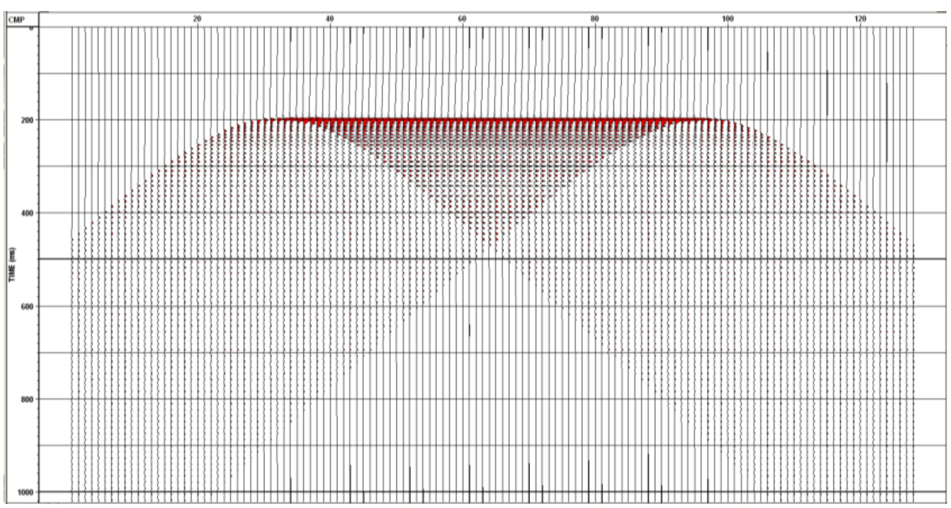

c)

EOM hyperbolae

John C. Bancroft

SUMMARY

The equivalent offset method of migration is a prestack migration that spreads energy from one input time sample to all the neighbouring gathers. In a time migration, the energy is spread along a hyperbolic path in a constant time plane defined by the input sample. This path is referred to as the EOM hyperbola. Moveout correction of this hyperbola creates the prestack migration ellipse.

Properties of the EOM hyperbola are displayed relative to the prestack migration ellipse to evaluate the extent of the EO hyperbola, and to establish an ad hoc method for applying amplitude scaling.

Comparisons of EOM with conventional prestack time migration are provided.

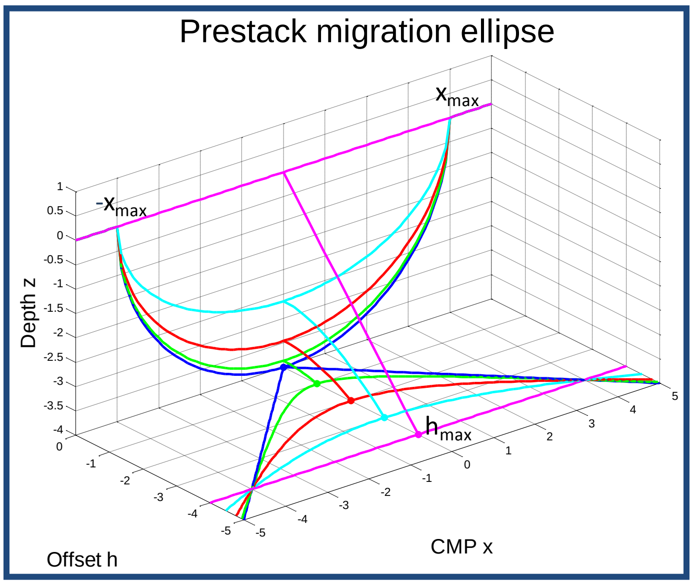

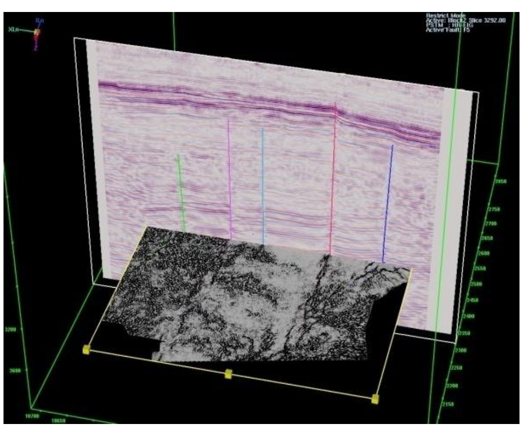

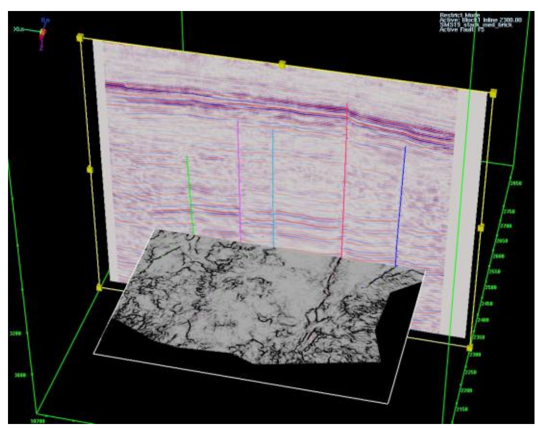

Conventional prestack time migration

EOM

Estimating an accurate RMS velocity for locating a microseismic event

John C. Bancroft

SUMMARY

The location and clock-time of a microseismic event (x_0, y_0, z_0, t_0) can be computed analytically using the Apollonius method that requires the first arrival clock-times at four known receiver locations. The velocity is assumed to be known and constant. If the velocity is not known, it can be estimated by using an iterative technique that minimizes the error of the traveltimes between the source and receiver. Improving the accuracy of the velocity improves the estimate of the source location.

The convergence to the correct solutions is dependent on the geometry of the source and receiver locations.

Five receiver locations allow five combinations of four receivers. An analytic solution for each receiver combination provides five different estimates of the source location. The difference in the raypaths and their traveltimes aid in converging to the correct velocity, and to the correct source location.

The figure below displayes the five estimated values for t_0. The correct velocity is 1.0, and the correct time is t_0 = 2.0.

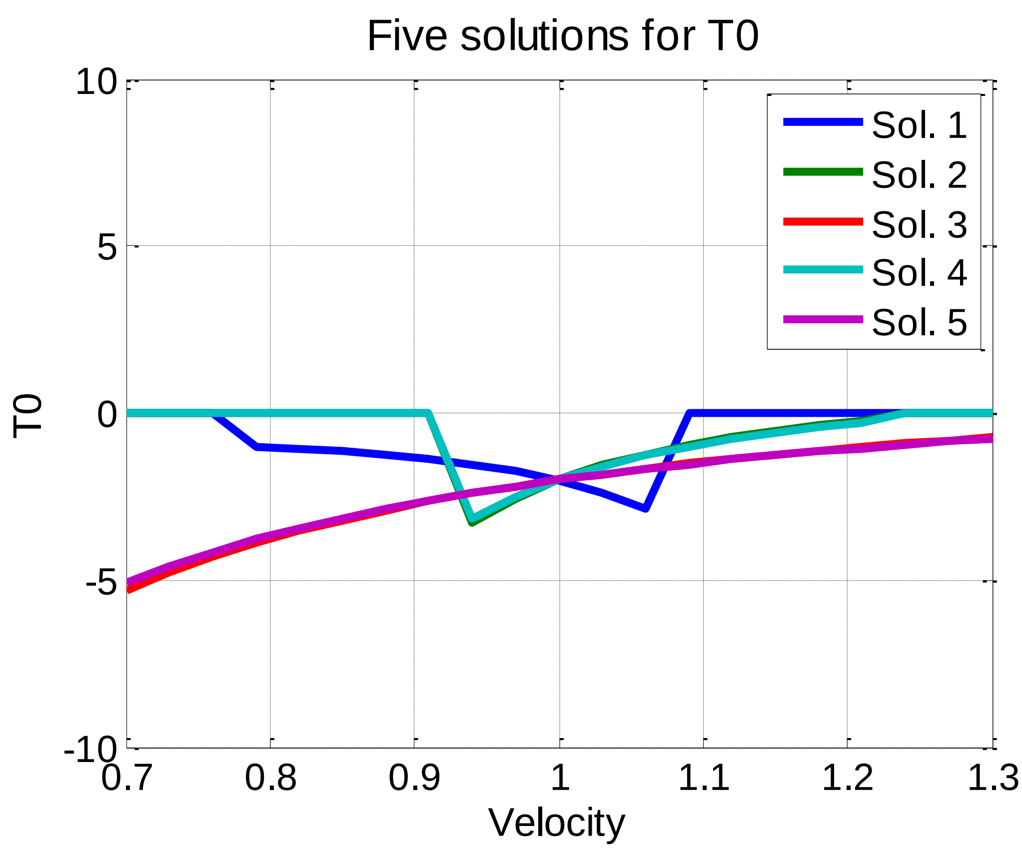

Estimating the location of a microseismic event when using a vertical array of receivers

John C. Bancroft*

SUMMARY

The accuracy of using a vertical array of receivers is investigated for locating microseismic events. Only clock times are used to estimate the location of the source. Noise was added to the clock-time of the receivers, and the errors in estimating the source locations displayed. The errors vary with orientation and distance from the receiver array and the size of the receiver array.

The following plots illustrate two algorithms for estimating the source location; P using analytic solutions, and V using vector intersection. Noise, with a standard deviation (Std) of 1.0 ms, was added to the receiver times. The vertical receiver arrays are identified by a green "X" and the sources with a blue "+". Errors in the estimated source locations and their Stds are shown in red. Figures (a) and (b) have sixteen receiver while (c) and (d) have eight receivers.

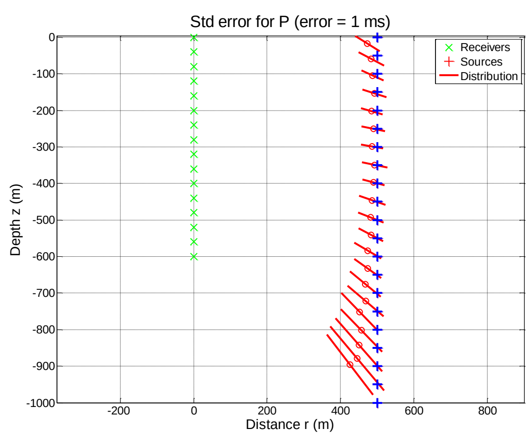

a)

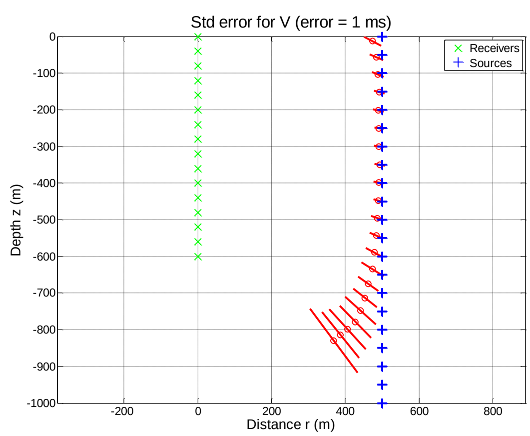

b)

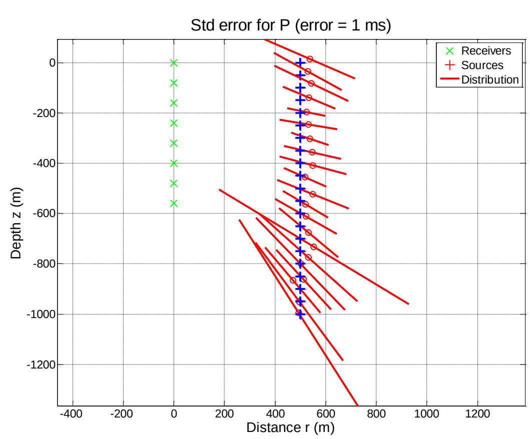

c)

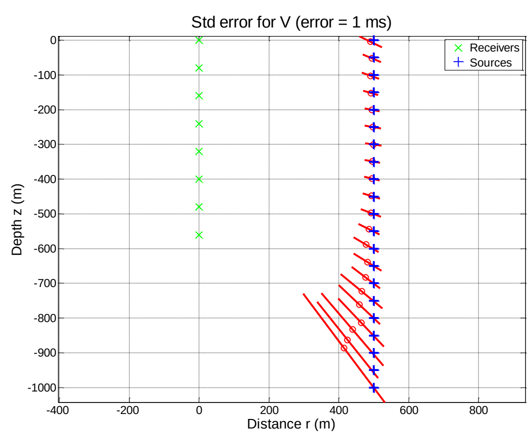

d)

Sensitivity measurements for locating microseismic events

John C. Bancroft, Joe Wong, and Lejia Han

SUMMARY

The first arrival clock-times from a number of receivers are used to estimate the clock-time and location of a microseismic event. The 3D solution is based on a 2D source location scheme based on the Apollonius method. This 3D solution requires four receivers that are non-coplanar or non-collinear. These restrictions are typically violated when receivers are placed in a large grid on the surface or in a linear array in a well. Non Apollonius solutions are presented for these restricted cases along with an analysis that relates the accuracy of the estimated source location to clock-times at the receivers.

It is anticipated that these methods will be part of a larger system where these analytic solutions can be used with data extracted from the large arrays.

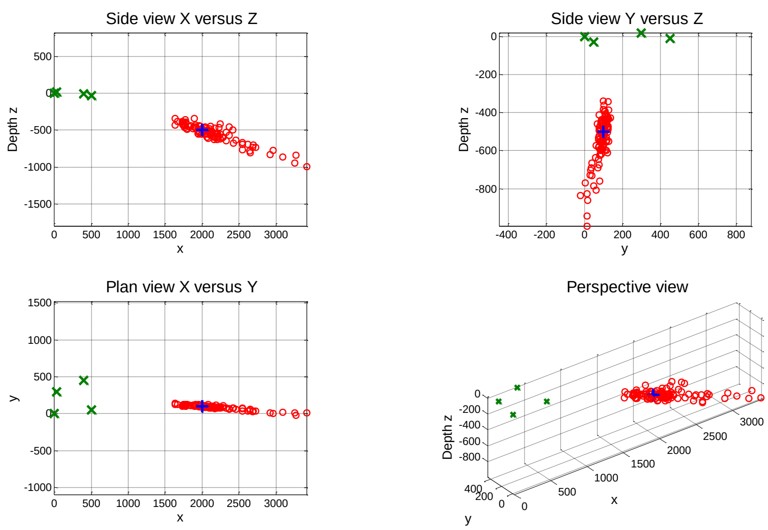

Fig. 1 Distribution of estimated source locations.

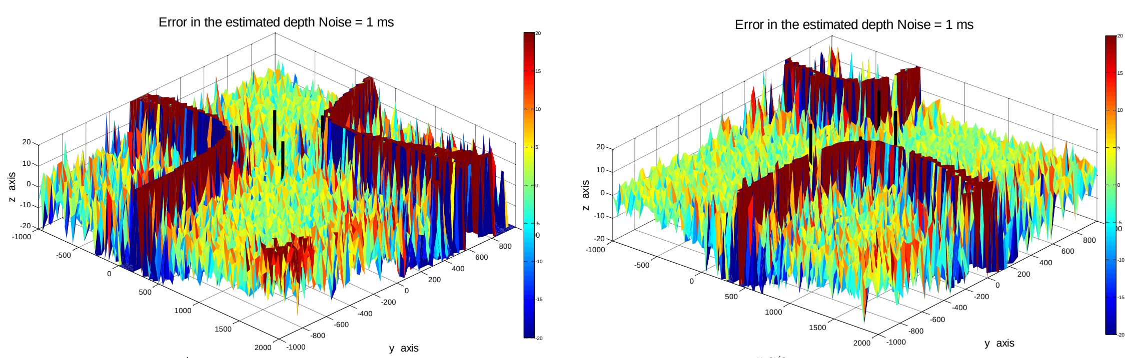

Fig. 2 Plot of the vertical error of source locations from an event at a depth of 500 m when estimated by four receiver close to the surface. The difference in these two figures is a result moving one receiver in the y direction from 300 m to 600 m. The location of the four receivers can be identified by the vertical black lines.

Seismic acquisition projects 2009

Malcolm B. Bertram*, Kevin W. Hall, Gary F. Margrave, Don C. Lawton, Joe Wong and Eric V. Gallant

SUMMARY

Since the CREWES meeting in November 2008, several acquisition projects have been undertaken. These include: a) a 9-C VSP and 3-C 2D line recorded in March 2009 at the Priddis observatory, the VSP to provide data for near surface attenuation studies and geophone orientation algorithm development, and the 2D line to evaluate the area for the proposed injection test site embedded array, as well as provide another data set for noise analysis; b) a set of evaluation records recording weight drop thumps and low frequency vibrator sweeps into comparison spreads of geophones, MEMs sensors, and seismometers acquired in August 2009 to evaluate the low frequency response of the seismic sensors compared to seismometers, and investigate surface propagation at low frequencies; c) the 2009 University of Calgary Geophysics Field School (GOPH549), this year recording a 3-C 2D line in the Spring Coulee area.. Also, during the last year, a new small weight drop source using an elastic band for acceleration has been developed and constructed at the University of Calgary.

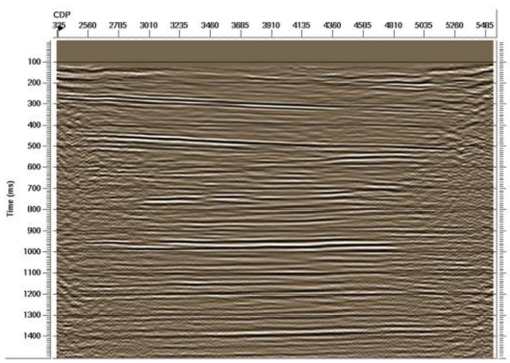

Section from the March 2009 3-C 2D survey

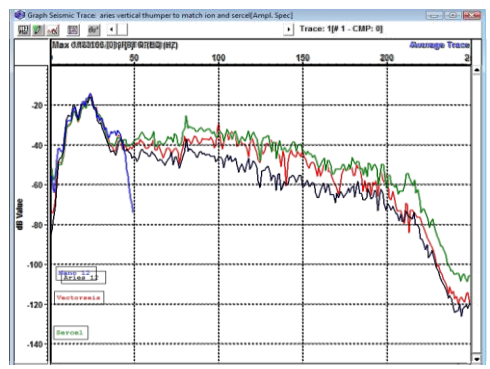

Spectrum comparison from the low frequency study

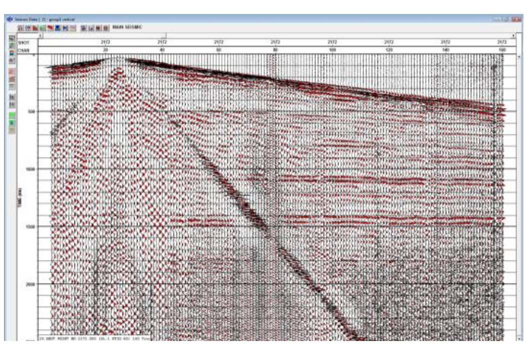

Shot gather from U of C Field School August 2009

New thumper seismic source

Seismic data modelling using parallel distributed MATLAB

Kayla Bonham and Robert J. Ferguson

SUMMARY

Numerical modelling of seismic wave propagation is central to seismic imaging and inversion. Modelling of 3D heterogeneous anisotropic media can, however, simultaneously be both costly and of low fidelity. To address some aspects of the fidelity / cost problem, we present our implementation of seismic modelling within the Rayleigh-Sommerfeld algorithmic framework and implemented in a parallel computing environment. We demonstrate through example, that knowledge of relationships among hardware architecture, support software systems, and resource usage of our algorithm, is of crucial importance to the achievement of worthwhile performance using parallel computing.

Our initial naïve MATLAB implementation using the built-in construct for the "outer loop" uncovered unsatisfactory parallel performance. By paying attention, however, to both the hardware architecture and the software support system, we have been able to substantially increase parallel performance without disturbing the simplicity of the code (much).

Time elapsed, T_3, is plotted for the observed runs of version 3 of the parallel program, in Figure 1. We find that a ‘sweet spot’ exists at about 48 workers on 6 nodes with 8 workers per node – not too many nodes reserved, something close to minimum elapsed computation time of 508 seconds. With 48 workers and 6 nodes, half the cluster is left to do a second computation or to let other users make use of the resources.

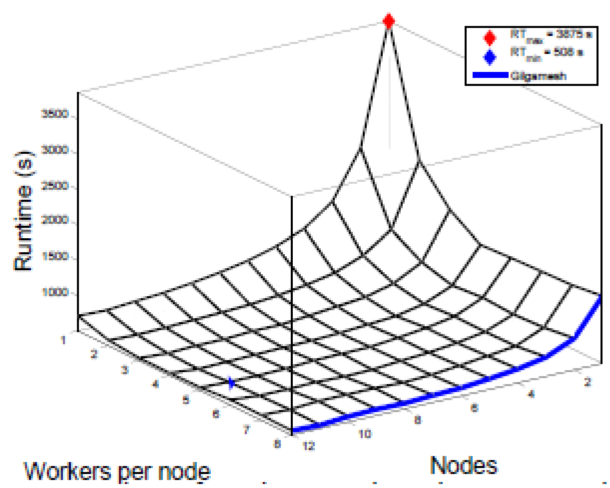

FIG. 1. Plot of runtime versus number of workers and workers per node. Maximum and minimumruntimes are indicated (RT_{max} = 3875s and RT_{min} = 508s) respectively, RT for the 8 worker pernode configuration of Gilgamesh.

VSP processing for coal reflections

Salman K. Bubshait* and Donald C. Lawton

SUMMARY

Five VSP surveys were acquired in Alberta as part of a study of Mannville coals. The zero-offset VSP survey was processed using the VISTA software through to corridor stack and shows high reflection quality of P waves with no significant multiples in the data. Also, the three walkaway VSPs along different azimuths were processed through to the VSPCDP stage. A recommendation is suggested to have an overlap of a receiver in the borehole to minimize shot static errors. The walkaways displayed high reflection quality of both P and S waves that highlighted the Mannville coals. A slight improvement of the reflection of the coals is noticed in the SV waves over the P waves as offset increases.

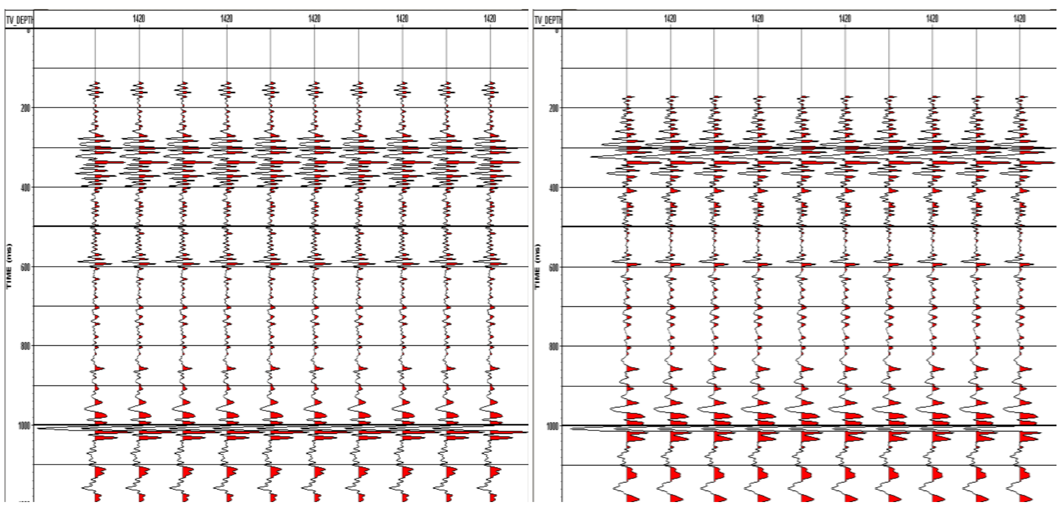

FIG. 1. Zero offset VSP inside Inside (left) and outside (right) P-wave corridor stacks.

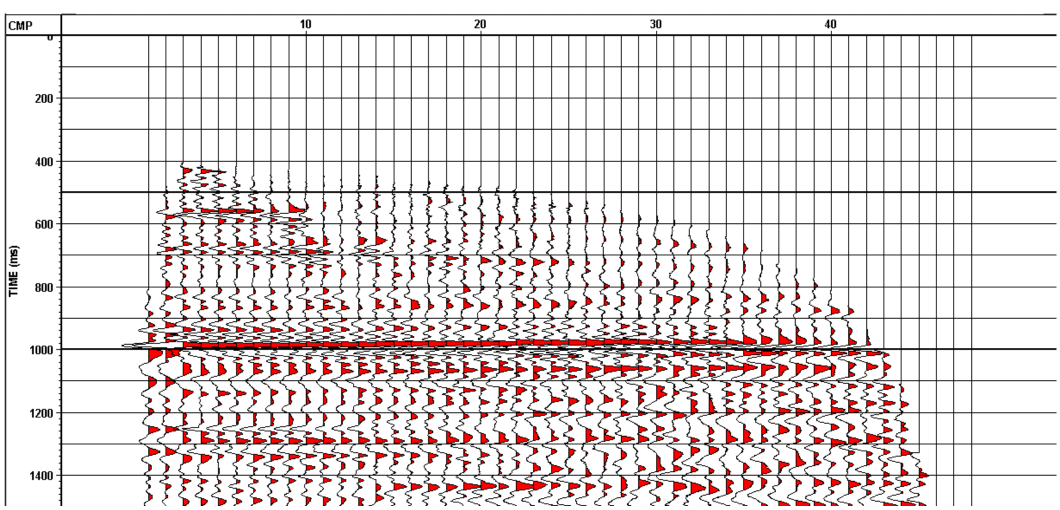

FIG. 2. VSPCDP (P-wave) multi-offset stack of a VSP walkaway survey.

The influence of reflectivity color on Gabor deconvolution

Peng Cheng and Gary F. Margrave

SUMMARY

This article analyzes the influence of nonwhite reflectivity in Gabor deconvolution. Testing on synthetic data shows that large phase rotations and distorted amplitude estimation can be attributed to the reflectivity's spectral color and temporal color respectively.

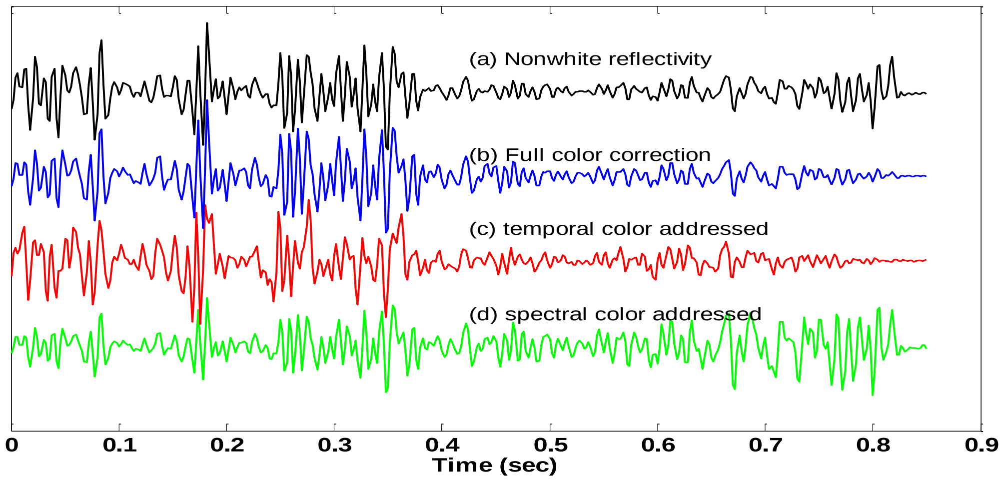

FIG.1. Reflectivity series: (a) true reflectivity; (b) full color correction estimation; (c) temporal color addressed estimation; (d) spectral color addressed estimation.

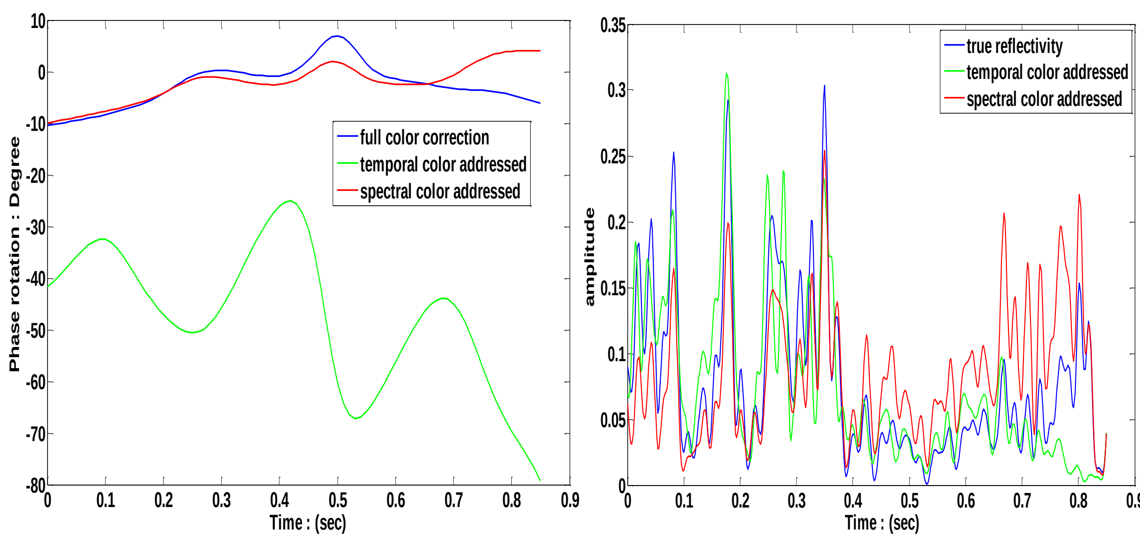

FIG. 2. (Left) Phase rotation of estimated reflectivity series shown in figure 1; (Right) Envelopes of the reflectivity series shown in figure 1.

Q analysis using synthetic viscoacoustic seismic data

Peng Cheng and Gary F. Margrave

SUMMARY

The spectral ratio method is used to conduct Q analysis with synthetic VSP and reflection data. Testing results show that the spectral method can deal with frequency independent energy loss including geometric spreading and transmission loss, and can also be used to derive the layered Q structure of subsurface. For real data, the notches in spectrum, due to reflectivity, are a severe problem for spectral ratio calculation. The adaptive multitaper method for spectral estimation is shown to give a smooth estimate with little evidence of notching, and is superior to both DFT and Burg spectral estimates.

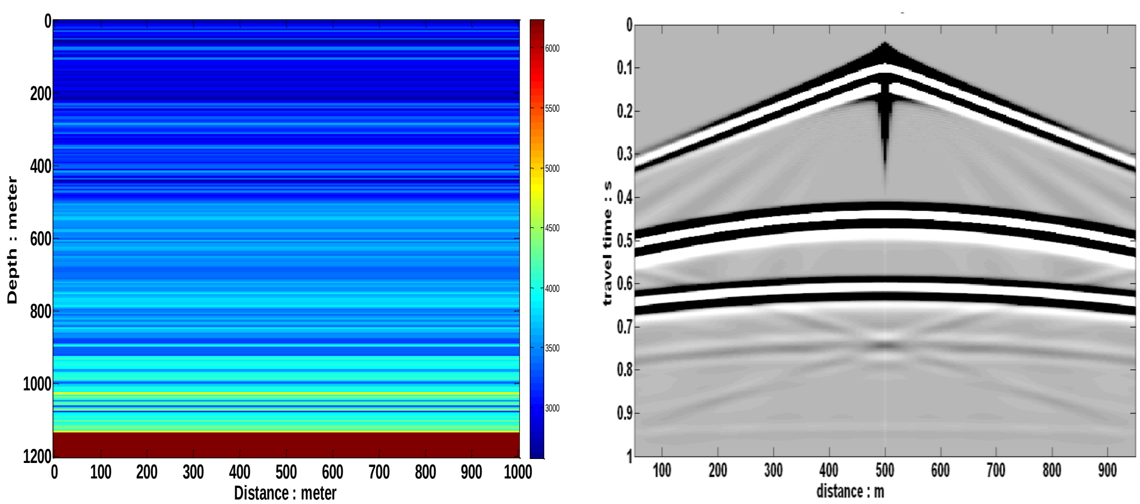

FIG. 1. (Left) A true velocity model calculated from a well log; (Right) Shot record gather using the left velocity model and a constant Q of 50.

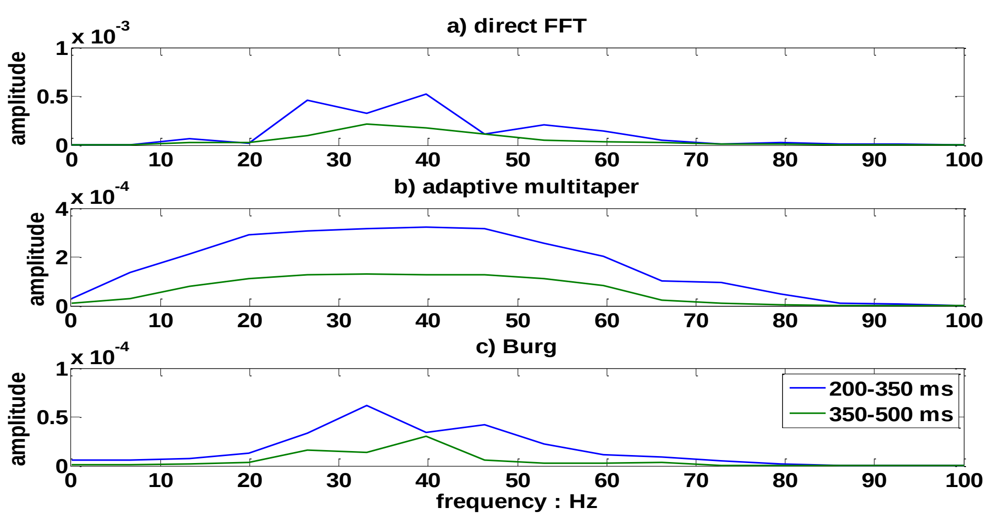

FIG. 2. The amplitude spectra of the 200-350ms and 350-500ms segments of the zero-offset shot record in figure 1 using three spectrum estimation methods; Estimated Q values are 137.4, 34.2 and 38.4 in order.

Delta weights for footprint suppression in 3D prestack migration

Joanna K. Cooper*, Gary F. Margrave, and Don C. Lawton

SUMMARY

When compared to prestack-migrated images of a fully-sampled ("exhaustive") numerical model seismic dataset, images from decimated (under-sampled) datasets display acquisition footprint artefacts. In this study, a weighting scheme for prestack Kirchhoff migration that attempts to compensate for irregular illumination of image points, which was previously shown to have promise in 2D, was implemented in 3D using MATLAB. The method was applied to the exhaustive and decimated datasets, with the purpose of examining its ability to suppress footprint artefacts. The scheme involves hit counting of delta angles for traces input to the migration, where delta describes the dip and azimuth of the vector bisecting the source-to-image-point and receiver-to-image-point rays. Though the method does not address footprint related to the aperture of the survey, it does appear to reduce the severity of footprint artefacts consisting of periodic amplitude variations in the interior of the survey, without losing the ability to resolve edges in the migrated images. The method produced results that are better than a comparable common-offset-weighted migration.

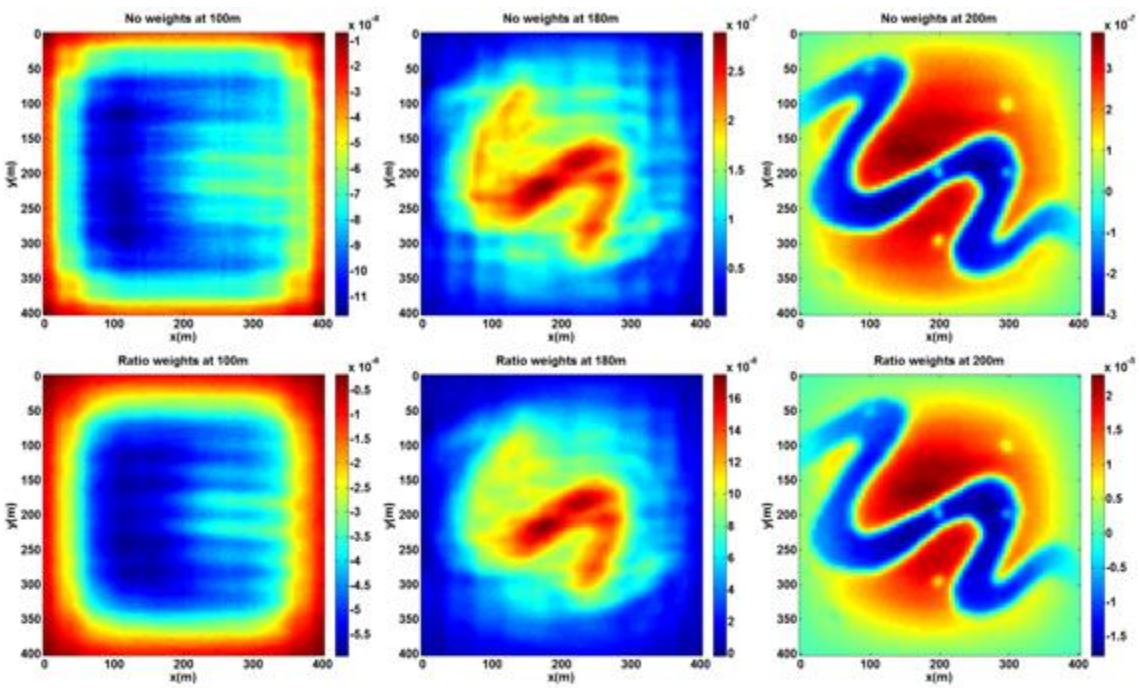

FIG. 1. Prestack-migrated depth slices at 100m (left), 180m (middle), and 200m (right) for an orthogonal 3D survey with a hole in shot coverage. Top row: no weights; bottom row: delta-ratio weights.

Anelastic media: wave propagation near vertical incidence

P.F. Daley

SUMMARY

A number of topics regarding wave propagation in anelastic media are considered. These include normal incidence reflection at an interface where the only parameter that varies between the two media is the quality factor Q. For reference purposes, the PP acoustic reflection coefficient for an elastic over an anelastic medium is discussed for varying values of Q in the lower media and a range of incident angles, $\theta, \left(0 \le \theta \le 90\right)$. Examples of normal incidence synthetic seismograms are presented for a plane layered medium with variations of Q in the layers.

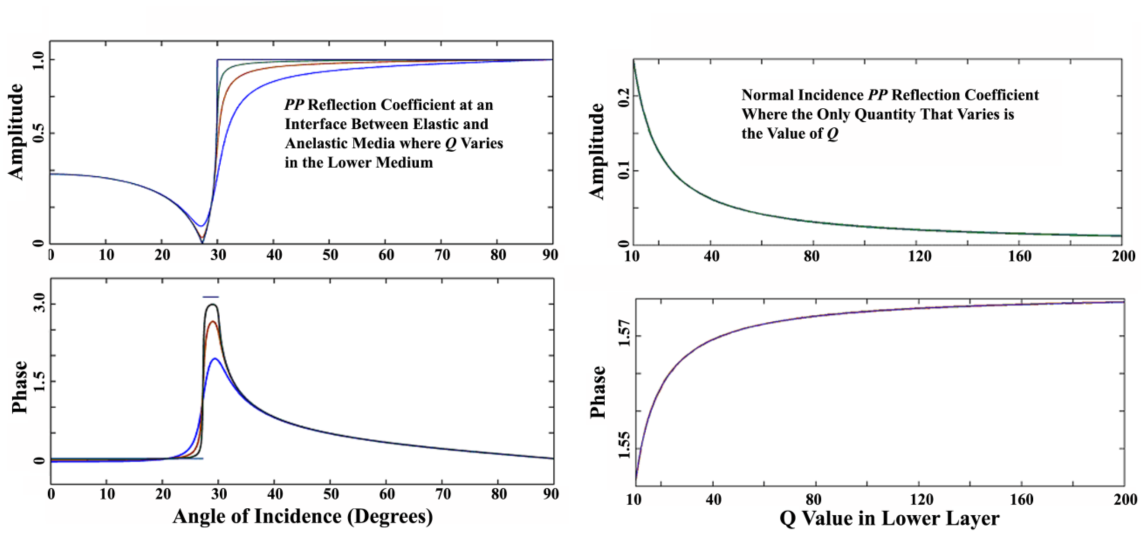

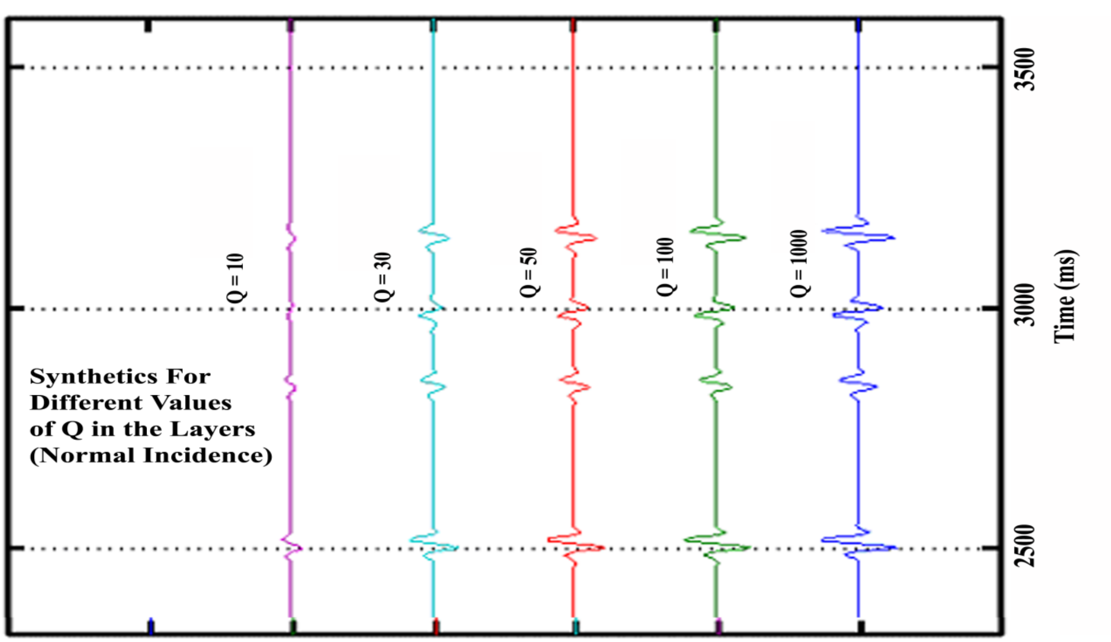

P and S velocity approximations in a poroviscoelastic medium

P.F. Daley

SUMMARY

Biot's equations of particle motion for wave propagation in a fluid saturated poroviscoelastic medium are manipulated to obtain zero and first order approximations to the fast compressional (P) wave and shear (S) wave velocities. The expressions obtained are used in the numerical investigation of the effects on these velocities resulting from the variation of quantities defining the solid and the fluid, specifically porosity and permeability, as well as others, inherent in the theory. In addition, the first order velocity approximations are complex functions, in terms of the quality factors, Q_P and Q_S, which define the attenuation properties in a poroviscoelastic medium. Zero and first order expressions for the complex fast compressional wave velocity and the shear wave velocity are obtained and used within the context of viscoelasticity to obtain some initial insight into the more general poroviscoelastic problem.

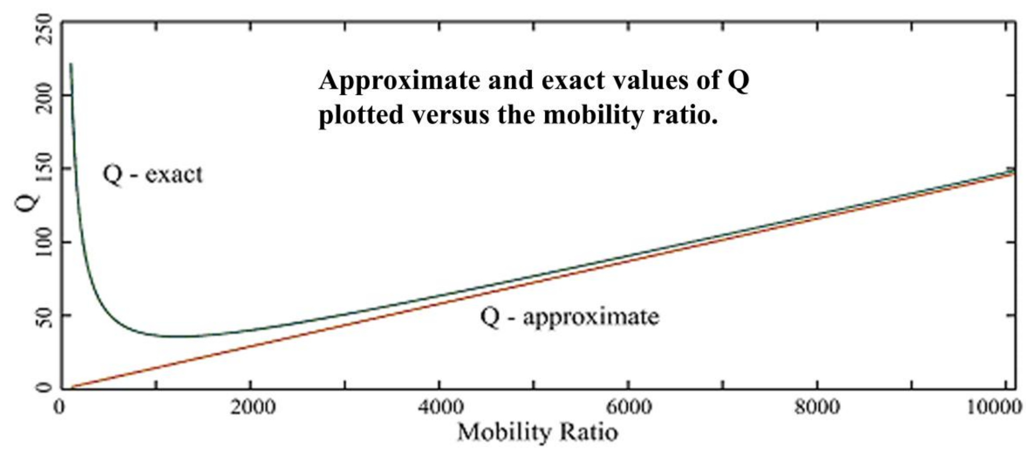

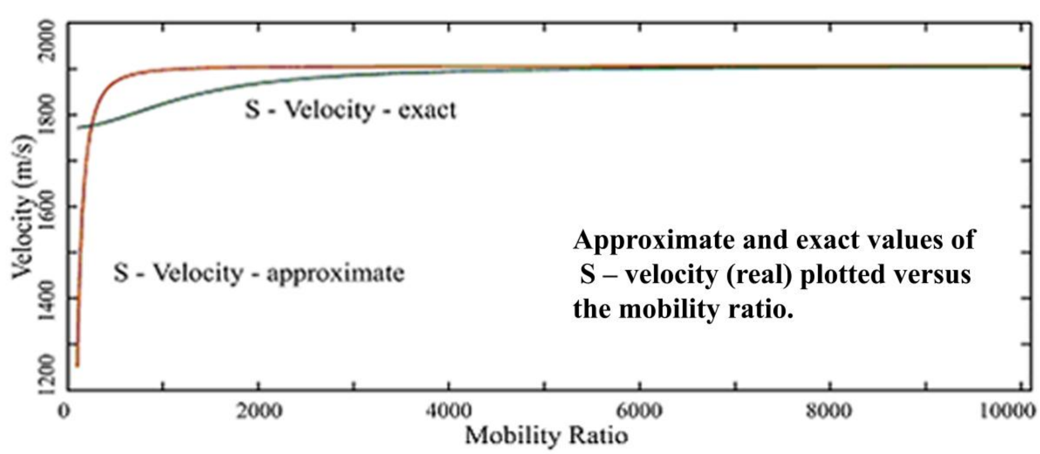

Reflected PP arrival in anelastic media

P.F. Daley and E.S. Krebes

SUMMARY

A homogeneous wave incident on an interface between two anelastic halfspaces in welded contact is considered. Certain distributions of the quality factor, Q, can result in anomalous behaviours of both or either of the amplitude and phase of the PP reflection coefficient when displayed versus the incident propagation angle or equivalently the real part of the horizontal component of the incident slowness vector. In an earlier work (Krebes and Daley, 2007) the question of anomalies in the amplitude and phase of the PP plane wave reflection coefficient for these distributions of the quality factor Q in adjacent anelastic halfspaces was discussed in considerable detail. The problem of the PP reflection coefficient is addressed again within the context of two selected approximate methods, of varying complexity.

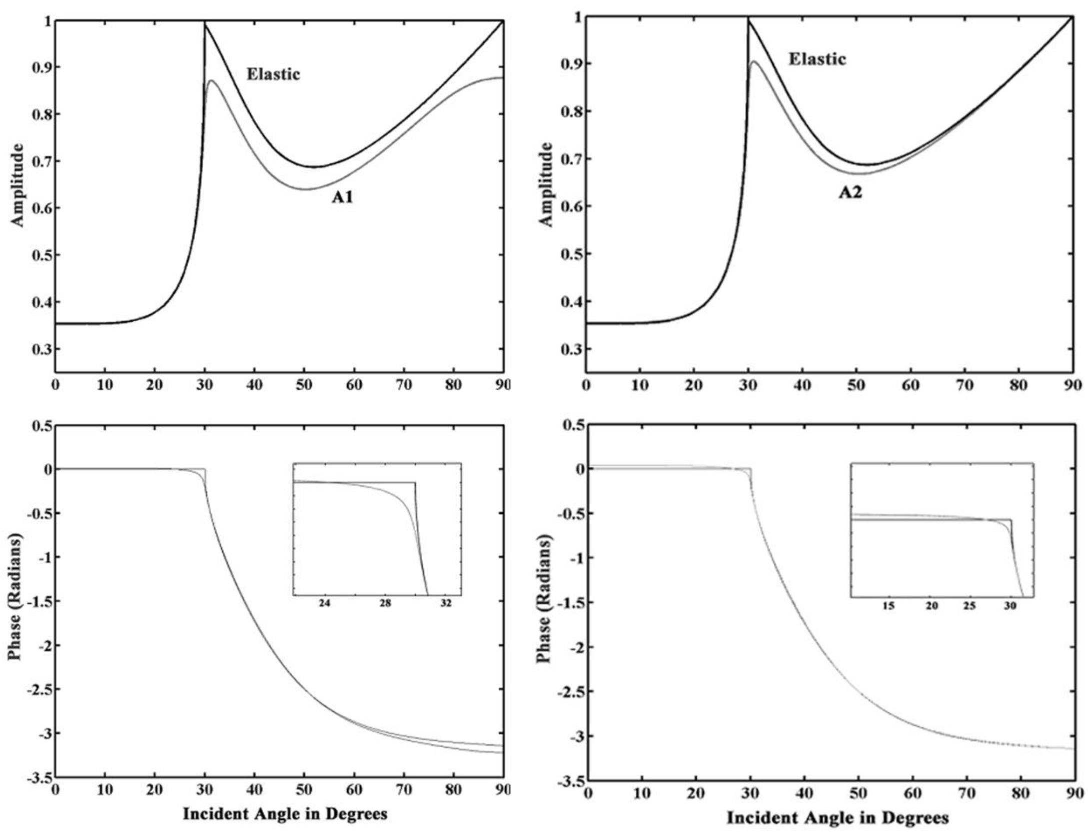

Absolute strain determination from a calibrated seismic field experiment

David W. Eaton*, Adam Pidlisecky, Robert J. Ferguson and Kevin W. Hall

SUMMARY

The concepts of displacement and strain are fundamental to our understanding of how elastic waves propagate in the subsurface, but accurate absolute determination of these quantities is rare. In August 2009, a field experiment was conducted on University of Calgary lands near Priddis, Alberta (Rothney Astrophysical Observatory) using various seismic sources (minivibe, weight drop) and receivers (geophones, accelerometers and broadband seismometers). A 3-component shot gather using a weight-drop source was recorded by 8 broadband seismometers and used to verify the absolute instrumental response of 80 3-C 10 Hz geophones, recorded using the university's ARAM-24 acquisition system. Although significant lateral amplitude variability is evident, an empirically derived average response for the ARAM system agrees with manufacturer specs to within < 4 in the frequency range 2-40 Hz, representing the bandwidth overlap between the geophone and seismometer systems. Based on this calibration, the strain associated with ground roll and refracted P- and S-wave energy is ~ 10^{-7}.

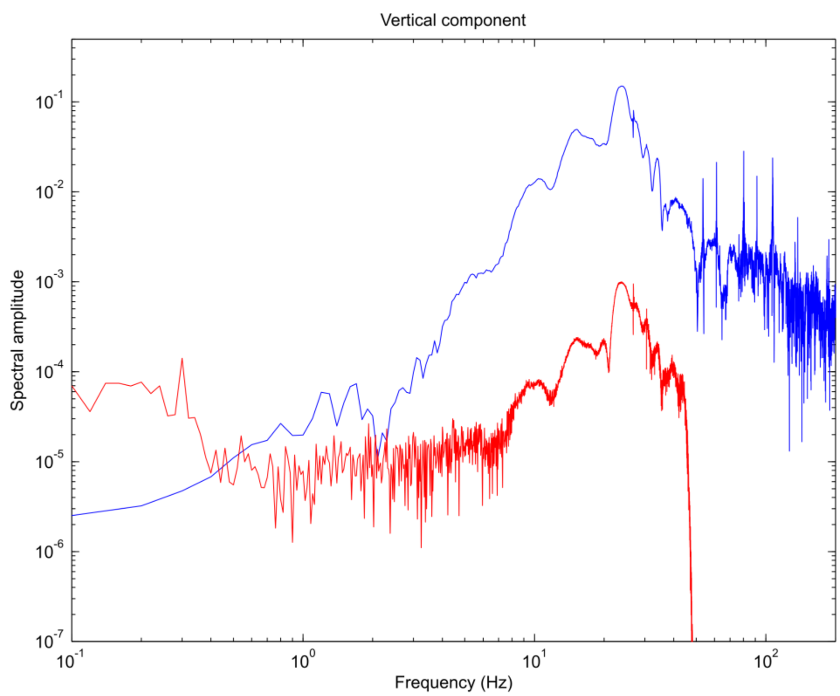

Comparison of a calibrated vertical-component spectrum for the Trillium-240 seismometer (lower curve; red) with the corresponding raw spectrum for the SM-24 geophone – ARAM system (upper curve; blue).

Antialiasing and wave equation statics by series approximationand inversion

Robert J. Ferguson

SUMMARY

To address the problems of irregular trace spacing and statics correction, simultaneous regularization and wave equation statics (WE statics) is implemented by least-squares inversion. In general, inversion is found to be intractable currently in 3D, so series approximation is made to reduce significantly the number of required integrals. The resulting operator is suitable for both direct inversion, or for use with gradient methods.

Real and synthetic data are used to demonstrate the viability of the inversion. Synthetic data show that even for severe velocity variation and topography, inversion converges to an acceptable solution, and that aliasing is significantly reduced. Similarly for real data, inversion is shown to return a regularized result with WE statics applied that is anti-aliased.

A severely decimated trace gather is given in Figure 1. Large trace gaps are present in the data (Figure 1a), and it's spectrum is severely aliased (Figure 1b). Following inversion, reflection events 1 through 5 are now well constructed (Figure 1c), and much of the aliasing is eliminated (Figure 1d).

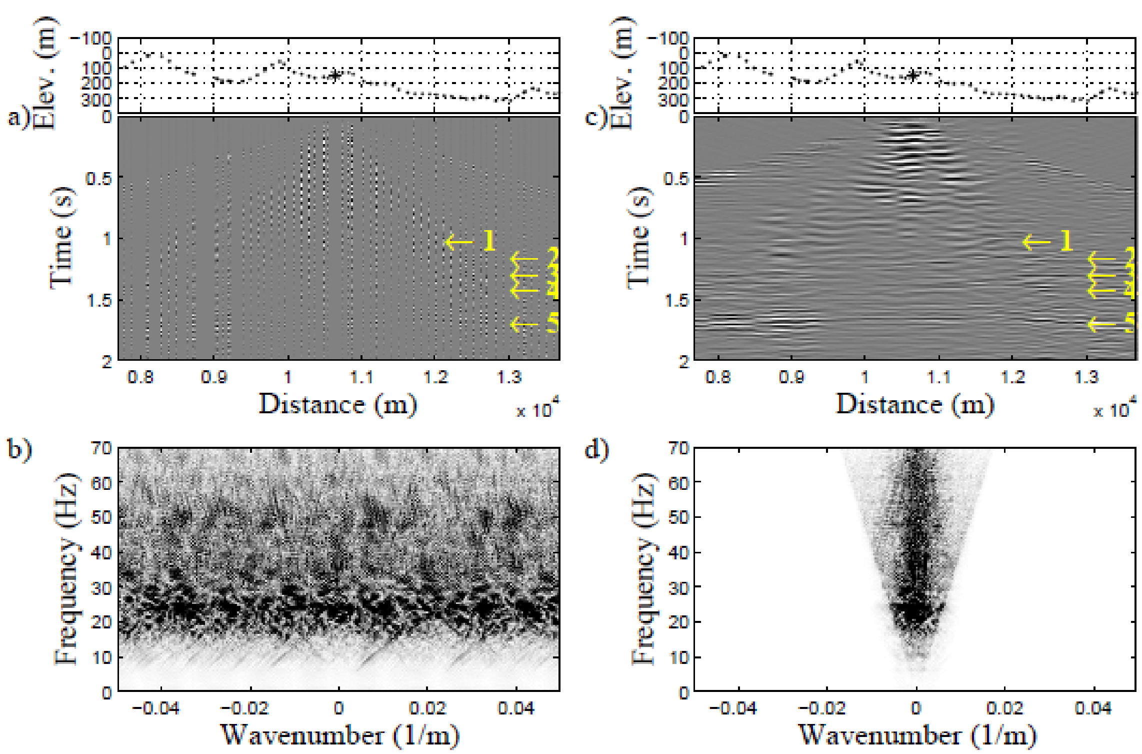

FIG. 1. Irregularly sampled shot gather from the Husky dataset. a) Seismic data (60 / 306 traces randomly spaced) plus an elevation profile. b) Spectrum of a). c) Regularization and WE statics by inversion. d) Spectrum of c).

Gabor domain analysis of Q in the nearsurface

Robert J. Ferguson*, Gary F. Margrave, and Kevin H. Hall

SUMMARY

We present a *Q* estimation method based on traveltime derivatives applied to multilevel vertical seismic profile (VSP) acquisition. Long, narrowband vibroseis sweeps provide approximately monochromatic wavefields over short time windows, and analysis is done in the Gabor domain (Figure 1a and b). There, attenuation β is estimated as a function of frequency *f*, and *Q*(*f*) is computed through inversion of β.

We provide an example based on a 7-level, near-offset VSP. Each VSP level consists of a 3-component receiver with inline, crossline, and vertical sweeps. Eight, narrowband sweeps are used to span 10 Hz - 250 Hz for each source orientation, and they are found to help reduce noise in the data due to baseplate harmonics.

Two subunits are identified within the local formation that correspond to an expected 50 m of unsaturated media underlain by an aquifer. Our results demonstrate that β varies near-linearly with frequency for the 95 m depth range, Strong values of β that increase with *f* are found in the unsaturated unit, and weaker, decreasing β is found in the saturated unit.

Q for the formation is estimated only approximately due to excessive powerline noise and and strong harmonics in the well. For both units and the overall formation, *Q* increases linearly with f until about 100 Hz.

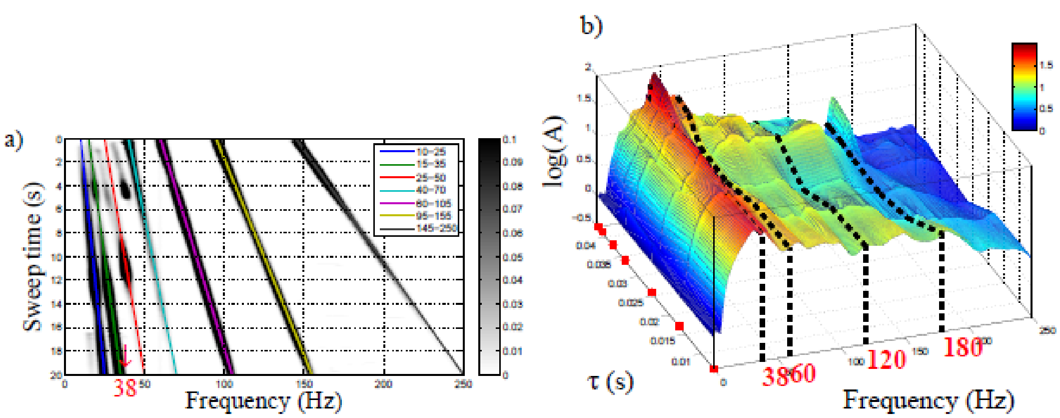

FIG. 1. Gabor data domain and derived analysis domain. a) Source V Gabor power spectra for $z = 50$ m. b) Source V derived $\log A$, where $A = \sqrt{G G^{\dagger}}$.

Geophone rotation analysis by polarity inversion

Robert J. Ferguson

SUMMARY

A technique is presented by which multicomponent geophone data are rotated such that the preferred geophone component is aligned with the direction of the incident wave form. Wave forms of interest are restricted to first-arrival P-waves, and S-waves polarized normal to the plane that contains both the source and the geophone. Rotation is based on that fact that the geophone orientation, and the apparent rotation that it imparts to the incident waveform, is equivalent to the application of a 3×3 unitary matrix, and that the inverse of the operator is also unitary.

Given a 3C recording, the inverse operator is deduced from a processed version of the recording through inversion by least-squares. This inverse operator is then applied to the raw recording to achieve the desired orientation. Decomposition of the inverse operator yields the dip and azimuth of the geophone orientation.

Synthetic examples are presented that demonstrate the performance of this inversion in the presence of noise. Inverted waveforms are compared to the idealized input waveforms, and dip and azimuth estimates are made. It is found that waveform comparisons compare very well qualitatively in the presence of noise, and that dip and azimuth estimates degrade with increased noise. Dip and azimuth estimates are found to improve to acceptable accuracy with judicious application of band-pass filters to the input.

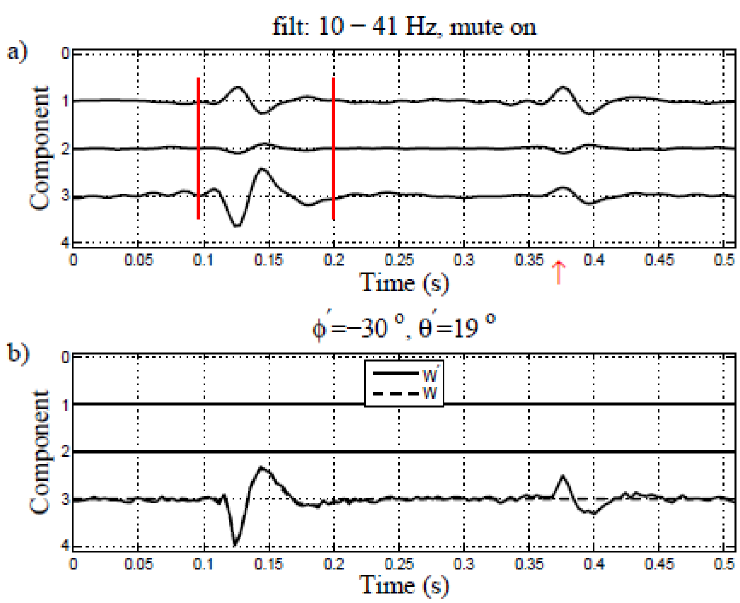

FIG. 1. 3C rotation for a P-wave source. a) 3C recording in the wellbore. Red lines indicate the analysis window. The arrow indicates a S-wave. b) The inversion estimate. Dip $\phi = -30^o$ (no error) and azimuth $\theta = 19^o$, $\theta_{true} = 20^o$.

Microseismic monitoring: Insights from moment tensor inversion

Farshid Forouhideh* and David W. Eaton

SUMMARY

This paper reviews the mathematical tools used for describing microseismic source mechanisms. In addition, based on analysis of synthetic seismograms we develop and evaluate a workflow for inverting source mechanisms (moment tensors). We consider several types of focal mechanisms including double-couple (representative of a slip on a fault) and more complex mechanisms that include tensile forces. Our inversion strategy uses a least-square approach that attempts to fit P- and S-wave amplitudes measured using multicomponent borehole geophone array. An important final step in the inversion process is decomposition of the recovered moment tensor into isotropic, compensated linear vector dipole (CLVD) and double-couple components. These three end member focal mechanisms provide the basis for describing most common classes of microseismic events. Our preliminary inversion tests for noise-free synthetic data suggest that the isotropic component is likely to be the least well-resolved parameter.

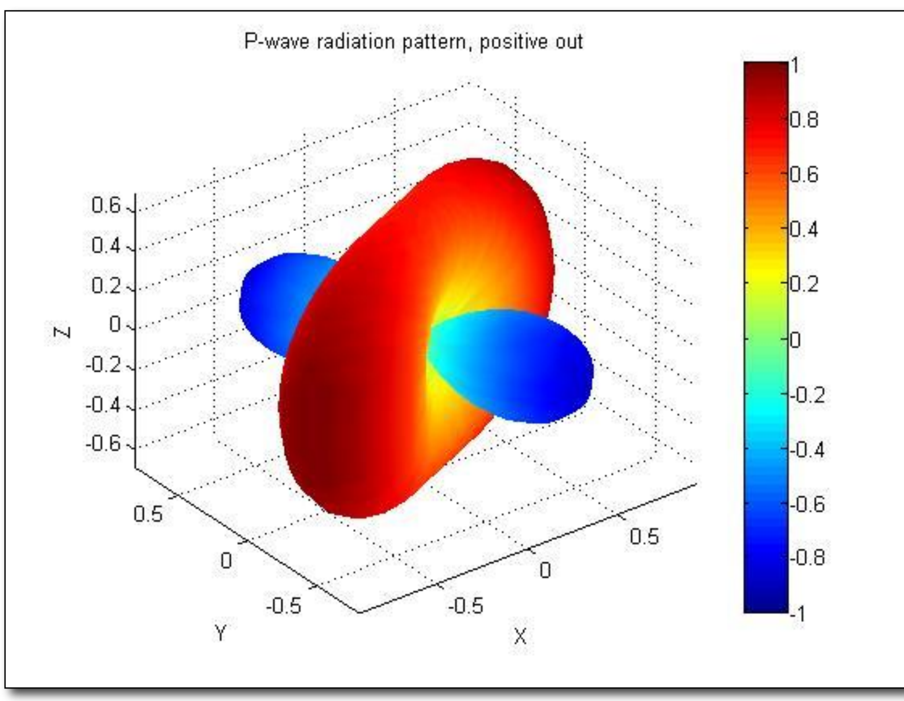

This figure shows the P-wave radiation pattern of a seismic source composed of 20% isotropic, 50% double-couple and 30% compensated linear vector dipole (CLVD) components. The isotropic component corresponds to the volume change. These sources represent the so-called tensile earthquakes.

Converted wave prestack migration in the presence of topography: Synthetic cases

Saul Guevara and Gary Margrave

SUMMARY

Converted waves can provide valuable structural and stratigraphic information, which requires suitable processing methods such as prestack migration. Rough topography, present at many places of interest, can reduce the quality of the resulting images. A method of Kirchhoff prestack migration for converted wave in the presence of topography is presented here. It was used a prestack depth migration code for shot gather data. The input data sets, shot gathers with topography, were created using an elastic FD method. The velocity model used for modeling was also an input for the migration code. An eikonal ray-tracing code allowed creating the time tables for the pre stack depth migration.

An example is illustrated in the following Figures. Figure 1 shows the geologic model with their velocities and geometry. The receivers are located at the surface with topography (below "Air"). A flat interface is approximately at 380 m below the energy source. Figure 2 shows the converted wave PSDM for the horizontal component. The two main events are marked with arrows. The number 1 corresponds to the PS converted wave and the number 2 to a pure S-wave, which keeps high energy in this case.

CONCLUSIONS

PSDM for converted wave in rough terrain using the Kirchhoff approach shows promising results applicable to structural and stratigraphic problems. Future research can take into account issues such as anisotropy and true amplitude recovery.

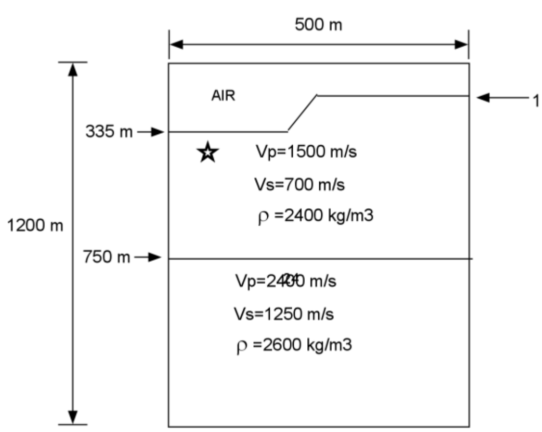

Figure 1. Geological model used to create the shot gather data set used for testing.

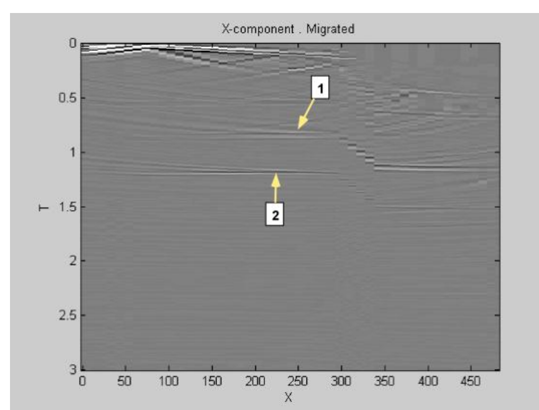

Figure 2. Converted wave PSDM result in time The arrow shows the main events. No. 1 corresponds to the PS.and No. 2 to the SS wave.

NFFT: Algorithm for irregular sampling

A. Gulati, Robert J. Ferguson

SUMMARY

The nonuniform discrete Fourier transform (NDFT) used in many processing schemes can be computed using a fast algorithm known as the non uniform fast Fourier transform (NFFT). The NFFT is not a new algorithm, but it is an approximation scheme that can be use to calculate an approximate spectrum. In one dimension, computational complexity of the NFFT is O(NlogN) which is a dramatic improvement from the $O(N^2)$ complexity of the NDFT. The approximate spectrum is calculated using simple algorithm scheme which involves convolution of an irregularly sampled signal with a truncated Gaussian in the spatial domain. A new empirical expression based on numerical experiment for the analytical Gaussian width is proposed. Synthetic data examples, some with analytical solutions, demonstrate the utility and validity of this approach. The approximate spectrum obtained can be use further in a reconstruction algorithm.

Figure 1a shows the uniformly sampled Ricker wavelet. Figure 1b and 1c show the analytically derived spectrum and the spectrum obtained using the NFFT algorithm. Figures 1b and 1c are validating the algorithm for a uniformly sampled wavelet. Figure 1d displays a non uniformly sampled Ricker wavelet, with its analytically derived spectrum in Figure 1e. Figure 1f shows the failure of the Fast Fourier Transform algorithm (FFT) for non uniformly sampling. Figure 1g shows the spectrum obtained for non uniformly sampled Ricker wavelet using NFFT. Figure 1h shows the comparison between the NFFT and analytical derived spectrum. The NFFT algorithm gives the correct spectrum. There is loss of amplitude due to missing Fourier coefficients, which can be corrected if desired using general processing schemes.

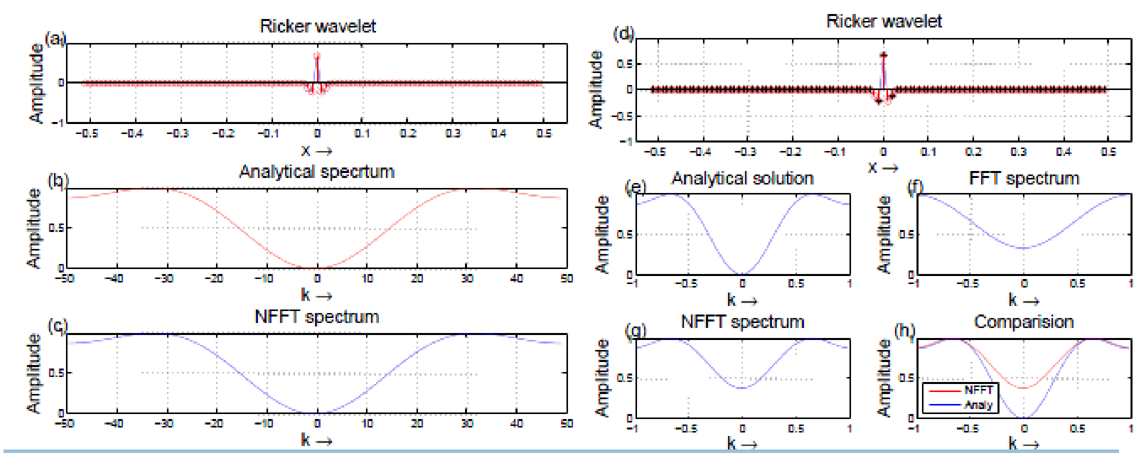

FIG. 1. a) Uniformly sampled ricker wavelet. b)Analytical spectrum. c)NFFT spectrum. d)Nonuniformlysampled ricker wavelet. e)Analytical spectrum. f)FFT spectrum. g)NFFT spectrum. h)Comparison of NFFT and analytical spectrum.

Q-estimation from uncorrelated Vibroseis VSP model data

Arnim B. Haase*

SUMMARY

A known method for velocity dispersion estimation and Q-factor calculation from uncorrelated Vibroseis records is investigated. In this method pilot sweeps are partitioned into time segments by successive windowing, each with a different central frequency. These segments are cross-correlated with the entire received sweep at all VSP-stations allowing the automatic picking of frequency and depth dependent travel times and the calculation of velocity dispersion. The method is tested with two synthetic zero-offset VSPs. Q-factors can be recovered fairly accurately away from the near-field in the special case of a homogeneous earth. Velocity dispersion and the Q-factor derived from it are quite sensitive to stratigraphic effects.

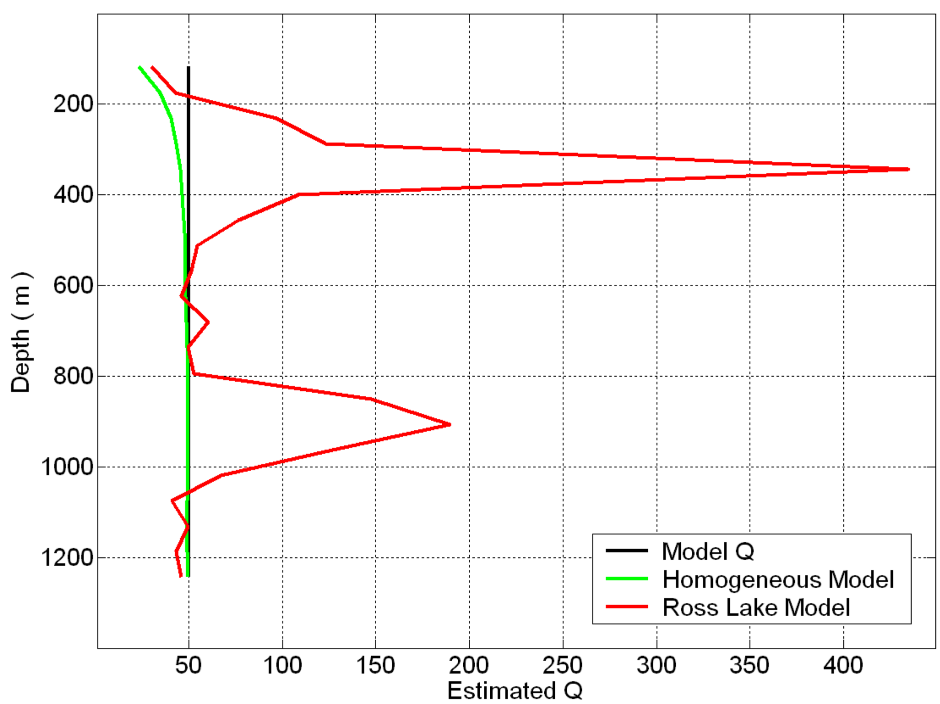

FIG. 1. Contrasting velocity dispersion method Q-estimates of, firstly, a homogeneous model with an intrinsic Q-factor of 50 and, secondly, a well-log derived model (Ross Lake) also with an intrinsic Q-factor of 50.

Residual converted wave statics

Arnim B. Haase and David C. Henley

SUMMARY

First estimates of S-wave receiver static shifts are applied to selected common receiver gathers of the Spring Coulee three component survey. Pre-processing of the input common receiver gathers includes NMO-correction, deconvolution, P-wave shot statics application, AGC and a band-pass filter. Residual S-wave receiver static shifts are computed from shot records obtained by resorting the chosen subset of receiver gathers. Prior to this computation of residuals the shot records are preconditioned by estimating and removing *DC-bias* as well as *residual normal move-out*. When stacking *residual-receiver-static* corrected shot records, little difference is found on comparing to shot stacks without residual application. Further analysis by velocity-sweep trial-stacks and residual normal move-out removal reveals *non-hyperbolic move-out* as a possible cause for the observed stacking response.

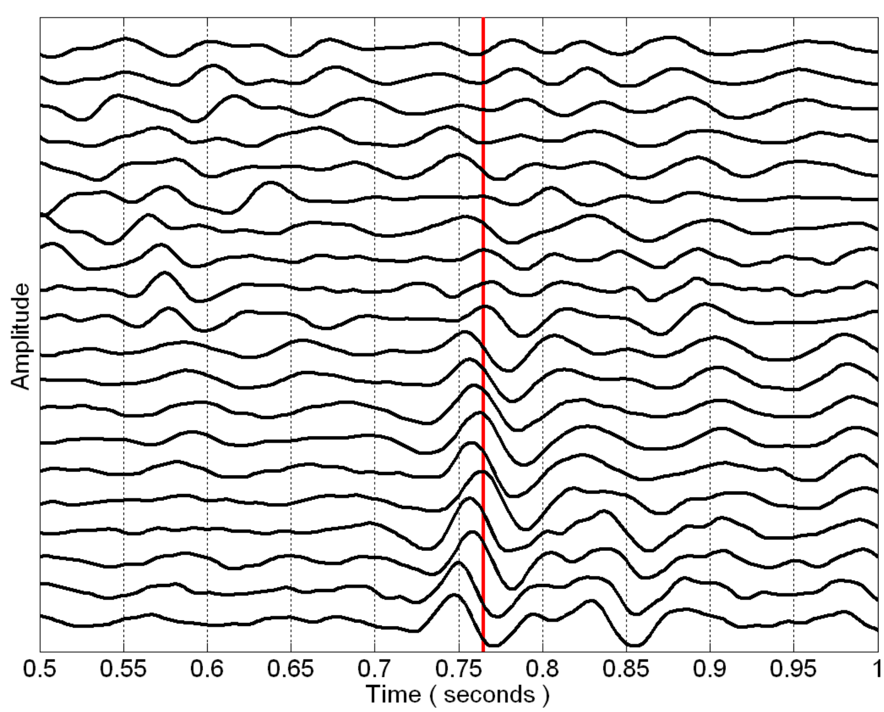

FIG. 1. Shot Record with initial and residual receiver static corrections applied. Hyperbolic residual NMO is also removed. The remaining move-out is non-hyperbolic.

Sommerfeld integral based spherical wave field computation applied to multi-interface VSP models for stratigraphic **Q investigations**

Arnim B. Haase

SUMMARY

A method developed from the Ewing algorithm for *point sources in layered media* is employed to compute the complete spherical wave field for synthetic zero-offset VSPs. For the elastic case of six embedded Class 1 reservoir layers, the transmitted wave spectrum below the stack of layers shows a clear trend of amplitude decay with frequency which the *spectral ratio method* of Q-estimation interprets as a finite Q-factor; because of the purely elastic model this represents *stratigraphic attenuation*.

For a more realistic multi-layer situation Ross Lake well-logs are introduced. The depth dependent Q-factor estimated from a synthetic Ross Lake VSP modelled with a constant intrinsic Q of 100 resembles Q(z) estimated from actual Ross Lake VSP-data. This observation suggests a dominant role of *stratigraphic attenuation* in the Ross Lake area. When implementing a first-order estimation-error reduction by *spectral normalization*, model Q recovery is improved but still unsatisfactory.

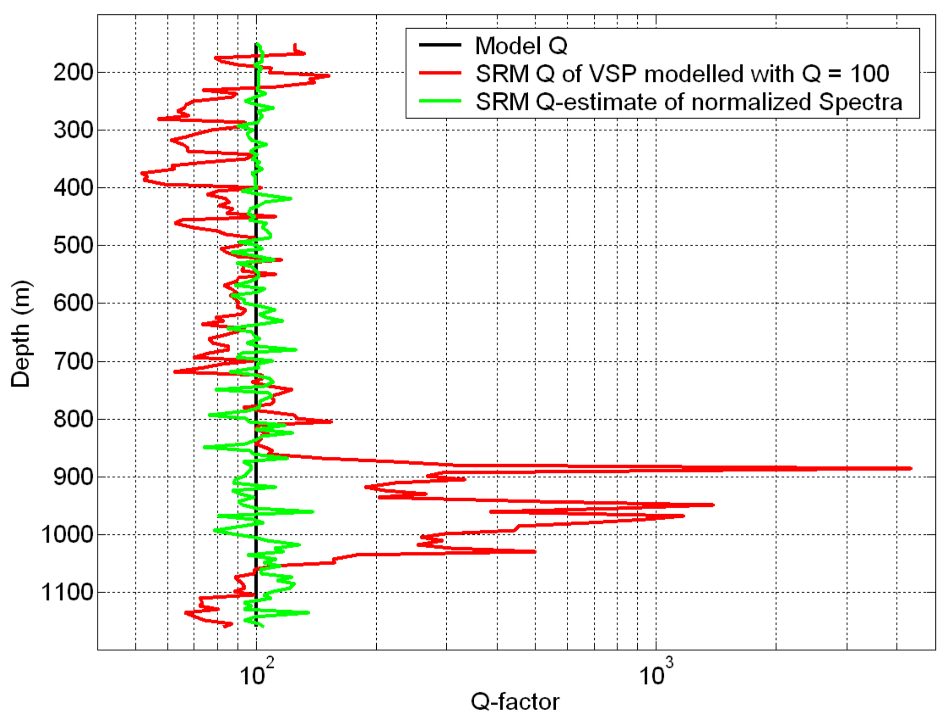

FIG. 1. Contrasting spectral ratio method Q-estimation of synthetic VSP model data with and without spectral normalization.

Comparison of low-frequency data from co-located receivers using frequency dependent least-squares-subtraction scalars

Kevin W. Hall*, Gary F. Margrave, Malcolm B. Bertram

SUMMARY

Eight-trace shot gathers were created from a subset of the data collected during the Priddis low-frequency comparison test (described by Bertam et al., this volume). For this comparison, we are only considering the 2-10 Hz EnviroVibe shots. The geophone data were decimated to a ten meter spacing to match the other datasets. The southernmost receiver station was dropped from the geophone and accelerometer data, as there was no seismometer to compare to for this station. Sixty seconds of seismometer data were extracted from the continuous data stream based on time of shot, debiased to remove the resulting (sometimes large) zero Hz component, and resampled from 10 ms to 2 ms to match the other data. The resulting datasets were aligned based on cross-correlations, and then compared by filtering the traces with a 1 Hz wide sliding bandpass filter (0.1 Hz increment from 2-10 Hz), and calculating a least-squares-subtraction scalar for each bandpass filter step. Figure 1 shows the results for the vertical component, sorted by receiver station. In general, the Sercel 428XL data is closest in overall amplitude to the raw Nanometrics/Trillium seismometer data but shows perhaps more variation over the frequency band. The Ion geophone and accelerometer data are 10^8 times smaller than the seismometer data and show less detail in the figure below, probably due to the mismatch in scale. The Sercel data show that the scalars likely depend on the quality of receiver placement in the ground, and may be offset dependent. All three exploration receivers compare quite well to the seismometers suggesting that frequencies as low as 2 Hz might be recoverable from any of them.

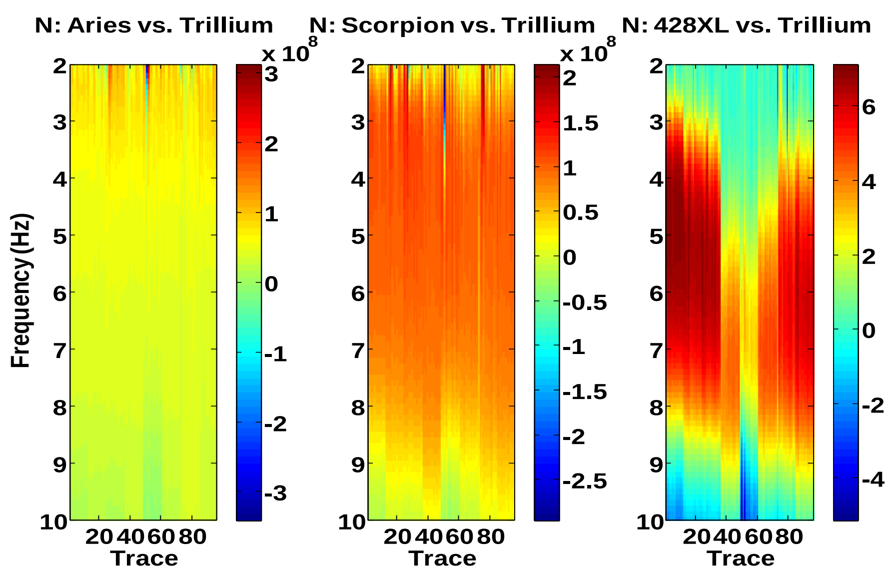

FIG. 1. Receiver gathers of frequency dependent least-squares scalars for all 2-10 Hz sweeps at the north vibe point. Left; Ion/Aries geophone compared to Nanometrics/Trillium Seismometer (NTS). Middle; Ion/Scorpion/VectorSeis compared to NTS. Right; Sercel/428XL/DSU3 compared to NTS. North is to the left.

Waveform tomography for areas of complex near surface

Hussain I. Hammad* and Gary Margrave

SUMMARY

We test the capability of waveform tomography in resolving a model in an area of very challenging near surface geology. The complex near surface of the model makes it difficult to image a low relief structure at depth. The goal of the inversion is to recover the near surface compressional velocity and to detect some indication of the of the low relief structure. We inverted the data using the multi scale technique and the efficient strategy of Sirgue and Pratt (2004). The resulting models contain substantially higher resolution than the initial models. We also compare statics provided by the estimated models. The statics of the estimated models agree with the statics of the true model to within +/- 15ms in most regions in the model. This statics correction is sufficient for a subsequent residual statics solution to be effective.

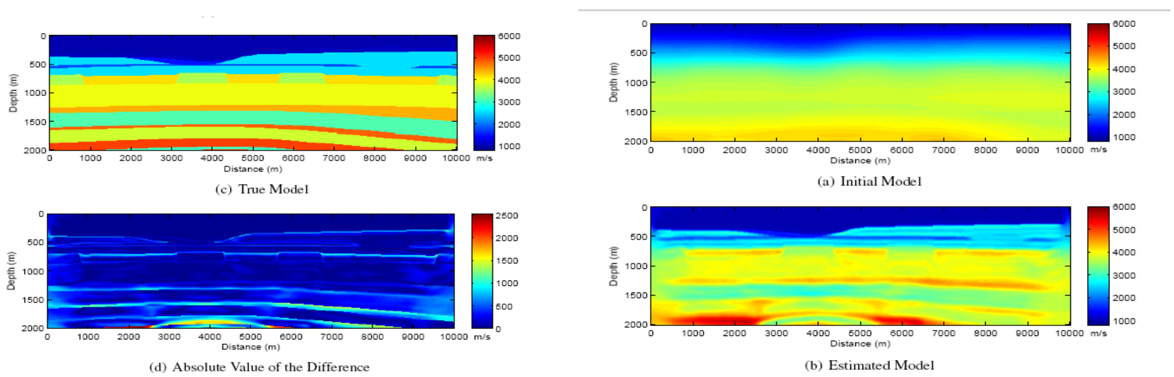

Fig. 1. Models for the sequential experiment.

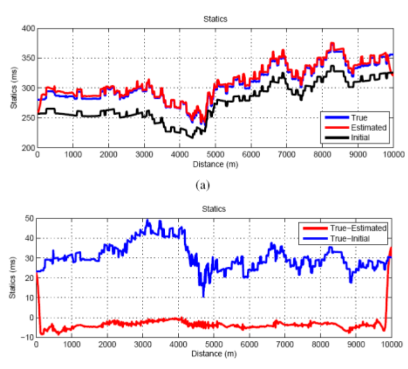

Fig. 2. Statics for the sequential experiment. a) shows all the statics b) shows the differences.

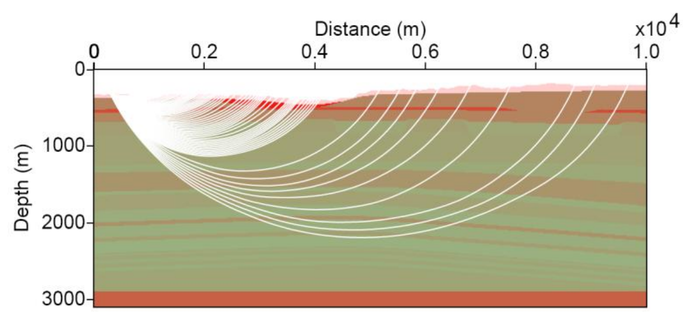

Fig. 3. Diving rays traced in a smoothed version of the true model. Diving rays indicate the maximum depth that can be reliably imaged for the given offset.

Hypocenter location using hodogram analysis of noisy 3C microseismograms

Lejia Han, Joe Wong, and John C. Bancroft

SUMMARY

Hodogram analysis and back-azimuth projection is one method used for mapping microseismic hypocenter locations in a homogeneous isotropic velocity field. The method works well when the input microseismograms have high signal-to noise ratios. However, when there are high levels of random noise on the raw seismograms, the mapping accuracy decreases significantly. To suppress noise and increase signal-to-noise ratios (SNRs) before hodogram/back-azimuth analysis, we applied frequency domain filtering, time domain windowing, trace averaging, and signal-noise separation (NSS). After noise suppression, the back-azimuth method coupled with statistical averaging of raypath intersections produces reasonably accurate hypocenter locations.

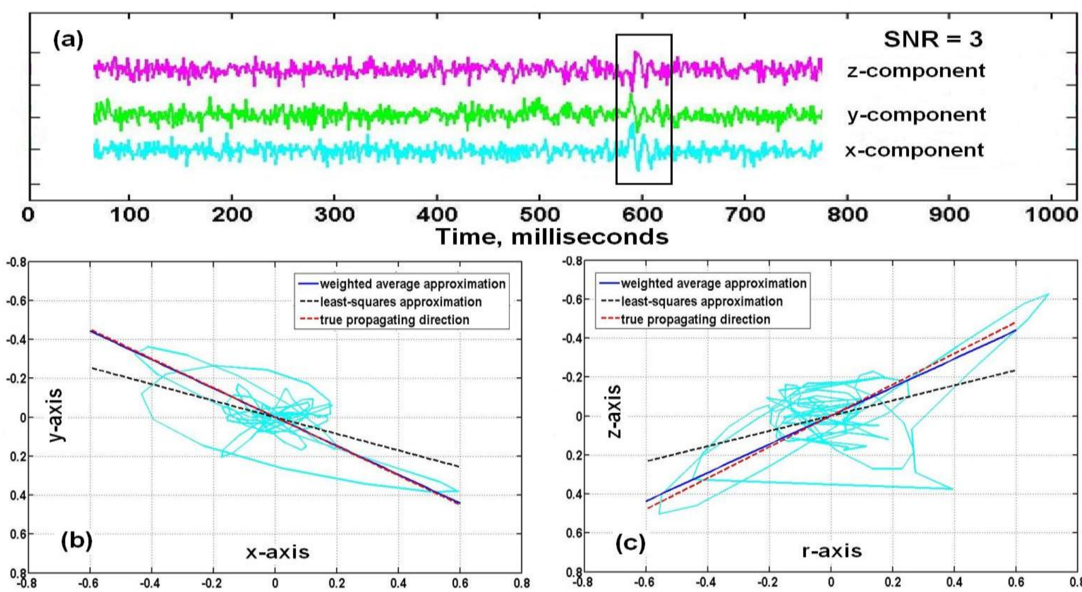

FIG. 1: (a) Synthetic noisy 3C seismograms for one geophone; (b) hodogram on map view; (c) hodogram on section view. Hodograms are time-parametric plots using seismogram points within the rectangle. Dotted red lines show true propagation directions. Dotted black lines show directions based on straight line least-squares fitting of points on hodograms. Solid lines show directions based on weighted average of vectors defined by points on hodograms

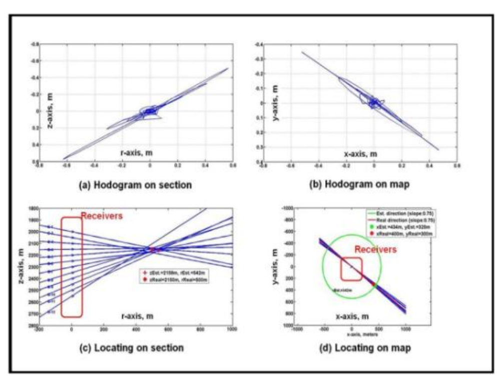

FIG. 2: Hypocenter location using back-azimuth method for 3C seismograms with SNR=10; (a) section view hodogram; (b) map view hodogram; (c) section view of raypaths back-projecting from geophones; (d) map view of raypaths back-projecting from geophones. The average of raypath intersections on (c) gives the depth and radial distance of the microseismic source. The intersection of the green circle on (d) with lines in the azimuth directions gives the map view source coordinates. The located (xs, ys, zs) coordinates are (434m, 325m, 2159m); The true coordinates are (400m, 300m, 2150m).

Time picking and random noise reduction on microseismic data

Lejia Han, Joe Wong, and John C. Bancroft

SUMMARY

Methods based on the STA/LTA ratio and the modified energy ratio (MER) were studied for their efficacy in automatic first-arrival time picking on high-noise microseismograms. Testing of the two methods on both field and synthetic data indicated that they can pick arrival times under signal-to-noise (SNR) levels as low as 1.7, but that MER time picking yields more consistent results. Moreover, MER time picking is significantly faster than STA/LTA time picking.

For many seismic processing procedures, reducing the random noise on the input seismograms will lead to improved results. Noise can be reduced by stacking over a group of traces aligned in phase to produce an average trace $s_{av}(t)$. We found suitable time shifts for trace alignment using (1) a minimum variance principle, and (2) using time picks from MER picking. A noise-signal separation (NSS) technique employing the noise-reduced average trace $s_{av}(t)$ as a reference separates the noisy seismograms into clean signal components and random noise components while largely preserving the relative signal amplitudes on the input seismograms.

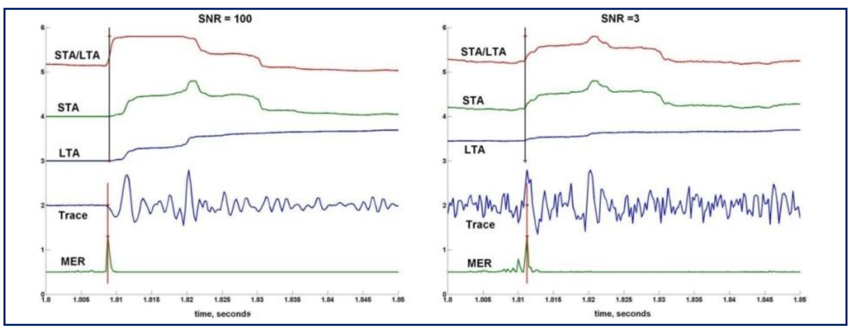

FIG. 4: STA/LTA and MER time-picking on clean and noisy traces. For the clean trace, both methods give an arrival time at the first break. For the noisy trace, the STA/LTA and MER picks occur somewhat later.

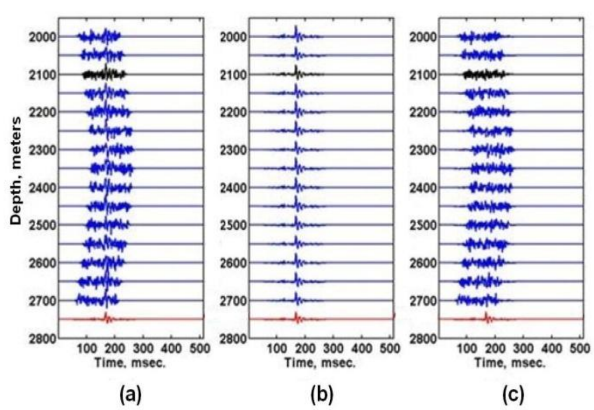

Fig.14: Noise-signal separation for SNR≈1.5. (a) Original seismograms; (b) noise-free components $s_b(t)$, and (c) Gaussian noise components $n_i(t)$. There appears to be little or no coherence between the average trace and the noise components, i.e., the dot product $n_i(t)\cdot s_{av}(t)$ is much less than the dot product $s_b(t)\cdot s_{av}(t)$.

Hunting reflections in Papua New Guinea: early processing results

David C. Henley and Han-Xing Lu

SUMMARY

Papua New Guinea is among the most notoriously difficult areas in the world for acquiring usable seismic reflection data. The rugged, forested terrain makes it very difficult to deploy both sources and sensors; and the complex near-surface layers contribute to serious coherent noise and statics on the resulting recorded seismic traces. Furthermore, the underlying geological structure is known to be complex, as well, adding to the difficulty of obtaining interpretable images. We show here some preliminary processing applied to very challenging data from a 2D-3C seismic line acquired in Papua New Guinea, which helps to image reflections.

EARLY RESULTS

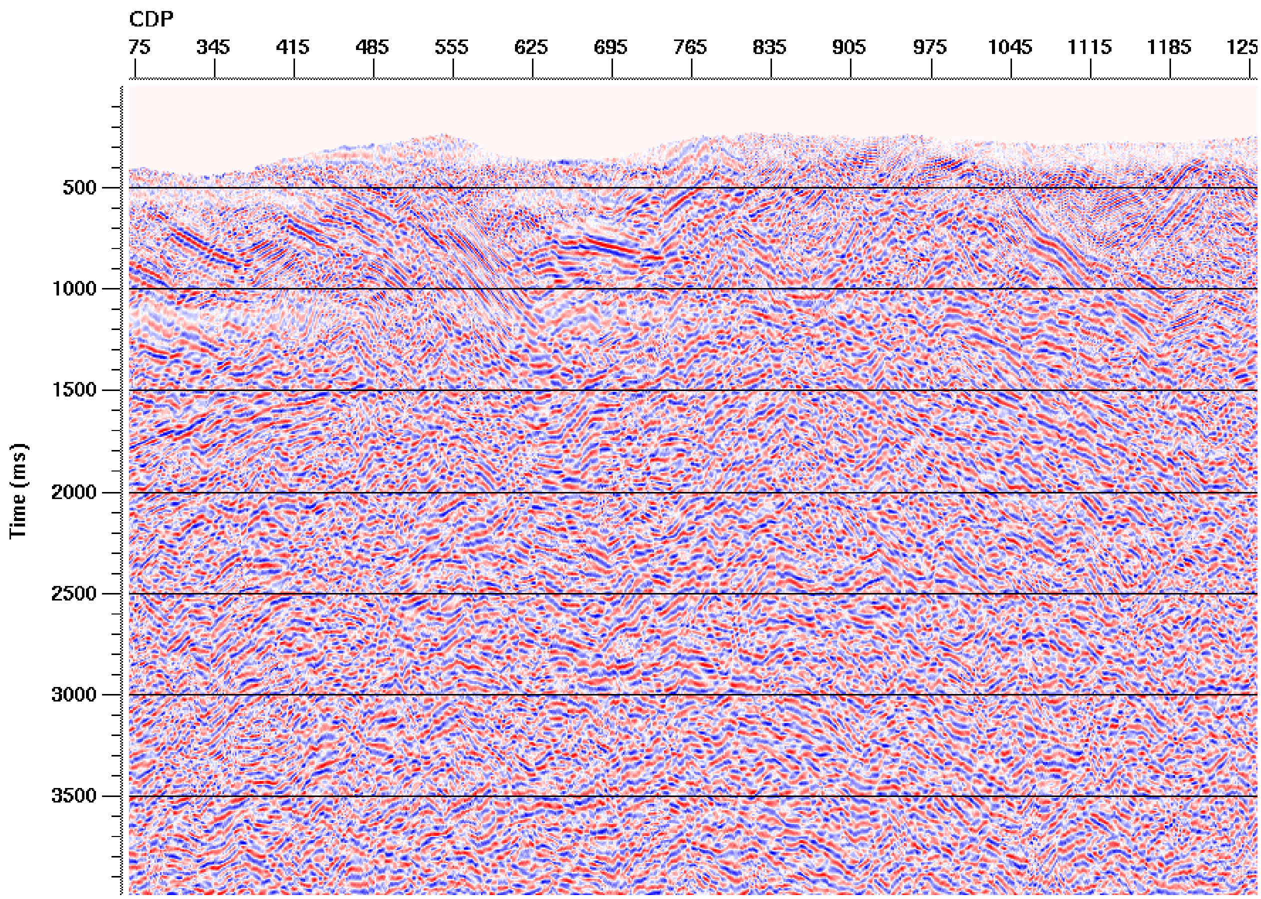

A portion of PNG line after brute processing, no noise filtering or decon

This figure shows a small portion of the PNG line vertical component, after preliminary processing to remove bad traces, and to correct for elevation and apply refraction statics.

Hybrid interferometry: surface corrections for converted waves

David C. Henley* and P. F. Daley

SUMMARY

Because interferometry can handle very large 'statics', as we have recently demonstrated with arctic data, we have attempted to apply similar techniques to converted wave data, but with limited success. We demonstrate here a more recent attempt to remove surface effects from converted wave data, using a 'hybrid' approach, in which we correlated traces from two different vector components at the same receiver positions in order to detect and remove the receiver 'static differences' by means of the technique which we term "raypath interferometry. The results show greatly improved coherence; but have yet to properly incorporate the 'structural' term. Although we expected the appearance of spurious events on the processed PS section, these may be a less serious problem than anticipated, with the appropriate choice of processing tactics during the interferometry. An accompanying model study appears to confirm this.

RESULTS

The Spring Coulee 2D-3C survey has been the subject of much study because of its good data quality. Since it exhibits large receiver statics on the radial component data, it is an ideal choice to demonstrate our technique. The results shown are considered 'promising' but are by no means final. The 'structural' part of the statics correction, since it was imported from a P-wave reflection event, is probably too 'mild' and needs to be adjusted by the Vp/Vs ratio.

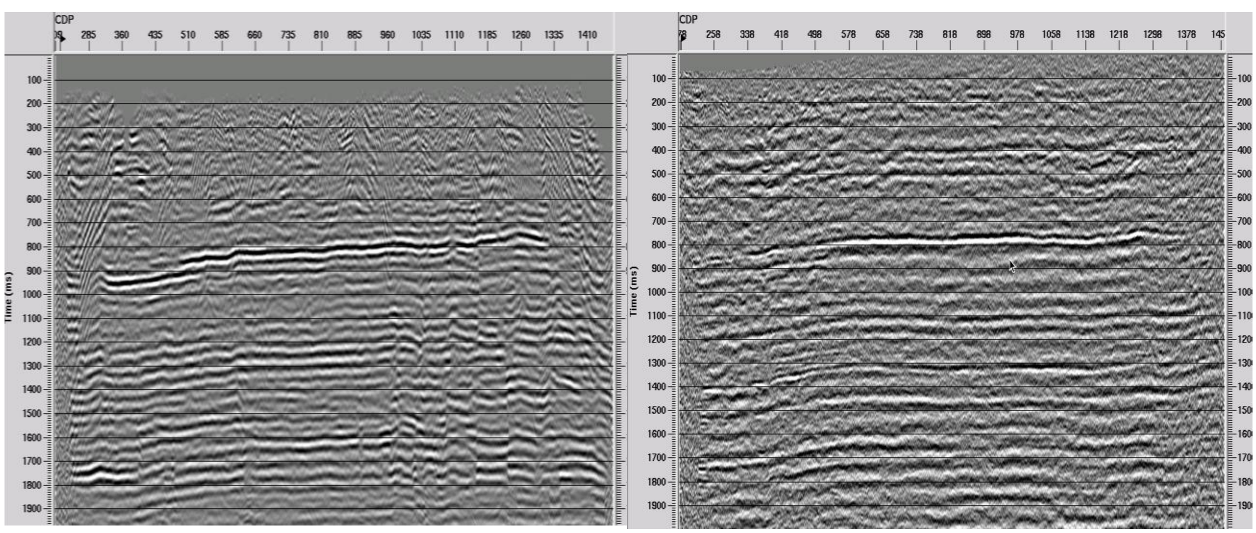

The best current result for hybrid raypath interferometry on Spring Coulee converted wave data. The CCP stack on the left is an earlier result obtained by hand picking statics, and the CCP stack on the right is our best interferometric result. The 'structure' of the events is probably not yet correct, but coherence and event resolution are greatly improved.

Intelligent design: the diagnostic mode of Gabor deconvolution

David C. Henley

SUMMARY

The diagnostic power of various displays of the Gabor transform has long been recognized, and such displays can be very intuitively instructive. Accordingly, we have extended the latest version of our surface-consistent, iterative Gabor deconvolution module, Gabor_sc, to include an alternative, diagnostic mode. In this mode, the program yields Gabor spectra, output as seismic traces, which can be displayed using Trace Display in ProMAX, or any other suitable seismic trace display operation. We demonstrate this new diagnostic mode here and show four examples where it has already proved its usefulness: studying parameter sensitivity; deconvolution operator design; deconvolution algorithm fine-tuning; and vibroseis sweep design.

AN EXAMPLE

Most of us have no idea what effect the number of coefficients used to estimate the Burg spectrum has on the details of the spectrum. The display below illustrates that the details of the spectrum are remarkably insensitive to the number of coefficients.

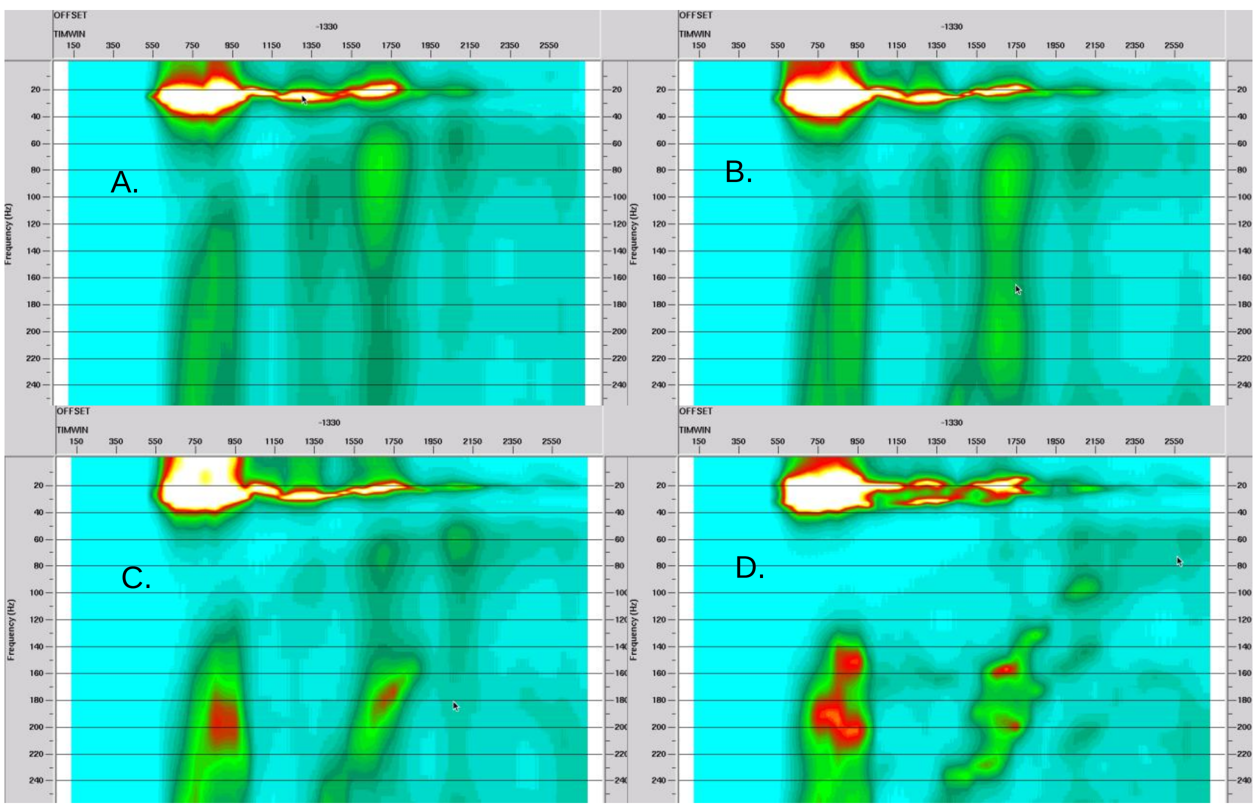

Burg wavelet spectrum estimate—A. 3 coefficients; B. 5 coefficients; C. 10 coefficients; D. 20 coefficients—no smoothing on any of these estimates

Gabor spectra displaying the details of burg spectral estimates of the wavelet spectrum for a seismic trace for different choices of burg coefficients.

Priddis pulse/probe experiment: still ambiguous

David C. Henley

SUMMARY

It has been conjectured that exciting the earth with a strong, stationary acoustic field will change the relative impedance of rock layer interfaces due to the induced motion of the pore fluids relative to the rock matrix, and that these changes in impedance should be detectable as changes in seismic reflectivity. A small seismic survey experiment to test this theory was conducted in 2008 at our Priddis test site; but the resulting analysis of the data yielded ambiguous results. The present report describes further analysis of those data. Specifically, we compared comparably processed CDP stacks of the survey data set acquired with dynamite only and the data set acquired with dynamite in the presence of a constant-frequency acoustic field excited in the earth. Comparisons were done using both straight subtraction and least-squares subtraction. We conclude from our analysis of those data that the results are still ambiguous, and the conjecture unconfirmed.

THE EVIDENCE

The figure below shows one of the comparisons between the CDP stack of the Priddis survey performed with dynamite only, and the CDP stack of the same survey performed in the presence of a 20 Hz monotonic acoustic field excited in the earth by our mini-vibrator.

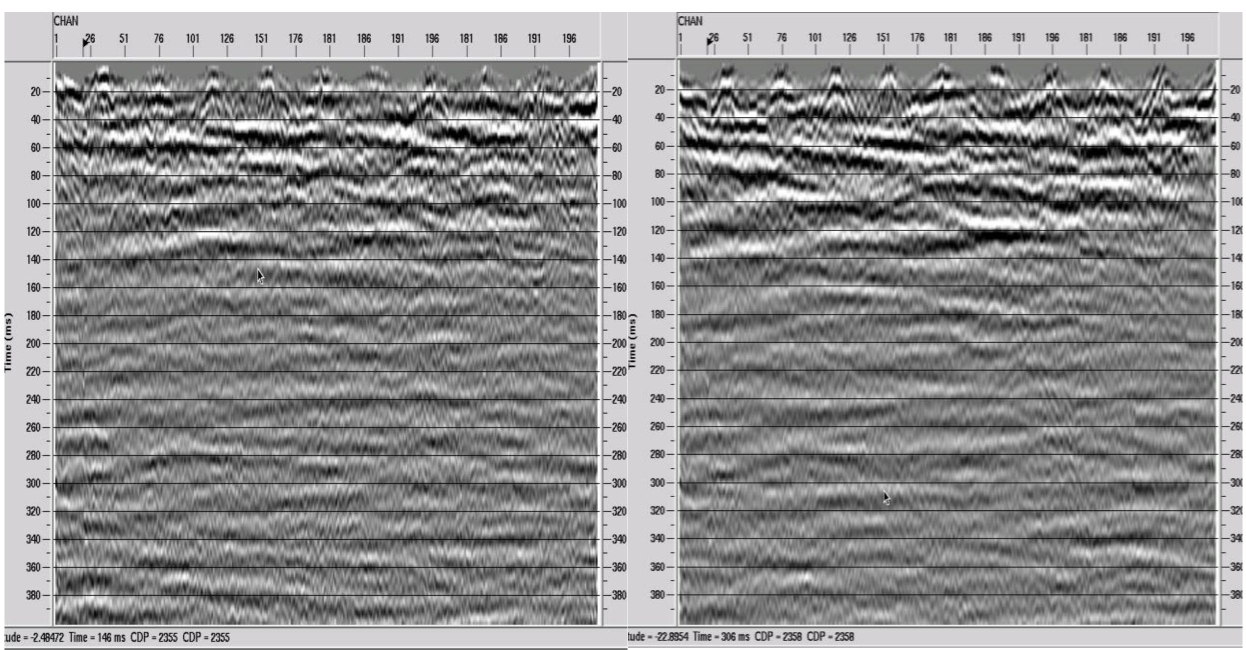

Dynamite plus 20 Hz minus dynamite. Arithmetic subtraction (left) vs least-squares subtraction (right)

Comparison between "dynamite only" survey and "dynamite plus 20 Hz", done with straight subtraction (left) and least-squares subtraction (right)

Radial filtering on steroids: the latest algorithm

David C. Henley

SUMMARY

Coherent noise attenuation is an ever-evolving technology, and radial trace domain filtering algorithms continue to change and advance, as well. Our previous version of the ProMAX radial filtering module provides several ways in which to attenuate coherent noise, including the recommended one of estimating coherent noise with a low-pass filter in the radial trace domain, then subtracting the noise estimate from the original trace gather in the X-T domain. We now have a new option in which the X-T noise subtraction is done by a least-squares subtraction algorithm. We demonstrate here that the new method provides significantly better noise attenuation, both with single filter applications and with sets of cascaded filters.

AN EXAMPLE

Since radial filtering is used extensively in coherent noise attenuation on our high resolution experimental surveys, its effect is most evident after several passes of filtering. Our recent Priddis 2D 3C survey is a case in point.

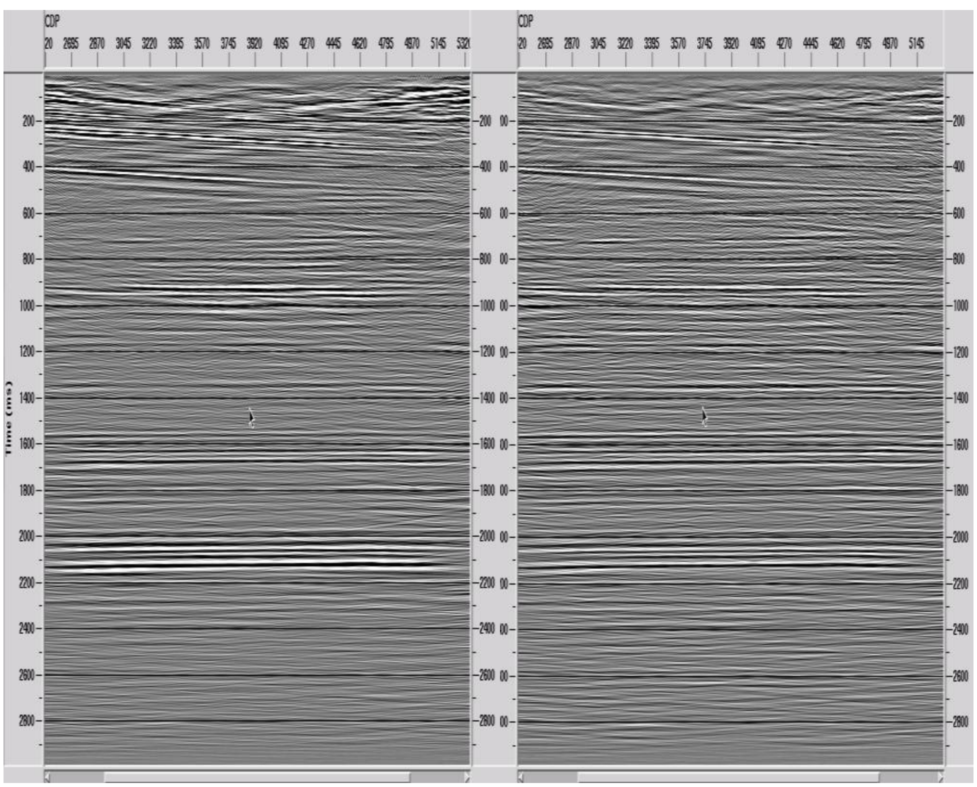

Old radial filters New lsq radial filters

Priddis 2009 2D-3C experiment—new radial filter algorithm leads to broader bandwidth, better resolved reflections (right), since residual noise is more effectively removed.

Shaken, not stirred: Priddis 2009 3C-2D hi-res acquisition

David C. Henley, Kevin W. Hall, Malcolm B. Bertram, Eric V. Gallant, Han-Xing Lu, and Rolf Maier

SUMMARY

Over the last several years, CREWES has designed and conducted several field experiments intended to explore the limits of seismic resolution, coherent noise attenuation, and the practical and logistical limits of field acquisition pertaining to source effort and sensor density. We describe here the latest experiment in the sequence, carried out in March 2009 at our Priddis field site. The goals of this experiment were two-fold: we wanted a 3C-2D profile through the proposed site of our future permanent 4D test site; and we wanted yet another test of high-resolution seismic acquisition, this time increasing receiver spacing to obtain longer offsets, but decreasing source spacing to retain spatial resolution. We display here some of the results of that field work, which show that, in conditions of good source and receiver coupling, we can, indeed, increase receiver spacing and compensate by decreasing source spacing. This gives us the same processing power over surface wave noise, and the increased source effort results in remarkably good depth penetration, showing reflections down deeper than 2.5 seconds.

CONVENTIONAL VS HI-RES PROCESSING

On a high-fold high resolution survey such as Priddis 2009, conventional processing leads to good seismic images, but pre-stack processing leads to even better images.

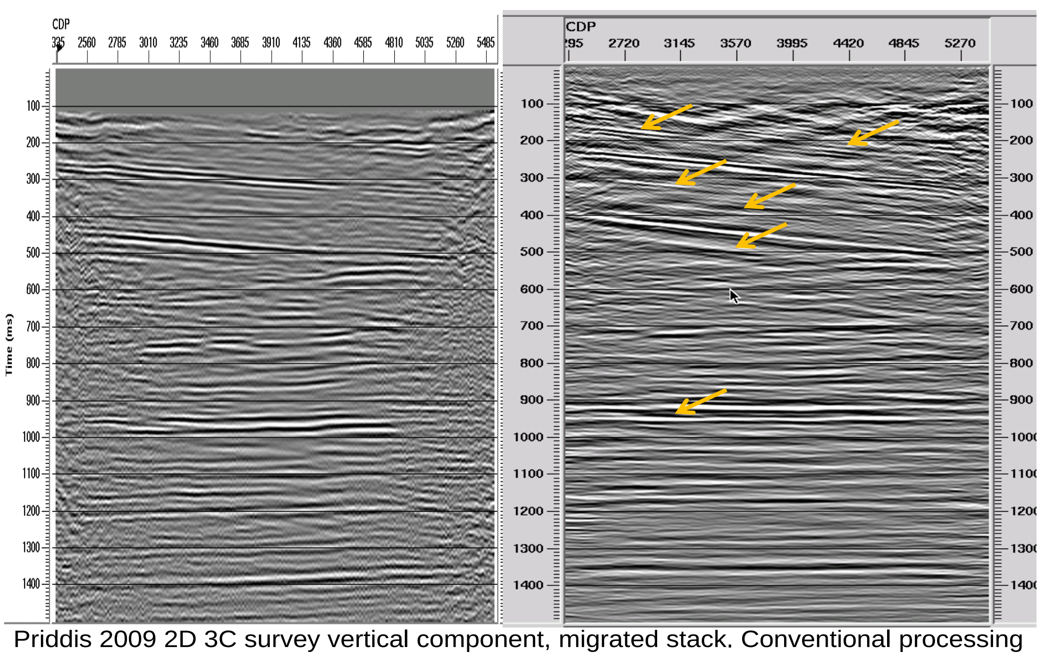

Priddis 2009 2D 3C survey vertical component, migrated stack. Conventional processing (left), vs. high resolution processing, including prestack filtering (right). Arrows mark parts of the section where particular improvement in resolution may be seen.

Smoke and Mirrors: demonstrating interferometry on synthetic converted wave data

David C. Henley

SUMMARY

Over the last several years, we have developed and demonstrated techniques for removing the near-surface effects (statics) from seismic traces, using interferometric methods, and have shown how to generalize constraints like surface-consistency and stationarity. We have shown significant results using field data from the Canadian arctic. More recently, we have adapted these methods to converted wave data, where the receiver corrections are difficult to determine using conventional methods. Here, we test interferometric methods on synthetic seismic models designed to study particular issues encountered in converted wave interferometry. We introduce various procedures for improving our results, and show them in practice on the model data. Our insight for processing real data has been significantly increased by the study.

RAYPATH INTERFEROMETRY DEMONSTRATED

Figure 1 below compares a PS common-angle gather after raypath interferometry with the same gather before interferometry, while Figure 2 shows the CDP stack of the data after interferometry compared to a shot gather with no statics (for event identification).

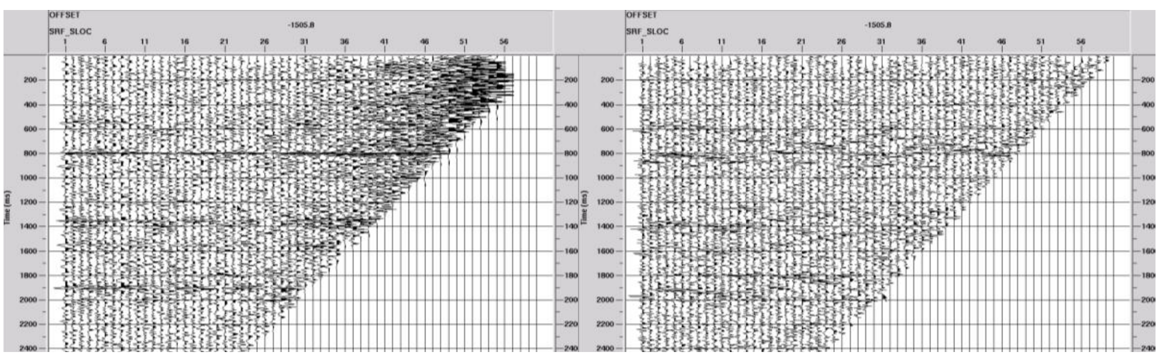

FIG. 1. PS common angle gather corrected by raypath interferometry (left) vs. original gather (right)

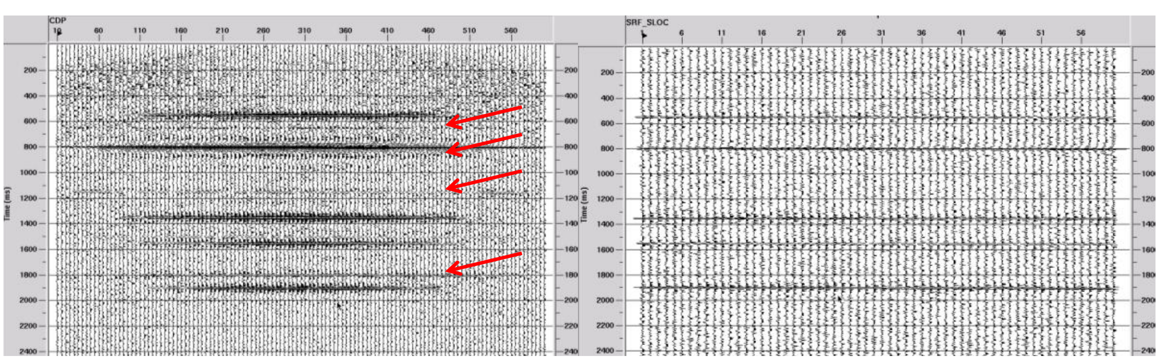

FIG. 2. CDP stack of PS data after raypath interferometry (left) vs. shot gather with no statics. Red arrows indicate spurious events generated by correlation of unrelated PP and PS events.

Timath and frmath: experimental trace ensemble modules for ProMAX

David C. Henley

SUMMARY

Much of the experimental software developed by CREWES is implemented within the MATLAB environment because of the sophistication of the MATLAB mathematical structure and the large library of functions and algorithms available. For testing programs in a production seismic environment, however, using many data sets of varying sizes and characteristics, it is often preferable to use an established standard seismic processing package such as ProMAX to apply a new algorithm. While several mature CREWES algorithms have been embodied in their own ProMAX modules, it is time-consuming and often tedious to write a complete new module to test each new idea, particularly if the idea is relatively simple, or the concept being tested is speculative. Hence, we have created two new ProMAX modules intended to apply computations of virtually any kind to the data samples in a 2D array (trace ensemble). We introduce these modules here and demonstrate their currently available functions. Our expectation is that they will find value as research tools as we continually add new test functions to their menus.

A TIMATH APPLICATION

The least-squares subtraction function implemented in Timath is demonstrated below, where it is used to help compare two nearly identical shot gathers, one using dynamite only, the other using dynamite as well as a continuous 20 Hz vibroseis signal, to test the concept that a strong stationary acoustic field can dynamically alter near-surface reflectivities.

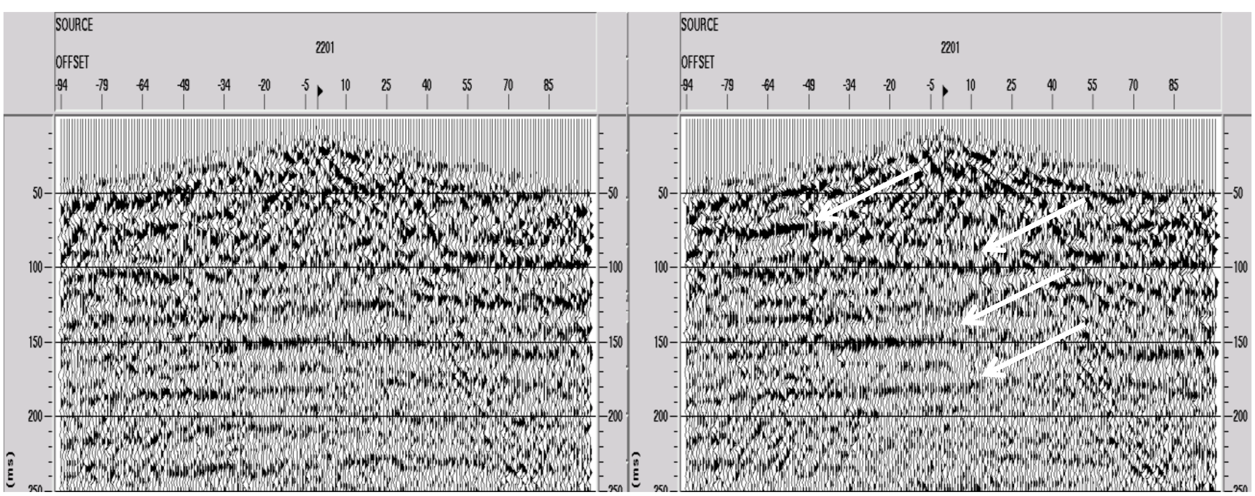

Priddis 2008 pulse/probe experiment: arithmetic subtraction (left) compared with least-squares subtraction (right) for the difference between a “dynamite only” shot and a “dynamite plus 20 Hz” shot at the same position. Arrows mark possible reflections that are stronger on the least-squares results.

An interactive velocity modelling tool in MATLAB

Chad M. Hogan, Gary F. Margrave

SUMMARY

An integral part of seismic data processing is the velocity analysis stage. Here we introduce an interactive GUI tool running natively in MATLAB that allows velocity analysis on shot gathers (real or synthetic data). This tool is now a part of the CREWES MATLAB toolbox.

Analysis of shot gathers is possible with both constant-velocity panels and with semblance, as shown in Figure 1. Currently, the tool uses the NMO/Dix equation approach to modelling. We hope to extend this tool in the future to allow for dip moveout, 3D velocity modelling and anisotropic models, migration velocity analysis, and more.

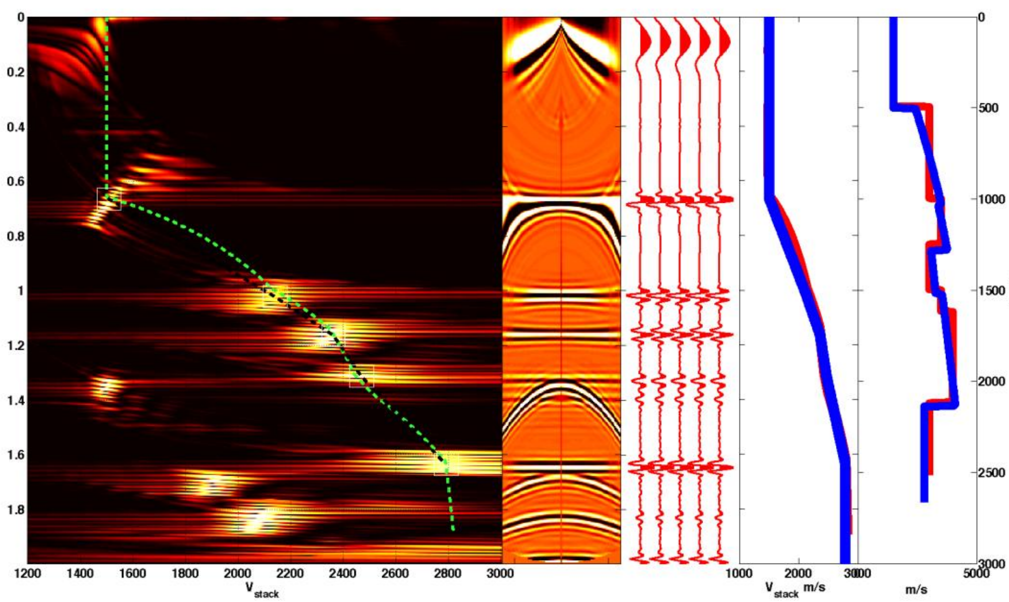

FIG. 1. Semblance plot in the velocity analysis tool. In the right-most plot, the red line shows well-log velocity, and the blue line shows the calculated velocity from the velocity analysis picks. In the second right-most plot, stacking velocity from the well-log is shown in red, with the estimated velocity from the velocity analysis picks in blue. The central wiggle plot shows a repeated stack of the gather with NMO correction applied. The center-left plot shows the shot gather with the NMO correction applied. The left-most plot shows semblance. The green dashed line shows stacking velocity as estimated from the well log. The black dashed line shows stacking velocity from the velocity picks, with velocity picks marked with a white square.

Deriving the eikonal approximation: a scattering diagram tutorial

Kris Innanen

SUMMARY

"Diagram analysis" is a way of parsing, classifying, and manipulating the non-linear terms of inverse scattering, ultimately aiding in the derivation of new seismic processing algorithms. Diagrams originate in forward as opposed to inverse scattering, and so an introduction to these topological organization devices is best accomplished by considering the forward problem. I will use them to help derive a familiar expression in wave theory. The eikonal approximation, a relative of the WKBJ approximation, can be arrived at in several ways, for instance by direct integration of the Lippmann-Schwinger equation. In this paper I will demonstrate that, by retaining only Born series terms that correspond to a certain class of scattering diagrams, the same approximation can be recovered.

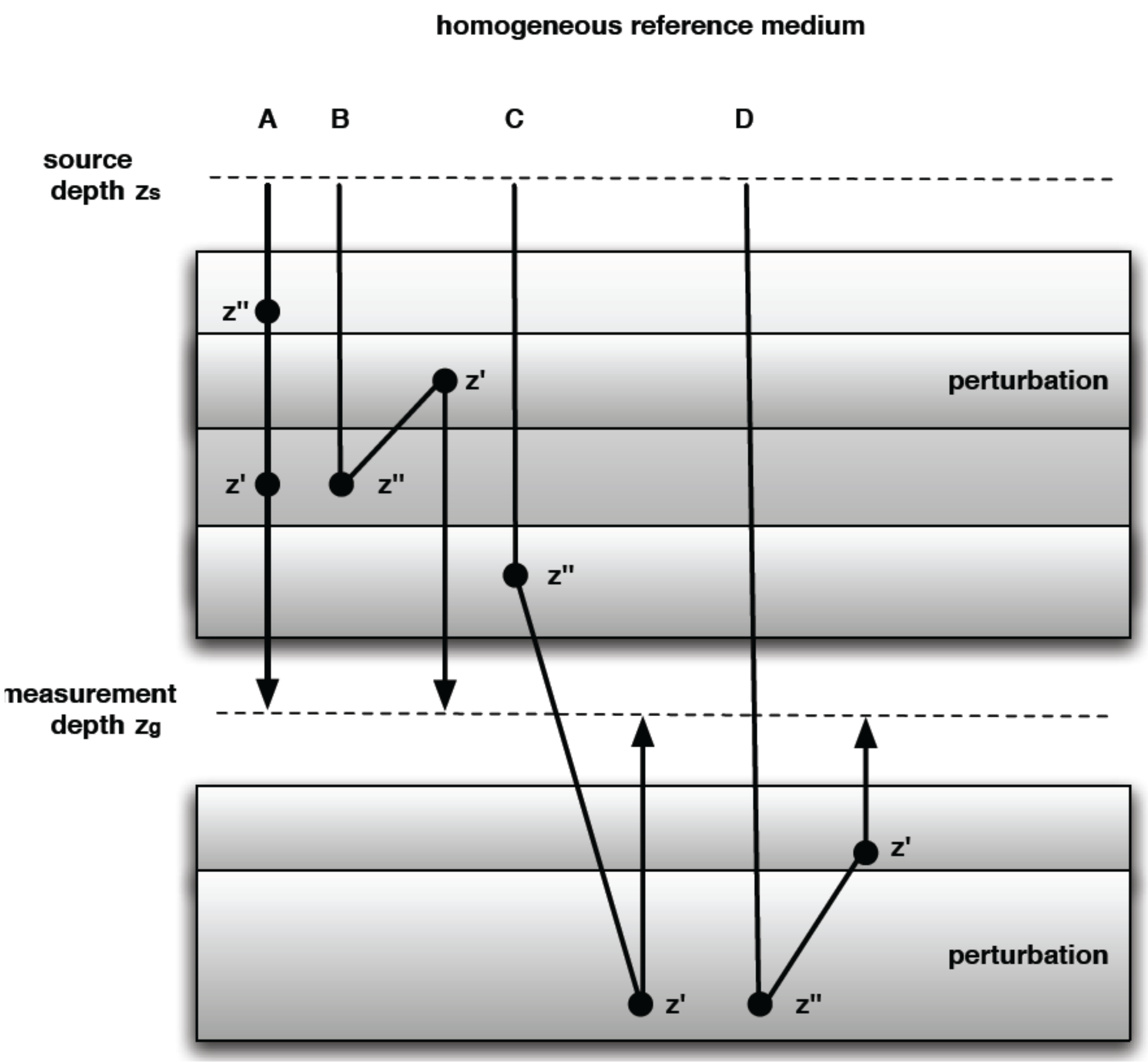

Inverting absorptive reflections: an inverse series tutorial

Kris Innanen*

SUMMARY

Non-linear inverse scattering, when it is applied to the big interesting seismic imaging and inversion problems, can be very complicated, and in a tutorial setting one risks losing all the basic concepts and insights in a morass of arithmetic. We can usefully proceed, however, by considering direct inversion within a highly simplified model: reflections from a single interface at a known depth, with known medium parameters above the interface and unknown medium parameters below. The seismic data reduce in this case to a single reflection coefficient, and the medium to be solved for reduces to a few scalar values. We consider the case of an absorptive target medium. A simple absorptive reflection coefficient may be expanded about small parameter contrasts and incidence angles, and used, angle by angle (AVA), or frequency by frequency (AVF), to directly determine simultaneous wavespeed and Q contrasts. Linear and non-linear inversion may occur algebraically or using an inverse series. The latter (in addition to being similar to inverse scattering) appears to be the better approach, with the former becoming less tractable for cases involving large angles and large contrasts.

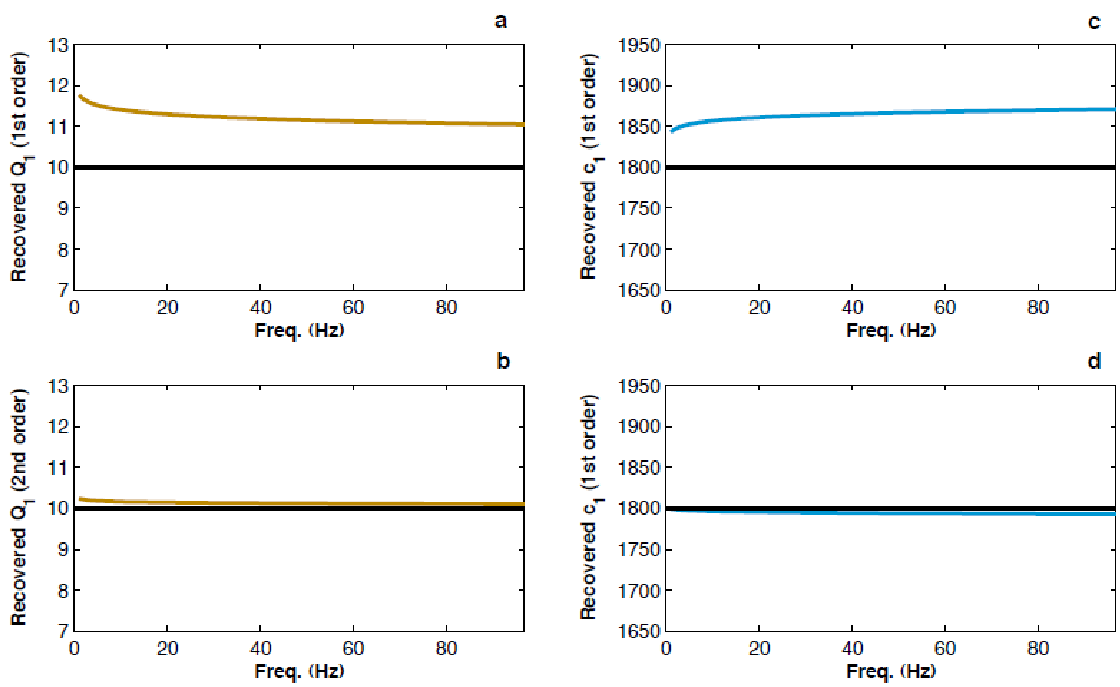

AVO analysis of carbonates

J. Helen Isaac and Don C. Lawton

SUMMARY

We analyzed amplitude variations with offset (AVO) in 2D seismic data from the Redwater area of Alberta to investigate whether it is possible to differentiate between limestone and dolomite carbonates of the Middle Leduc Formation. We used the P-wave sonic and density logs from two wells; one with dolomite in the Middle Leduc and the other with limestone. The dolomite has only a subtle signature on the gamma ray, sonic and density logs. Shear wave sonic logs had to be estimated from the P-wave logs. Supergathers were formed from cdp gathers of seismic data processed to retain amplitude information. Synthetic offset gathers were calculated using approximations to the Zoeppritz equations. The correlations between the synthetic offset gathers and the seismic data at the location of the wells is poor, even when using wavelets extracted from the seismic data. We are not able to pick a consistent event on the offset gathers for limestone well. Modification of the dolomite well logs to replace the dolomite with limestone show only a very small change in the theoretical offset responses. Better modelling could be done with a shear sonic log rather than having to estimate one using a constant Vp/Vs ratio. Better quality seismic data would help, too.

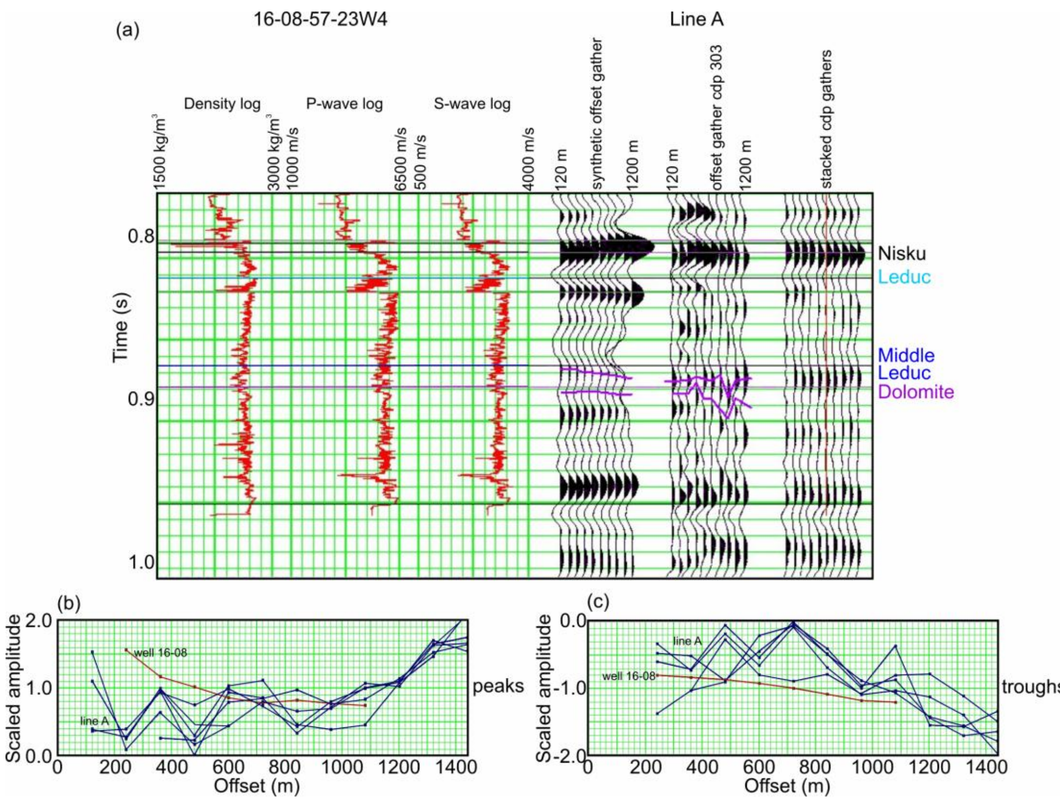

The density, P-wave and S-wave logs used in the creation of the synthetic offset gather for well 16-08-57-23W4, the seismic offset gather and part of the stacked seismic section centred on the location of the well at cdp 303 (a). The peak (b) and trough (c) picks close to the top of the dolomite, shown in purple in (a).

Combining absorbing and nonreflecting boundary conditions for elastic wave simulation

Zaiming Jiang, John C. Bancroft, and Laurence R. Lines

SUMMARY

The absorbing boundary conditions and the nonreflecting boundary condition are two of the most popular solutions to the computational boundary condition problem. We report our implementations of these boundary conditions within our staggered-grid finite-difference applications and describe their features. Then we present a method combining the absorbing boundary conditions and the nonreflecting boundary condition (Figure 1).

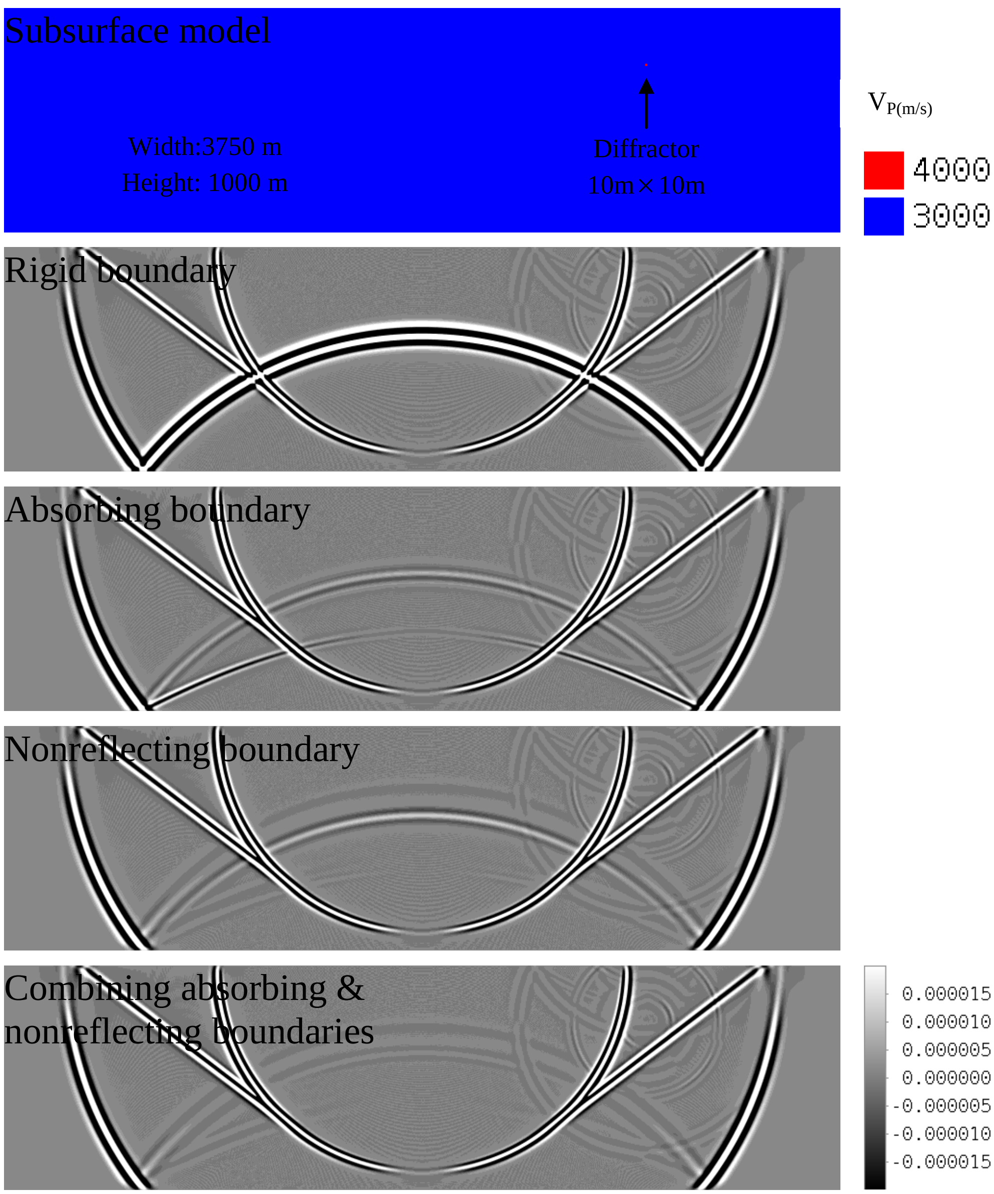

FIG.1. A model with a scatter point, and the boundary reflections by different boundary conditions.

Elastic prestack reverse-time migration using a staggered-grid finite-difference method

Zaiming Jiang*, John C. Bancroft, Laurence R. Lines, and Kevin W. Hall

SUMMARY

Both staggered-grid finite-difference schemes and non-staggered schemes are popular in elastic wave modelling, while conventionally reverse-time migration is carried out through the non-staggered grid schemes. We present an elastic prestack reverse-time migration method using a staggered-grid finite-difference scheme.

The causes and characteristic of imaging artifacts of source-normalized imaging condition are analyzed. Based on this analysis, we practiced artifacts removal by subtracting neighborhood averages, by taking first derivatives, and by applying high pass filters.

The migration method is tested using a point diffractor model and a reduced set of the elastic Marmousi2 model (Figure 1 and Figure 2).

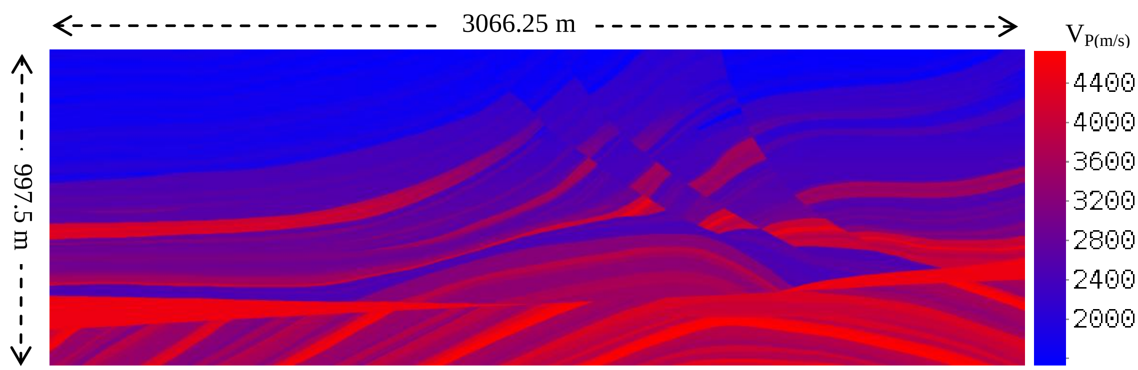

FIG 1. New Marmousi model extracted from the Marmousi2 model. It keeps the structure and elasticity of Marmousi2, but the size is much smaller.

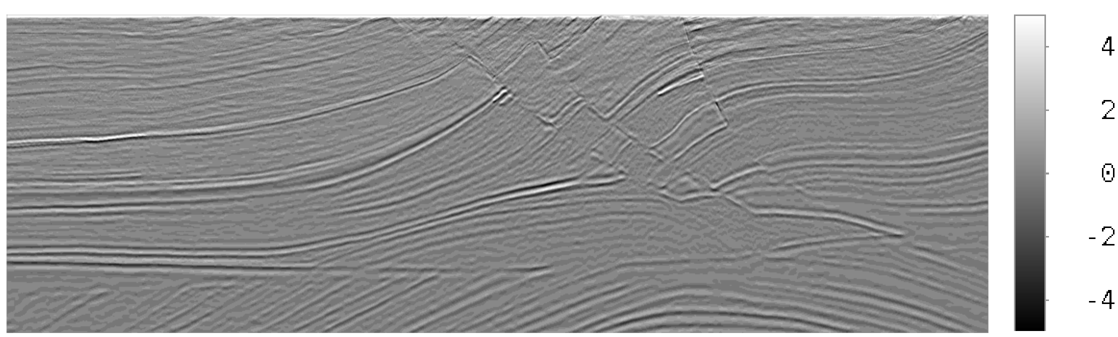

FIG. 2. Reverse-time migration result. The processing procedure is: modelling of 64 shots, reverse-time migration on each shot, stacking of shot-images, and filtering the stacked image by a high pass filter along each trace.

Overcoming computational cost problems of reverse-time migration

Zaiming Jiang, Kayla Bonham, John C. Bancroft, and Laurence R. Lines

SUMMARY

Prestack reverse-time migration is computationally expensive. Program run times are long, in terms of the total number of CPU cycles, and it requires large amounts of hard disk free space.

To accelerate computing, we do parallel processing using Intel Threading Building Blocks (TBB) and multi-core computers, for both the forward-time modelling and reverse-time migration phases of the computation (Figure 1). To solve the problem of limited free disk space, we use a technique that may seem counter-intuitive: the forward modelling phase is done twice instead of once (Figure 2).

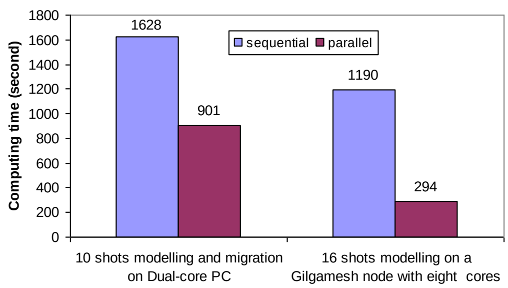

FIG. 1 (Up). Computational costs of sequential and parallel programs on a Dual-core PC, and a Gilgamesh node with eight CPU cores.

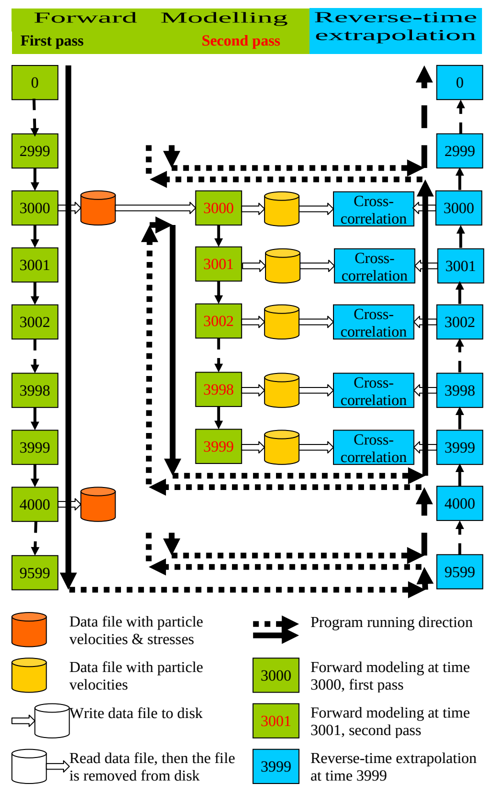

FIG 2 (Right). Do modelling twice instead of once, to keep the disk space requirements within available limits. During the first pass, we save the wavefield state (subsurface particle velocities and stresses) for only a few times; during reverse-time extrapolation, the snapshots for each time step are re-modeled from the stored data.

Two other enduring problems are described at the end of the paper: the requirement for large working memory, and limited access speeds of mass storage (hard disk) relative to the speed of computation.

Using three-point difference approximation to improve absorbing boundary conditions for elastic wave modelling

Zaiming Jiang, John C. Bancroft, and Laurence R. Lines

SUMMARY

Absorbing boundary conditions are partial difference equations, for which only forward or backward difference approximations instead of central difference approximations can be used. Usually two-point approximations are used for first order derivatives; however, three-point approximations result in less reflection from the computational boundaries. A comparison of the two-point and three-point approximations is illustrated.

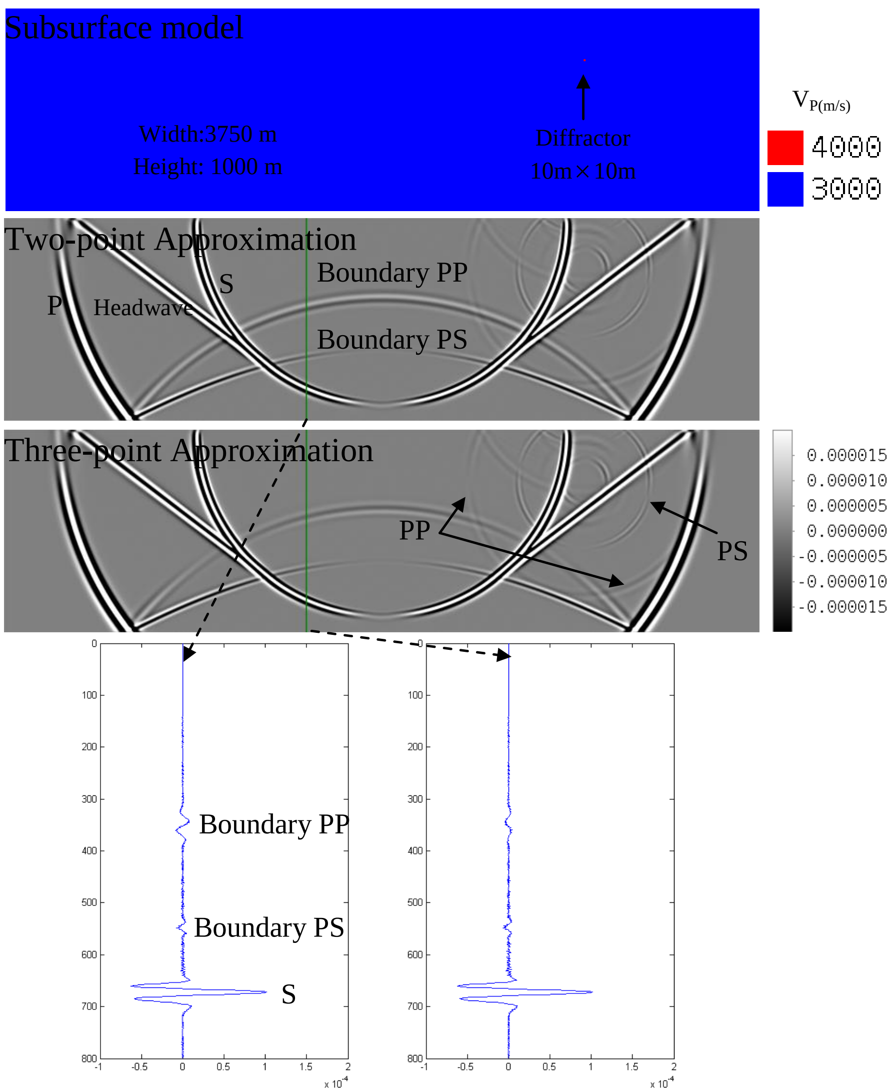

FIG. 1. A model contains a scatter point and the boundary reflections by absorbing boundary conditions of two-point and three point approximations.

Enforcing minimum phase on nonstationary filters

Michael P. Lamoureux and Gary F. Margrave

SUMMARY

We discuss designing nonstationary filters that preserve the minimum phase property: minimum phase signals in, must produce minimum phase signals out. Such filters are important in deconvolution: by accurately representing the physics of wave propagation through the earth, one aims to build algorithms that give better seismic images. These filters model the observed physical phenomena that the minimum phase property of an impulsive source is preserved even as it passes through an attenuating, dispersive medium.

To summarize: a causal, minimum phase preserving nonstationary, linear operator is represented by a triangular matrix, each column of which forms a minimimum phase signal (possibly a different signal for each column), and these column/signals have the spectral decay property – the Fourier amplitude spectrum of each successive column is decreasing.

A stronger result may be true: that a minimum phase preserving operator is characterized by exactly two minimum phase signals. The first signal generates a stationary filter, the other that generates a contraction of the unit disk in the complex plane, which is physically the decay operation. This second part results in a model of frequency-dependent Q-attenuation.

a_{00}	0	0	0	...
a_{10}	a_{11}	0	0	...
a_{20}	a_{21}	a_{22}	0	...
a_{30}	a_{31}	a_{32}	a_{33}	...
...	...	...	...	...

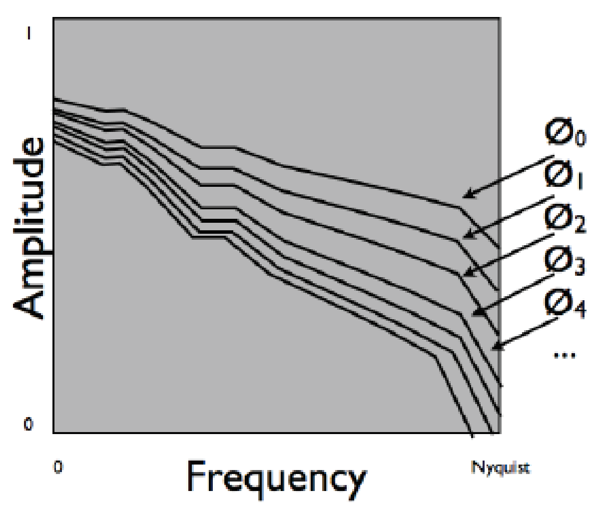

FIG. 1. Each column of the matrix represents a signal, with a Fourier amplitude spectrum. A plot of the spectra shows a decreasing sequence of functions.

Generalized frames for Gabor operators in imaging

Michael P. Lamoureux*, Gary F. Margrave and Peter C. Gibson

SUMMARY

In numerical wavefield propagation, it is useful to decompose a complex geological region into small local regions of nearly constant velocity, and propagate pieces of the wavefield through each region separately. The total wavefield is then obtained by reassembling all the pieces. This decomposition and reassembling is represented schematically in Figure 1. Mathematically, the total operator is written as a sum of localized operators, written as

$$A_{loc} = \sum_i Q_i^* A_i P_i,$$

where the $P_i;Q_i$ are the windowing operations that localize the wavefield both before, and after propagation, and A_i is the appropriate localized propagator for that window pair. This is the methodoly of Gabor multipliers that is the basis for many numerical algorithms in seismic imaging.

In this article we show how this decomposition/reassembling is captured mathematically using a windowing procedure which is accurately described by so-called generalized frames. By applying frame theory, we show that a collection of local wavefield propagators combined via a suitable partition of unity, remains a stable propagator, which is a highly desirable property in numerical simulations. These results apply more generally to combinations of linear operators that are useful for many nonstationary filtering operations. We discuss why symmetric windows are often required, and indicate directions for future work.

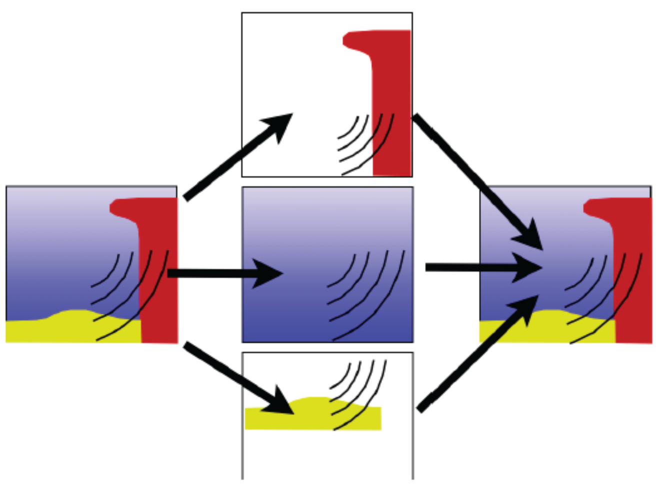

FIG. 1. Propagating a wavefield through a complex medium, as separate local operations.

Multicomponent seismic survey at Spring Coulee: a data repeatability study

Don Lawton*, Peter Gagliardi, Malcolm Bertram, Han-Xing Lu, Kevin Hall, Joanna Cooper, Eric Gallant, Kevin Bertram.

SUMMARY

A 3 km long 3-component seismic line was recorded at Spring Coulee, Alberta, using an Envirovibe source, with a nominal shot and receiver spacing of 10 m and a maximum useable source-receiver offset of about 1500 m. Offsets greater than 1500 m were limited primarily by wind noise overwhelming signal. The line was recorded twice over a time period of 10 days. The vertical and radial component data from the two surveys were processed using the same flows, but with independent static solutions and velocity analyses. Spring Coulee is a 'good' data area, with only a thin weathering layer, and P-P and P-S reflections from PreCambrian basement evident on processed sections. An nrms metric was used to assess the repeatability of shot gathers and processed P-P and P-S sections between the two surveys. For shot gathers, nrms values ranged from 0.3 to 0.9 for raw vertical component data, and 0.4 to 1.2 for radial component data (Figure 1). After an 8-12-50-60 Hz bandpass filter was applied, nrms values reduced by 0.2 for both vertical and radial component data, respectively. For migrated sections, nrms values for P-P data were about 0.4 in the high-fold, central part of the seismic line, but greater than 1.1 for P-S data. The poorer repeatability of the P-S data with respect to the P-P data is due to unresolved receiver static corrections and differences in ambient wind noise between the two surveys.

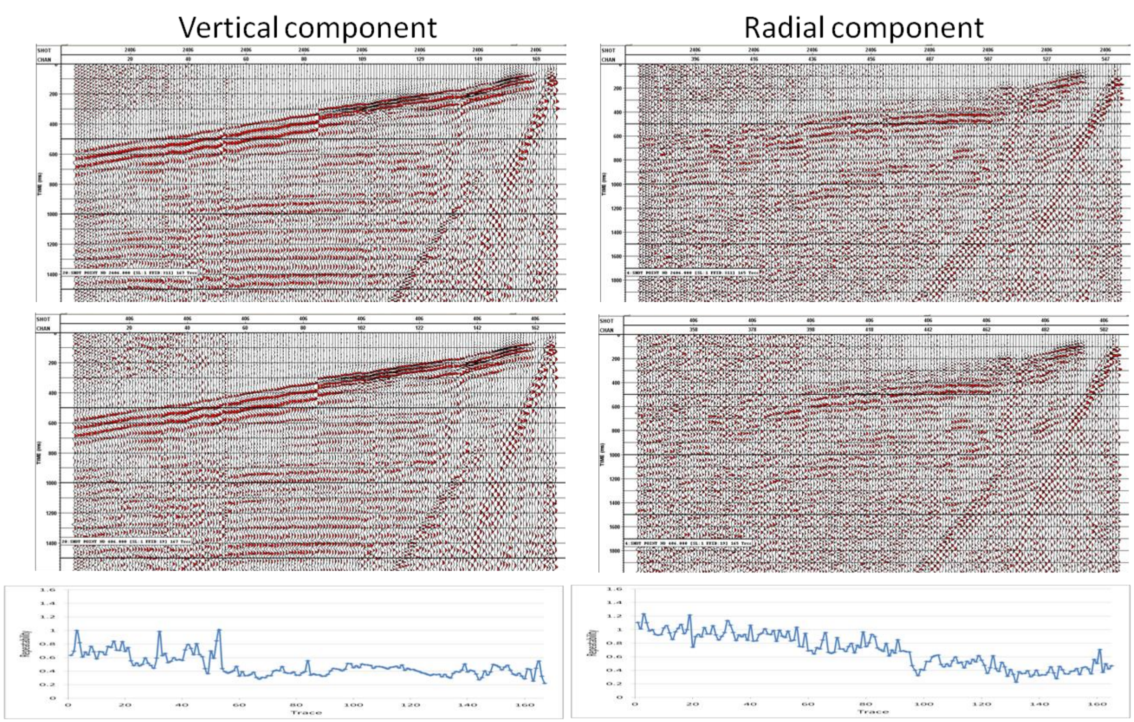

FIG.1. Filtered shot gather repeatability. Baseline (top), monitor (centre) and nrms (bottom)

The accuracy of dipole sonic logs with implications for synthetic seismograms and wavelet estimation

Laurence R. Lines* and P.F. Daley

SUMMARY

Sonic logs contain errors due to mud invasion and cycle skipping, and repeat logs may be recorded to validate measurements. For repeated dipole sonic logs, it is interesting to note differences in the (compressional) $P-$wave and (shear) S-wave velocities, as well as the resulting differences in reflectivity sequences and synthetic seismograms. Figure 1 shows a comparison of repeat P-wave velocity logs for a well at Long Lake heavy oil field. For synthetic seismograms with low-frequency wavelets, the differences are often barely perceptible, especially for $P-$wave synthetic traces. When correlating these different synthetic traces with reflected events on real seismic data, our interpretations would often not be affected. However, for the purposes of deconvolution, seismic wavelets are often estimated by using both sonic logs and real seismic data. In some cases, where there are noticeable differences in estimated log-based wavelets, it is advisable to check log-based wavelet estimates using statistical methods, such as minimum phase wavelet estimation. Also in these comparisons of dipole sonic logs, synthetic seismograms and wavelet estimates, we have generally found the repeatability of $P-$wave logs to be superior to that of the shear-wave logs. This is not surprising due to the difficulty of picking shear-wave arrivals compared to $P-$wave first break picks. In summary, repeat measures of dipole sonic logs will be worthwhile for insuring that the $P-$wave synthetic seismograms, shear-wave synthetic seismograms and wavelet estimates are accurate.

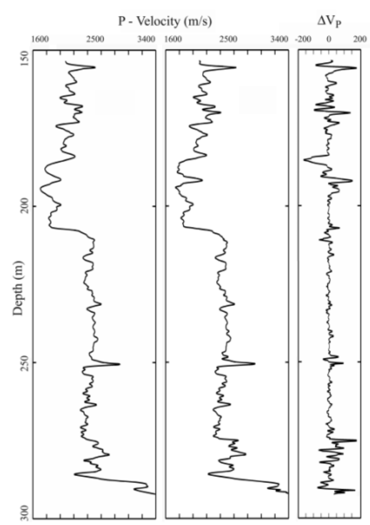

FIG. 1. A comparison of sonic logs from two wells (denoted in the text as log A and log B) spanning a depth range from 153.5-292.1*m*. The third trace in the plot is a discrepancy log giving the difference in velocities between wells A and B (log B velocities – log A velocities). Note that the biggest differences are at depths of about 155, 172, 192, 252 and 290*m*.

Revisiting the Blackfoot 3C-2D broad-band seismic data

Han-Xing Lu and Rolf Maier

SUMMARY

Four lines of 2D vertical and three-component seismic data were acquired in the Blackfoot area east of Calgary in July, 1995, were sorted by the frequencies for the 3C geophones, processed, and stacked.

The influence of the frequency is shown by focusing on a target zone. None of the stacked sections have an AGC or band-pass applied. The differences in the target zone are quite striking; in the 2 Hz case the event at 1080 ms shows a stronger discontinuity in the data from the lower frequency (2 Hz) geophones (figure 1), yet the higher frequency (10 Hz) phones (figure 2) show a gradual pinch-out which the low-frequency phones seem to partly obliterate.

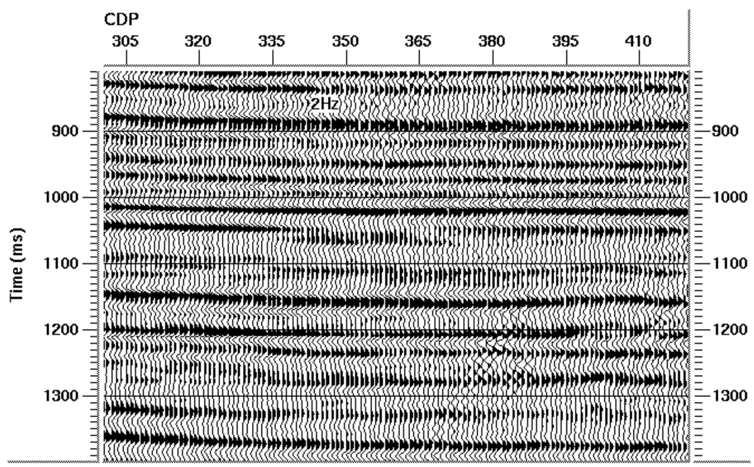

Fig. 1. Stack of the vertical component from 2 Hz 3-C geophones.

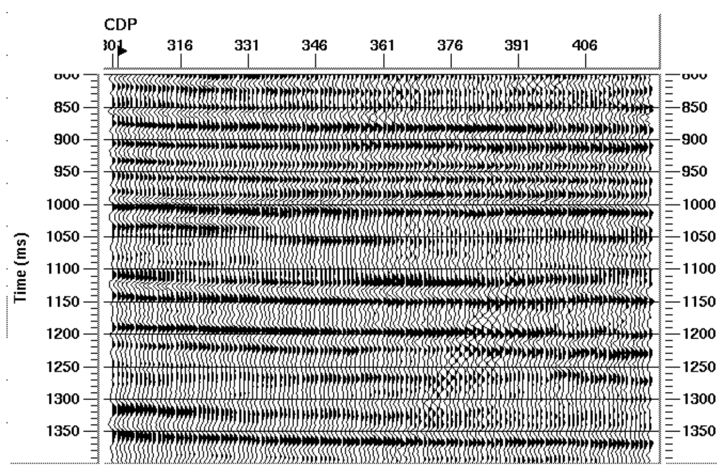

Fig. 2. Stack of the vertical component from 10 Hz 3-C geophones.

A review of angle domain common image gathers

Faranak Mahmoudian and Gary F. Margrave

SUMMARY

Common image gathers in the offset domain are used extensively in velocity analysis, and amplitude versus offset (AVO) studies. Imaged with the correct background velocity model, the events will appear horizontal in the seismic offset gathers. Any curvature or moveout in these gathers can be used as a criterion for updating migration velocities. If the geology is complex and the ray field becomes multi-pathed and the assumptions made for imaging data in the offset domain are violated. This will especially influence the quality of common-image gathers and, as a sequence make it difficult to perform any form of AVO or velocity analysis. Such complicated problems typically arise in seismic imaging beneath gas, salt domes, and basalt structures. Angle-domain common image gathers (ADCIGs) uniquely define ray couples for each point in the subsurface. Therefore each event in the data will be associated with only one subsurface location. It is possible to generate the ADCIGs with both Kirchhoff and wave-equation migration methods and these ADCIGs may be used for velocity analysis and amplitude-versus-angle (AVA) analysis. Common-angle migration creates seismic images for different reflection angles at the reflector, thus generating ADCIGs. The ADCIGs may be used for velocity analysis, and amplitude versus angle (AVA) analysis with the specific application in fracture study. AVA can provide information about fractures at existing wells, in reservoir characterization specially in predicting the production rates of new wells, and in structural interpretation. Because the AVA records the fracture information between the wells, it adds significant information to the interpretation of fractured reservoirs that cannot be easily obtained in other ways.

Disusing common-angle migration, a summary of the Kirchhoff-based method in based on the work of Bleistein et al. (2001) is presented. In addition the wave-equation-migration based method, which is discussed in the work by Sava (2001), is examined. Further, a brief review of the application of ADCIGs in amplitude-versus-angle and azimuth (AVAZ) analysis by Gray et al. (2002) is presented.

Numerical modeling of a fractured medium

Faranak Mahmoudian and Gary F. Margrave

SUMMARY

Fractures play an important role in hydrocarbon production. A fractured layer acts as a transverse anisotropy with horizontal symmetry axis (HTI) layer in response to seismic wave propagation. We have created numerical 3D seismic data from a fractured model, using a 3D finite-difference anisotropic program called TIGER. The effect of the fracture layer on seismic response has been examined; the HTI medium affected the amplitude and travel time of both P- and S-waves. P-wave amplitude is highest in the direction of fracture strike. Also, shear wave splitting occurred at the bottom of the fractured layer. The TIGER code was able to create an accurate 3D dataset with no dispersion. The investigation of synthetic data for fractured layer will help in fracture detection and estimation from surface seismic data. This model will be used to calibrate a common-angle migration algorithm, whose purpose is to generate common-angle gathers essential in an amplitude-versus-angle and azimuth (AVAZ) analysis, an effective method in fracture detection.

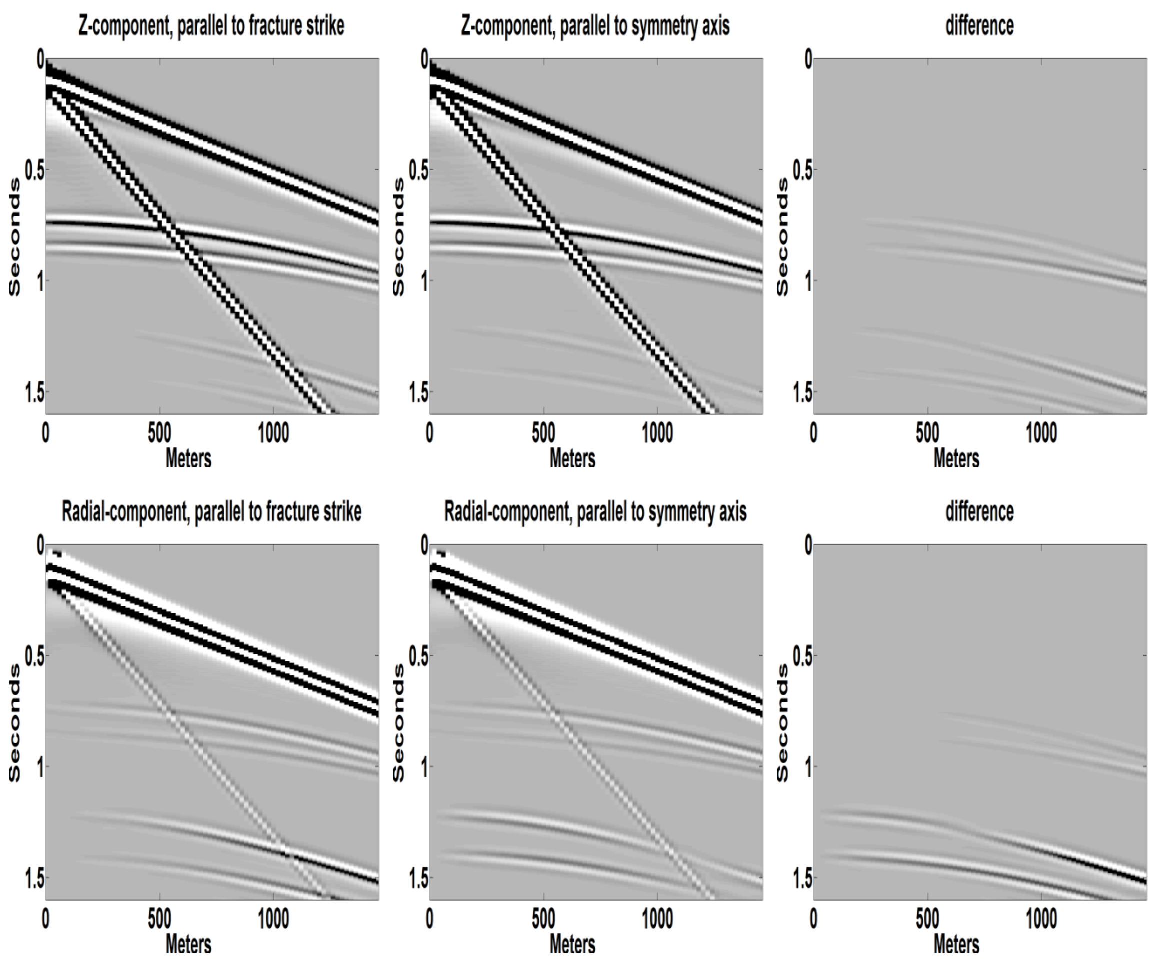

Z- and radial-component, 3D elastic finite-difference modeling of HTI model.

Taking steps toward generating angle-domain common-image gathers

Faranak Mahmoudian, Gary F. Margrave and P.F. Daley

SUMMARY

The amplitude of the output of any true-amplitude migration can be used to estimate the angular-dependant reflectivity. However, explicit information regarding the reflection angle will be missing after a standard true-amplitude migration. In a amplitude-versus-angle (AVA) study, the explicit relation of the reflectivity function to the reflection angle is needed. This motivates us to work toward having the reflectivity function in the angle-domain from migrated data.

This short note summarizes the steps that we take towards generating angle-domain common-image gathers (ADCIGs). Two approaches to generate ADCIGs are considered. In the first method, a shot-domain common-image gather (SDCIG), generated from true-amplitude common-shot Kirchhoff migration (Bleistein et al., 2001) is converted to the ADCIG; a postmigration mapping from surface-domain (shot-coordinate) to angle-domain. Based on the a priori knowledge of opening angle the calculated reflectivity function is placed in an angle bin. In standard common-shot migration, the reflectivity function for each subsurface point is stored in a vector of size $nz \times 1$ (*nz*: number of depth samples). In this method the reflectivity function will be stored in an $nbin \times nz$ array where the *nbin* is number of angle bins. In the second approach, a 2.5D version of common-opening angle migration discussed in Bleistein and Gray (2002) for constant velocity is presented.

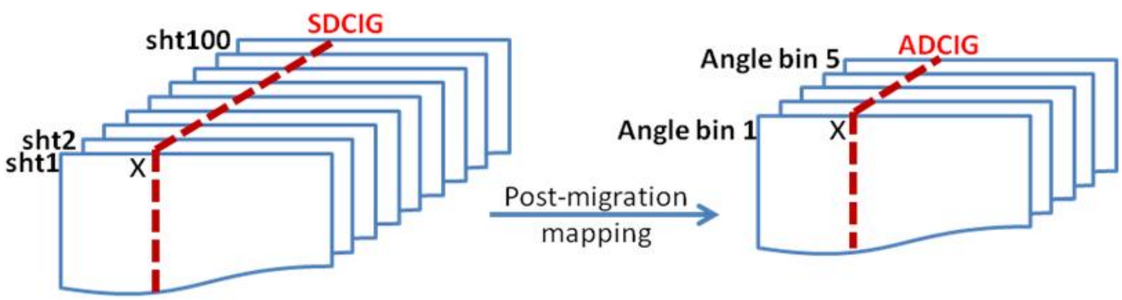

The CREWES data library

Rolf Maier, Kevin W. Hall, and Han-Xing Lu

SUMMARY

The data most frequently used by researchers and students are being put into a unified format described below.

Data on disk have always been easier and quicker to access than data on tapes. Hence, the data sets most frequently requested by researchers and students have been collected on disk over the last few years. This allows not only for quick access and backup, but also simplifies the task of converting the data into a common format following a common set of specifications.

The aim is to have data stored in one basic format, although there are two variants depending on the data's age and whether they have been prepared. Processed data sets are thus far all in a version of SEGY standard rev. 0 format while unprocessed, newly acquired field data, data from the physical modelling system, and data from numerical simulations, are in SEGY rev. 1 format. Since CREWES has enjoyed the availability of ProMAX for many years, the header word locations ProMAX assignes by default are used. Hence, for information such as first breaks, station number, inline number, and cross line number, we use the same (ProMAX) format for every dataset when written as a SEGY file. The location of any non-standard header word is defined in the text header. The following little table lists those trace header words which are not part of, or differ from, the rev. 0 standard:

ProMAX mnemonic	header bytes	type	description
sou_sloc	181-184	4I	source (station) number
srf_sloc	185-188	4I	receiver station number
iline_no	189-192	4I	inline number, in 3D
xline_no	193-196	4I	cross-line number, in 3D
cdp_x	197-200	4R	x coordinate of CDP
cdp_y	201-204	4R	y coordinate of CDP
R_LINE	205-208	4I	receiver line number, in 3D
S_LINE	209-212	4I	Swath or sail line number, in 3D
FB_PICK	213-216	4R	first break pick time
geo_comp	217-220	4I	the component number in 3C
tr_type	221-224	4I	1: live trace, 2: zeroed out bad trace

The first item is defined simply as a unique number pertaining to a shot. The standard calls this the energy source point number and uses bytes 17-20. Sometimes the field file ID (FFID) is used; we use the shot point. Using the shot point as a unique identifier implies that shots are not repeated, or that repeated shots are all bad but one, and only the good shot has been kept after preprocessing. The last item, the trace type, called the trace identification code in both versions of the standard, would be in bytes 29-30 if the standard were followed.

Finite-difference staggered-grid modelling in 3 dimensions

Peter M. Manning*

SUMMARY

The elastic finite-difference modelling method, which uses staggered grid displacement positions and which has proved effective in 2 dimensions, has been extended for use in 3 dimensions. The geometry of the grid positions is shown from selected viewpoints. For an isotropic, homogeneous medium, four types of finite-difference energy sources are examined, and the propagating wavefronts expected from them are shown. The accuracy of one of the energy source models is verified by comparison with the double-couple solution from known theoretical results.

FIGURES

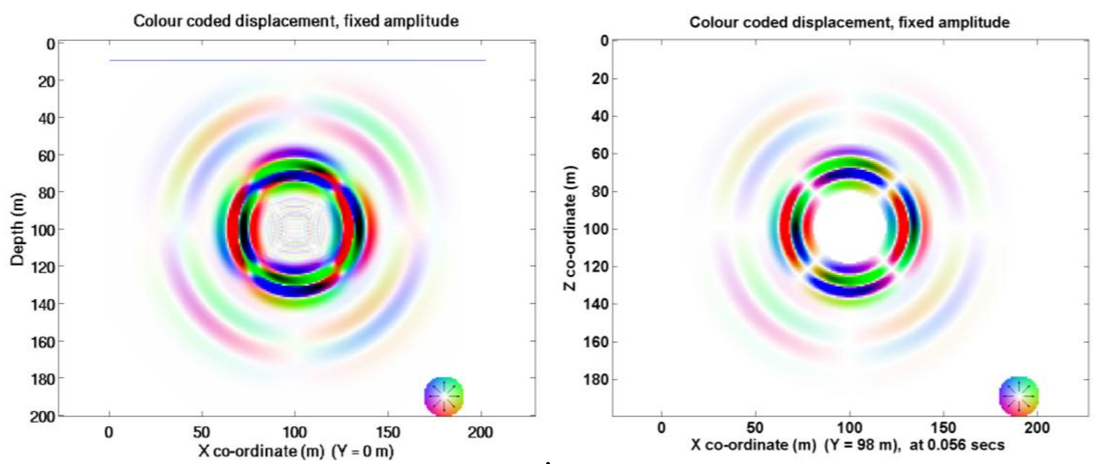

Left: A snapshot from the ‘double couple’ source propagated by the finite-difference algorithm for .056 seconds. The high amplitude inner ring is composed of shear waves, the outer ring is composed of pressure waves. Right: Propagated waves from a ‘double couple’ as described by equations from Aki and Richards.

Modelling from well logs with CREWES tools

Heather J.E. Lloyd and Gary F. Margrave

SUMMARY

In 1994, LOGSEC was written using the MATLAB programming language. Its original features included, importing logs, editing horizons, editing logs using LOGEDIT, propagating logs along the cross-section, converting the cross-section to time, and computing theoretical seismograms. Over time the code had to be modified to correct programming code changes and to add additional functionality to the program. Some of these new functions include computing a synthetic stack using the SYNGRAM algorithm and being able to export the section for further analysis with other tools. LOGEDIT also has new functions including a Gassmann Function which allows for fluid substitution in the logs, a Gardner Function and a Mudrock Line Function. A Blackfoot Channel model was created and used to illustrate the functions in both LOGEDIT and LOGSEC. Information on the functions in LOGSEC and LOGEDIT can be found in their respective User Guide or help files.

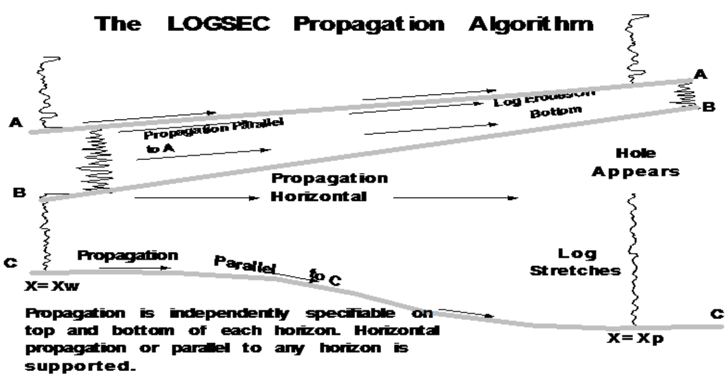

FIG. 1: The LOGSEC Propagation Algorithm

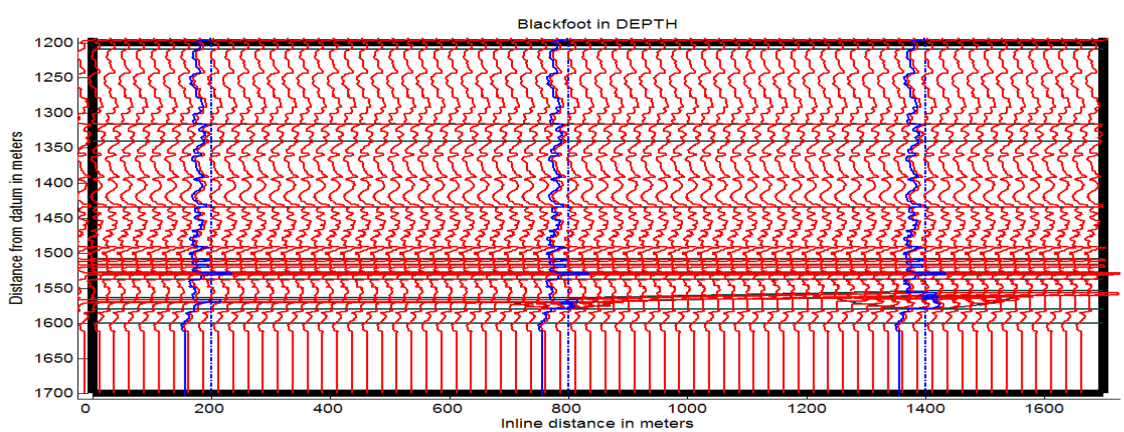

FIG. 2: this is a density log section. The red logs have been propagated by combining the logs at the wells indicated by the blue lines. The way the logs are propagated shows the how the channels would look if looking at a section of traces.

Nonstationary predictive deconvolution

Gary F. Margrave* and Michael P. Lamoureux

SUMMARY

We present a general method for construction of a uniform partition of unity (POU) that is exact over a finite segment of the real line and whose individual windows are constructed from asymmetric Gaussians. The spacing between windows need have no relationship to the Gaussian half-width. We illustrate the uses of such POU's to decompose a signal into a discrete set of temporally localized signals which we call Gabor slices. We then apply this theory to construct a time-domain nonstationary deconvolution method based on gapped prediction filtering. We call this new method *slicedecon* because it operates directly on the individual Gabor slices. We also prescribe the construction of nonstationary autocorrelation functions as an analysis tool. We then compare *slicedecon* with the more established Gabor deconvolution or *gabordecon*. When the prediction filtering is unit-lag, we show that *slicedecon* achieves results comparable to *gabordecon* on a nonstationary (Q attenuation) synthetic. For lags greater than unity *slicedecon* appears to suppress, though not eliminate, periodicities in the nonstationary autocorrelation of a signal. Testing on a synthetic with multiples has not yet indicated any dramatic elimination of the unwanted multiple reflections; however, we plan improvements to the method.

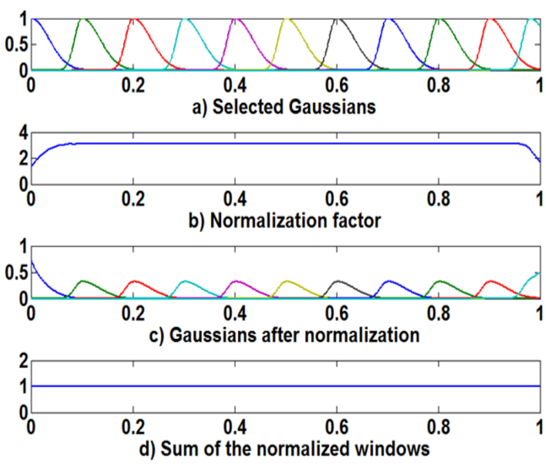

This figure shows the construction of a POU using asymmetric Gaussian windows (top). The initial Gaussians are divided by the normalization factor to make the POU exact.

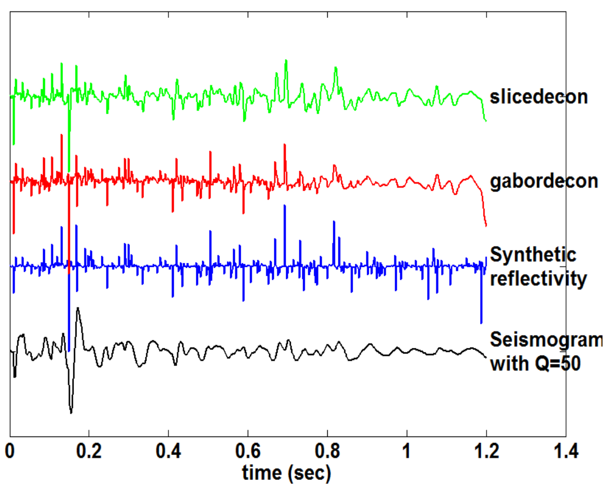

Here is an example of the performance of *gabordecon* and *slicedecon* on a nonstationary synthetic trace. The seismograms contains Q effects but no multiples.

Numerical fluid flow modelling and its seismic response in time-lapse

Vanja Milicevic* and Dr. Robert J. Ferguson

SUMMARY

A timelapse reservoir characterization study is performed on a model of a producing reservoir. This model reservoir has two injection wells and one producer. Pressure and saturation models are obtained from numerical simulation of reservoir properties and fluid flow for a number of calendar days. Integration of saturation models and Gassmann’s relations delivers compressional wave velocity models for each calendar day, and finitedifference algorithms are used to generate synthetic data for comparison; specifically, we compare 2D acoustic and 3C-3D elastic forward modelling. In Figures 1 and 2 examples show subtle similarities and differences between the models. Both, acoustic and elastic, models prove to be valuable tools in reservoir characterization.

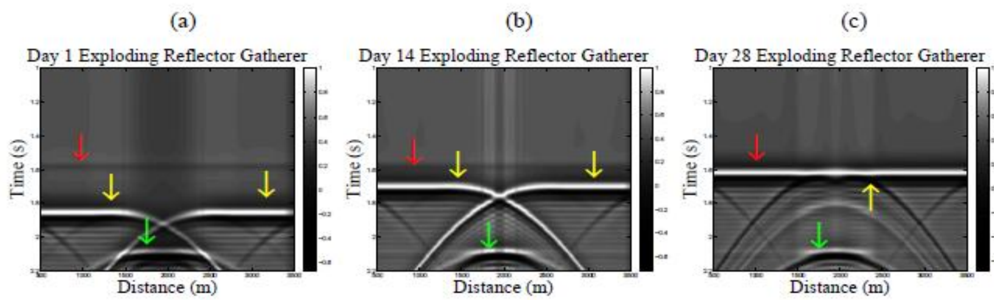

FIG. 1. 2D Exploding Reflector Seismic Gatherer models in acoustic medium. The red and green arrows point to the top and bottom of the resrvoir, respectively. The yellow arrows mark the two waterfronts. Note waterfronts progress upwards in time-lapse after day 1, 14 and 28.

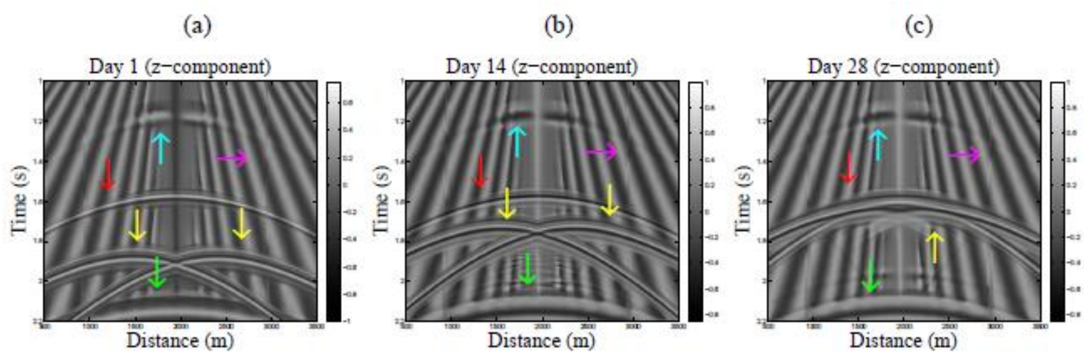

FIG. 2. 3C-3D Shot Gatherer Models: z-component velocity models in elastic medium. The red and green arrows point to the top and bottom of the reservoir, respectively. The yellow arrows point towads two waterfronts. The waterfronts on elastic models also progress upwards in time-lapse after day 1, 14 and 28. The 3C-3D models plot more detailes, hence we see numerical artefacts and projection of shear waves on the the vertical component, pointed by magenta and turquoise arrows, respectively.

True surface processing of Spring coulee

Carlos A. Montana

SUMMARY

The true surface processing approach takes into account the difference in the source and receiver raypaths introduced by variable elevation and weathering. In this project seismic data from the Spring Coulee line, in this case P-P, are processed using the true surface methodology. The near surface model created from refraction (figure 1) shows that in fact the elevation and weathering thickness variations are considerable. The post-stack time migrated P-P section (figure 2) obtained shows important differences with respect to other published results.

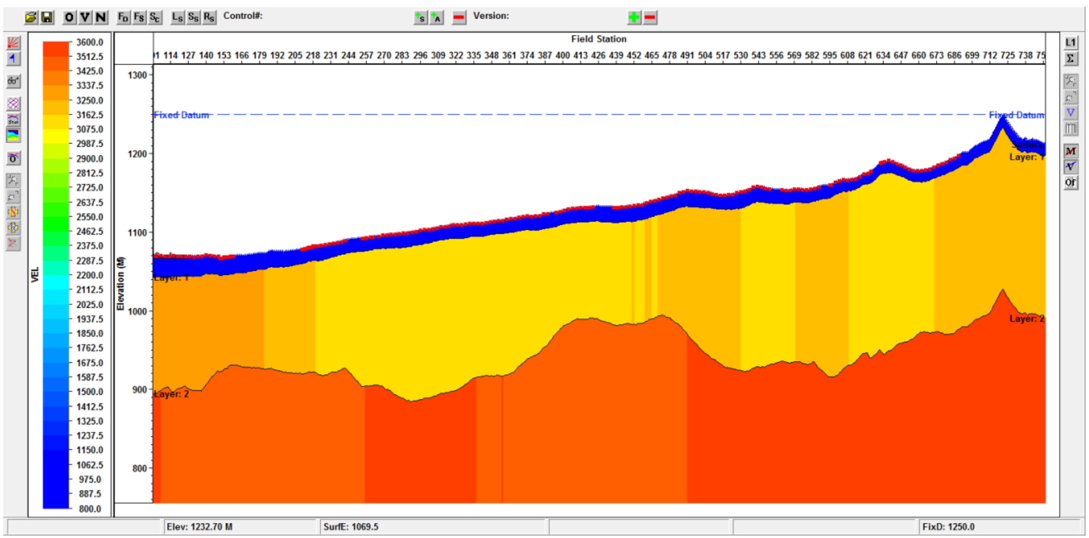

Figure 1. Near Surface model generated from first breaks. The color scheme corresponds to the near surface velocities.

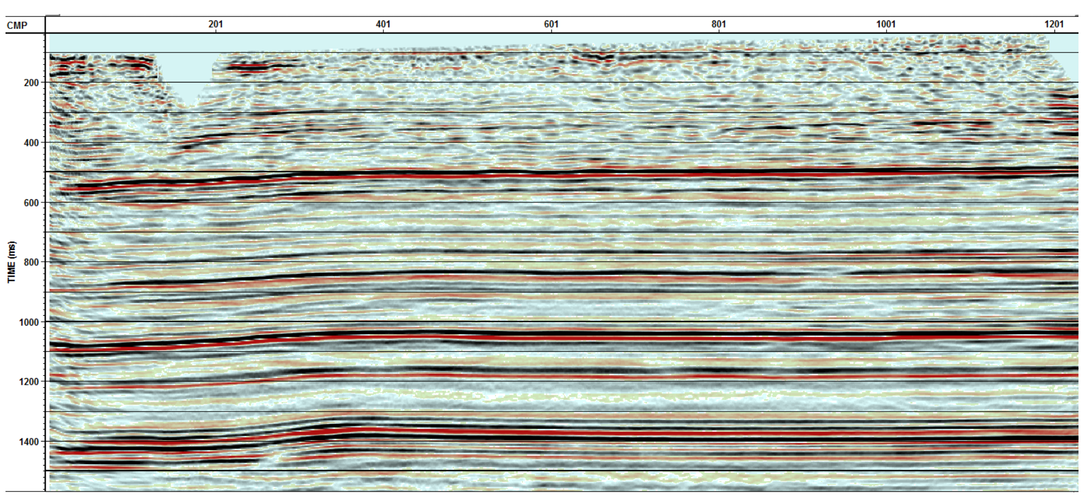

Figure 2. Finite Differences post stack migration of P-P section. North is left.

Spring Coulee seismic interpretation

Lauren A. Ostridge, Don C. Lawton and Robert R. Stewart

SUMMARY

Over the past two years, CREWES has recorded three seismic surveys near Cardson in southern Alberta, where the University of Calgary holds the mineral rights to two sections of land. Each survey consisted of multiple seismic lines, the main purpose being to map the sub-surface of the area and secondly to see if there could be hydrocarbon production potential. From nearby producing wells, we have chosen the Mississippian-aged Madison Formation as the primary target and strata of the Lower Cretaceous Mannville Group and Second White Speckled Shale Formation as the secondary targets. This paper gives an overview of the data acquired and summarizes the seismic interpretations.

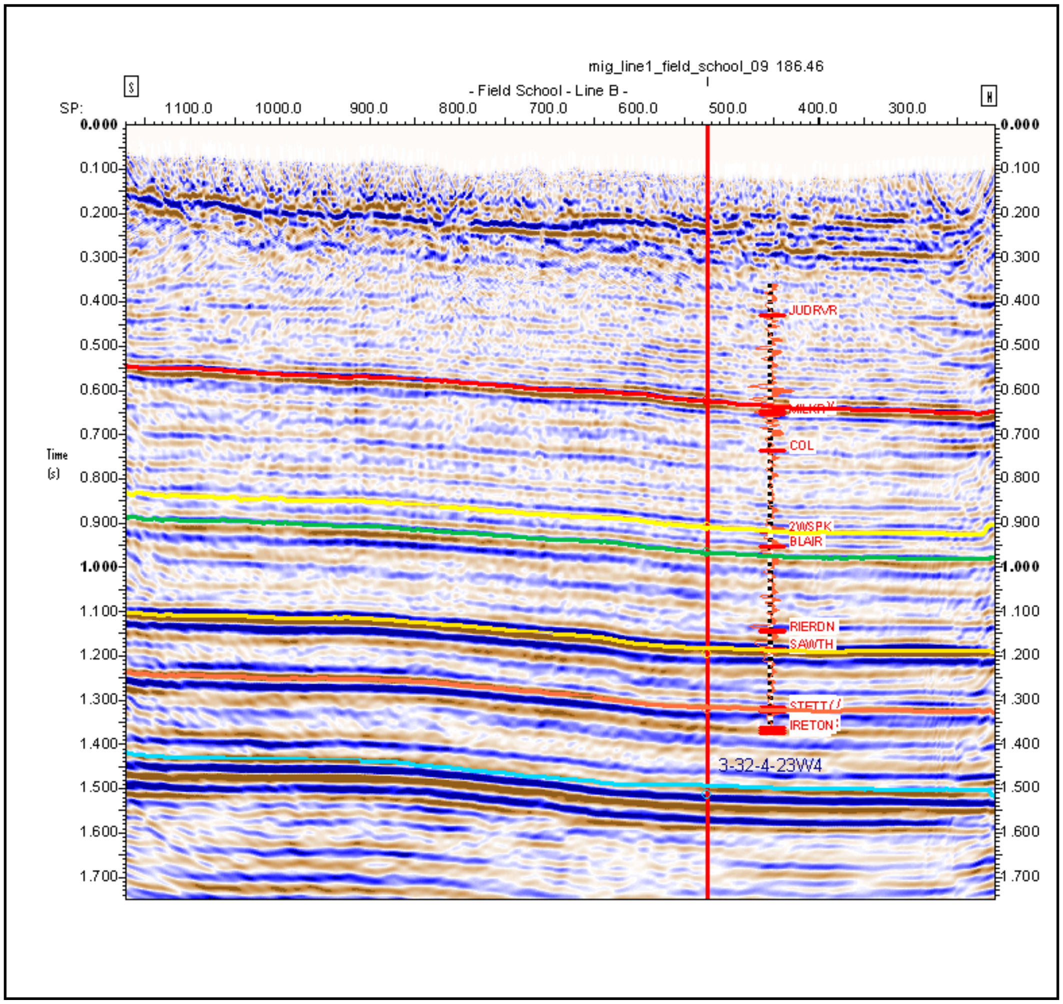

FIG. 1. Line B of the August 2008 Field School Survey, illustrating subtle structure affecting the entire sedimentary sequence. This line is oriented in a north-south direction and is located immediately west of the land where the University of Calgary holds mineral rights. The intersection with the 2009 field school line is shown in red.

Choosing reference velocities for PSPI migration

Baolin Qiao and John C. Bancroft

SUMMARY

When performing PSPI migration, the accuracy of migration result is mainly credited to how and how many reference velocities being chosen for a given downward extrapolation step. A method of selecting reference velocities is designed in this paper which can select reference velocities based on the complexity of velocity model at given depth. Migration results show that this method is basically satisfied.

SYNTHETIC EXAMPLE

Figure 1 shows the reference velocities from receiver R_{311} to receiver R_{331} at depth z=2.4km. Four typical points are marked in red dot. For R_{314}, neighbour reference velocities are used in linear interpolation; for R_{317}, reference velocities at its left side are used; for R_{318}, the reference velocity is true velocity, so interpolation is not necessary at this point; for R_{322}, reference velocities at its right side are used.

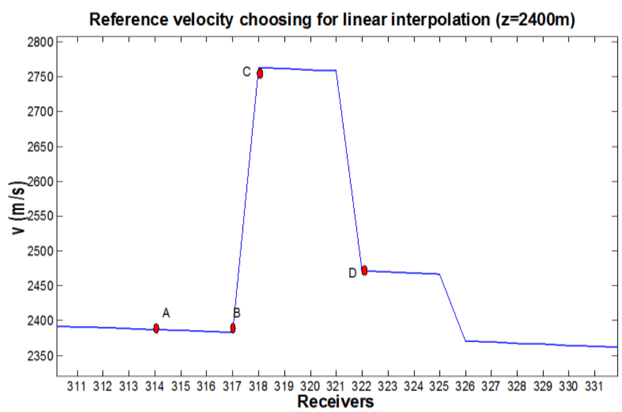

Figure 1. Illustration of choosing reference velocities at four typical points (red point).

Figure 2 shows the migration result. By using reference velocity interval dv=40m/s and linear interpolation, migration result is basically satisfied.

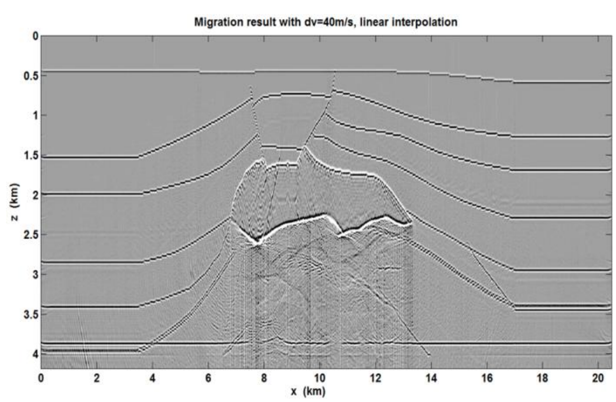

Figure 2. Migration result with dv=40m/s and linear interpolation method.

Error distribution when using first-break arrival times to locate microseismic events

Baolin Qiao and John C. Bancroft

SUMMARY

SVD method was used to estimate 3D hypocenter and origin time of a microseismic event. Given variance of observed first-break arrival times, 3D error distribution of hypocenter is calculated. It is shown that uncertainty in vertical direction is much bigger than that in horizontal directions.

Suppose that all receivers start to record data at arbitrary clock-time t_0, receiver R_i (x_i, y_i, z_i) recorded first-break arrival time at t_i. Solving the following linear equations can be used to estimate the location and origin time of hypocenter.

$$2(x_i - x_{i-1})x + 2(y_i - y_{i-1})x + 2(z_i - z_{i-1})z \; - 2v^2(t_i - t_{i-1})t_0$$
$$= v^2({t_i}^2 - {t_{i-1}}^2) + {x_i}^2 + {y_i}^2 + {z_i}^2 - ({x_{i-1}}^2 + {y_{i-1}}^2 + {z_{i-1}}^2).$$

Covariance of estimated parameters can be used to calculate the error distribution of hypocenter location.

EXAMPLE

The following figure shows 2D view of error distribution of a microseismic event. Standard deviation *std*=10ms is used to calculate error ellipses. The results show that the uncertainty in vertical direction is bigger than that in horizontal directions.

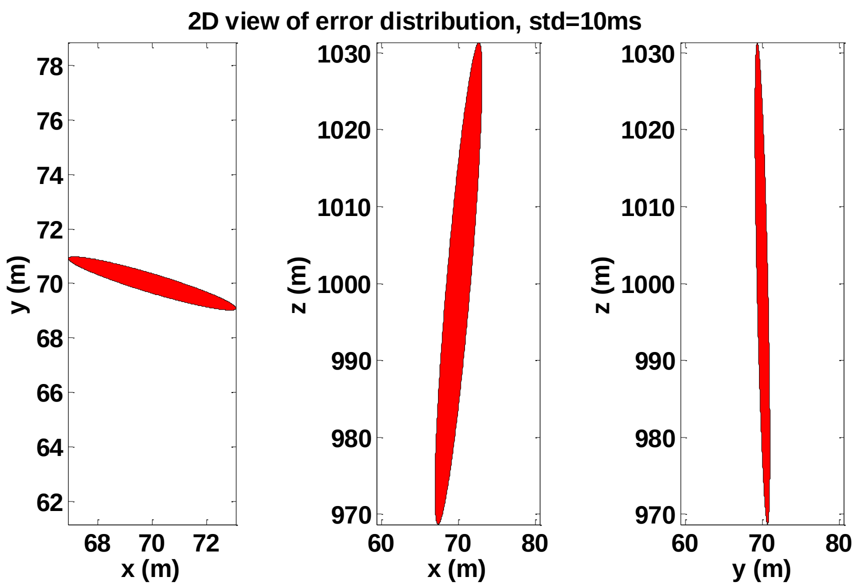

Error distribution of a microseismic event with hypocenter *S*(*x*=70, *y*=70, *z*=1000). Standard deviation *std*=10ms is used to calculate error ellipses.

An empirical study of hydrocarbon indicators

Brian Russell*, Hong Feng, and John Bancroft

SUMMARY

Numerous approaches have been published that derive fluid indicators, often called direct hydrocarbon indicators (DHI), from the amplitude variations with offset (AVO) method. These methods use linearized approximations to the Zoeppritz equations to extract physical parameters such as *P*-impedance, *S*-impedance, density, bulk modulus, shear modulus, Lamé's parameters and Poisson's ratio, and then infer the fluid content of a hydrocarbon reservoir from these parameters. Russell et al. (2003) used poroelasticity theory (Biot, 1941) to generalize several of these methods using a parameter dependent on the dry rock V_P/V_S ratio. The purpose of this study is to examine the generalized fluid method and compare this method with other fluid methods to see which indicator can most effectively discriminate between hydrocarbon sands and wet sands and which indicator is most sensitive to pore-fluid content estimation. To perform the sensitivity analysis we use an empirical dataset measured by Han et al. (1985), which covers saturated and dry sands with a wide range of porosities and clay contents at different pressures. As an indicator to evaluate the best method, we use the measure suggested by Dillon et al. (2003) in their analysis of fluid indicators. Using Han's dataset, we conclude that the generalized fluid method is in general the most successful fluid discriminant, given that we can get a reliable estimate of the dry rock V_P to V_S ratio. We are also able to make predictions about the dry rock V_P to V_S ratio as a function of porosity, clay content and pressure, which is related to depth.

Numerical estimation of angle of incidence with Bleistein approach

Ritesh K. Sharma and Gary F. Margrave

SUMMARY

The angle of incidence, Θ_i, of a ray is the angle measured from the ray to the reflectornormal. Historically, ray tracing is used to compute the angle of incidence. According to ray tracing, a wave can be modeled as a large number of rays (narrow beam), and a ray can be considered locally straight over a very small distance. In ray tracing, Snell's law is used to compute ray path and the angle of incidence. We investigate a method to compute the angle of incidence from the ratio of two reflectivity attributes known as β (reflectivity function) and β_1. Another method, the ratio of β_2 and β_1, is also proposed to compute the angle of incidence with less computation. The basic objective of this paper is to verify the proposed approach numerically. A comparative study of the two methods, β / β_1 and β_2 / β_1, is considered here.To verify the proposed approach, two models have been considered. The specular angle of incidence is then computed with both methods, namely, the ratio of β / β_1 and the ratio of β_2/ β_1. Both of these methods give approximately the same result for both the models. At the central part of the model the extracted values of the angle of incidence match with the computed values. The results may be improved with a common-shot seismic section of high resolution. Computationally, the time taken by both of these methods is same for 2D models but for 3D model, method 2 is more efficient than 1. Method 2 takes 18% lesser time than time of method 1.

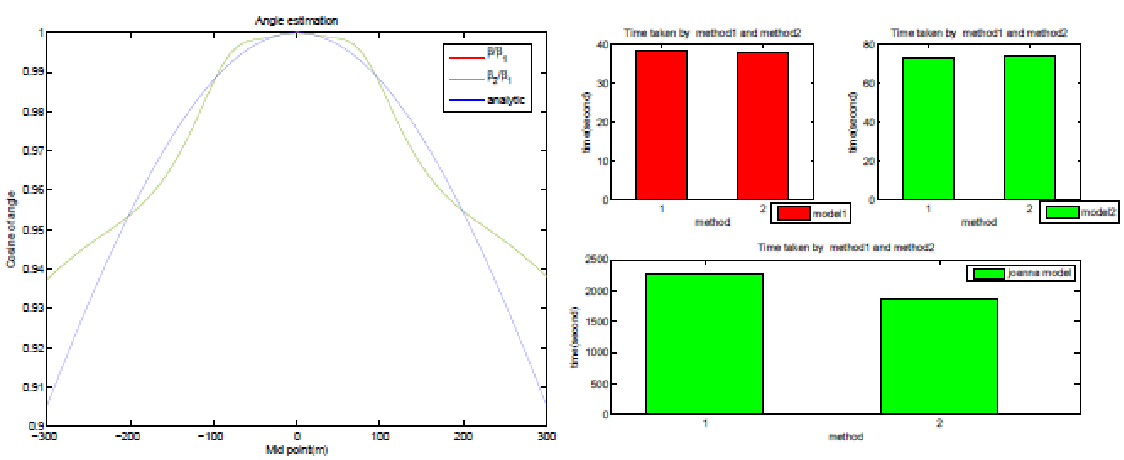

Figure 1(a) shows the estimated value of the angle of incidence with proposed methods and with analytic one. Time comparison of proposed methods for different models are shown in Figure 1(b)

Reflection and transmission coefficients for SH wave in plane wave domain

Ritesh K. Sharma and Robert J. Ferguson

SUMMARY

Classical reflection and transmission coefficients in plane wave coordinates are worked out for reflectors aligned with the computational grid. For non-aligned reflectors, those with dip and azimuth, computation of effective reflection and transmission coefficients is not straight forward, for this the coordinate system must be rotated. To do this, a normal for each individual plane wave based on local velocity and vector cross product of this normal with the normal to reflector is computed. This cross product yields a ray arameter that presently is used to compute corresponding reflection and transmission coefficients for a given plane wave. The importance of this approach is the automatic adaptation of the reflection and transmission coefficients expression to a special case of dipping interface. These coefficients can then be used to scale the amplitude component of plane wave extrapolation across a reflector as is done in seismic forward modeling. Another importance of reflection and transmission coefficients in plane wave domain, is their use in Rayleigh Sommerfeld Modeling(RSM) of seismic data. In line traces and cross line traces are required in order to model the plane wave inputs. Presently, the problem associated with data acquisition is studied here by changing the number of cross line traces.

Figure 1(a), (b) show the real and imaginary part of the reflection coefficient for horizontal interface. Real and imaginary part of the transmission coefficient are shown in Figure 1(c), (d). Figure 1(e), (f) show the real and imaginary part of reflection coefficient for dipping interface. Figure 1(g), (h) show the real and imaginary part of transmission coefficient in the case of dipping interface.

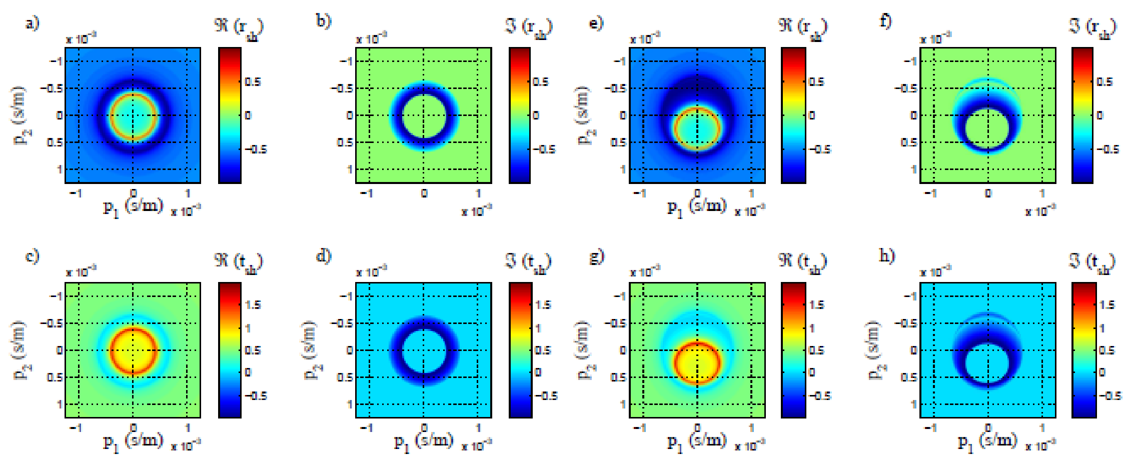

FIG. 1. a) Real part of reflection coefficient. b) Imaginary part of reflection coefficient. c) Real part of transmission coefficient. d) Imaginary part of transmission coefficient. e) Real part of reflection coefficient. f) Imaginary part of reflection coefficient. g) Real part of transmission coefficient. h) Imaginary part of transmission coefficient.

Seismic modeling of fluid substitution in Redwater Reef, Alberta

Taher M. Sodagar* and Dr. Don C. Lawton

SUMMARY

The objective of this study is to analyze and undertake seismic modeling of CO_2 saturation of the Devonian Leduc reservoir characterization at the Redwater reef by using Gassmann fluid substitution seismic modeling. This method was applied to the available wells inside the reef. Zero-offset synthetics were created for these wells before and after fluid substitution.

A distinct P-wave velocity decrease occurs from 0% to about 40% of CO_2 saturation. From around 40% to 100% of CO_2 saturation, the P-wave velocity starts increasing slightly, while the S-wave velocity increases almost linearly with the CO_2 saturation increase. There are slight changes in amplitudes between the wet in-situ reservoir reflections and the fluid substitution modeling reflections of Leduc formation. A time shift is observed at the base of the Leduc reservoir. The maximum time shift at the base of the Leduc reservoir and the highest amplitude difference changes are recognized at around 40% of CO_2 saturations.

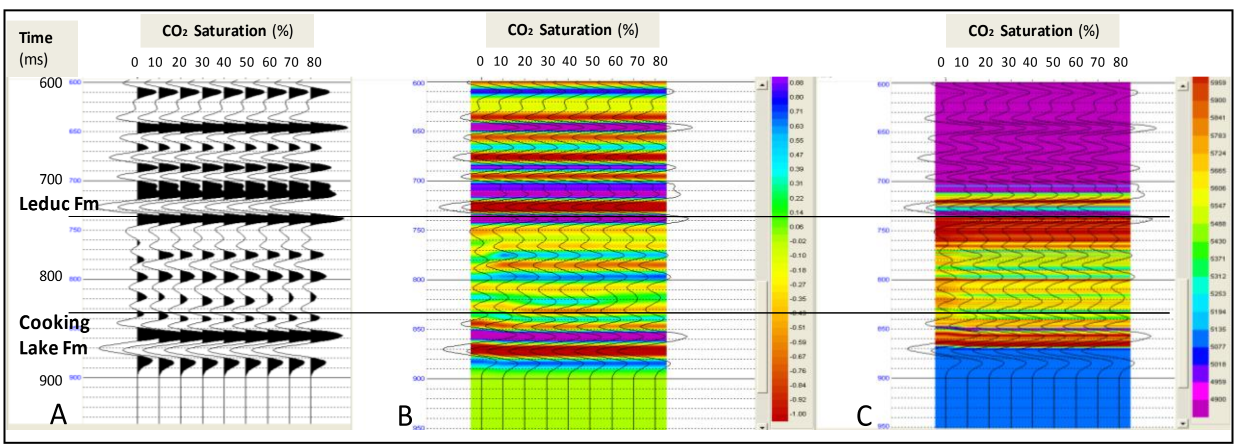

Figure 1: Zero-offset synthetic seismic traces for well 16-08-57-23W4, with CO2 fluid substitution from 0% (left) to 100% (right) in each panel. (A) wiggle-trace display, (B) color amplitude with wiggle-trace overlay, and (C) interval velocity with wiggle-trace overlay.

A brief history and extended future of full-wave seismic exploration

Robert R. Stewart

SUMMARY

This paper presents a short history - and extended future - of the multicomponent (full-wave/vector/elastic) seismic method. The goal of the method is to more fully generate and record complete vibrations in the earth; then, use these recordings to enhance traditional P-wave arrivals and create complementary shear- and surface-wave pictures. Of the additional wavetypes recorded, the converted wave (P-to-S on reflection) has found the most use in resource exploration (including imaging through gas volumes, sand-shale discrimination, and fracture assessment). Acquisition has progressed with many new land (e.g., MEMS) and marine systems (cables and nodes). Processing has also improved, with novel migration and anisotropy procedures making much better images. Commercial software for multicomponent analysis and interpretation has helped create a cascade of innovative uses and case histories. As the demand for more crisp and informative subsurface imaging grows, so does the need for multicomponent seismic application.

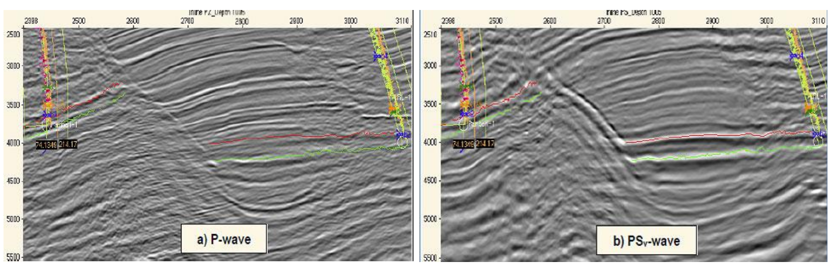

Figure P-wave (a) and converted-wave (b) pre-stack anisotropic depth-migrated sections from offshore Trinidad (Johns and Sarmiento, 2007).

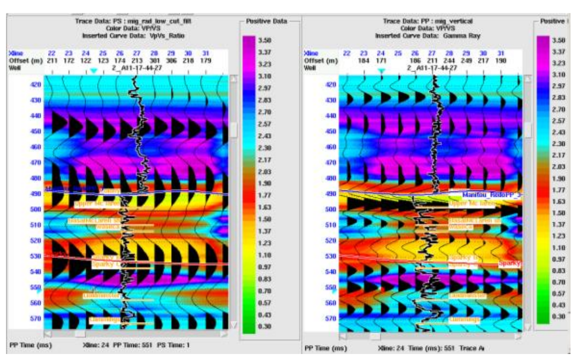

Figure PS (left) and PP (right) sections from a heavy oil reservoir registered in PP time with the background Vp/Vs mapping value shown in color. The yellow regions indicate a relatively low value and are interpreted as sand rich (Varga and Stewart, 2009).

Geophysics field education: Better learning by doing

Robert R. Stewart, Shuhab Khan, Joe Wong, Stuart Hall, and Christopher Liner

SUMMARY

A significant and exciting part of geophysics is its data acquisition (survey design, instruments, and measurement). As such, a complete education includes geophysical measurement and field surveying. Field camps play a role in allowing students to better understand the techniques of subsurface imaging.

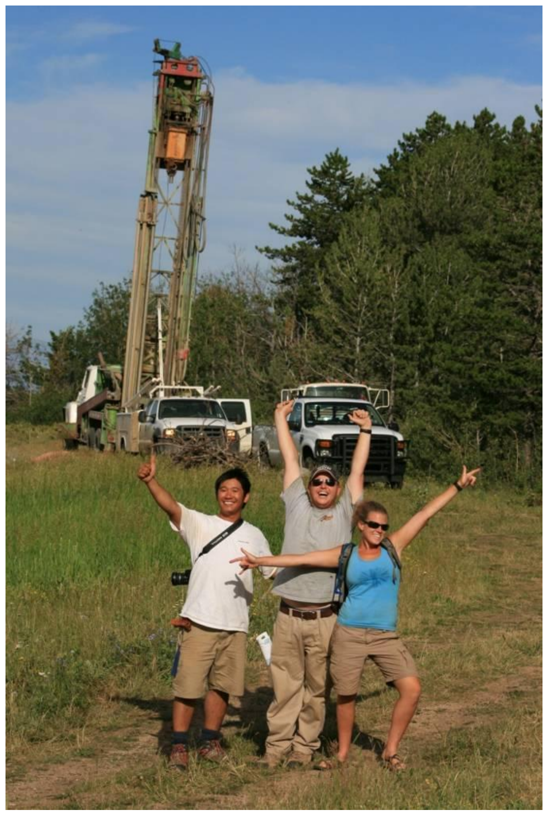

Variable-factor S-transform seismic data analysis

Todor I. Todorov* and Gary F. Margrave

SUMMARY

Most of today's geophysical data processing and analysis are based on the assumption that the seismic signal is stationary and employ an extensive use of the Fourier analysis. However due to various attenuation mechanisms of the Earth, the seismic signal is not stationary. The short-time Fourier transform (Gabor transform) has been developed to deal with non-stationary signals. The Variable Factor S-Transform is an extension of the Gabor transform and provides better time-frequency decomposition of a non-stationary signal for all frequencies. An S-transform deconvolution method is developed as an extension of the non-stationary Gabor deconvolution reported in the literature. The new methods is tested on a constant Q synthetic data and shows superior results over the traditional stationary Wiener deconvolution and an improvement over the non-stationary Gabor deconvolution. In a separate application an f-t-x CDP noise attenuation method is developed. A synthetic example proves the effectiveness of the f-t-x noise attenuation for both, high-amplitude linear noise and random noise.

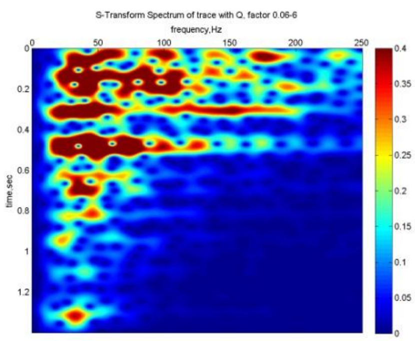

Variable factor S-transform time-frequency decomposition.

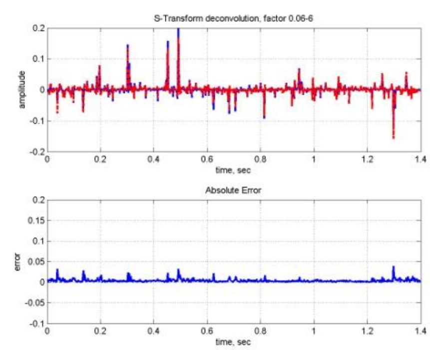

Variable factor S-transform deconvolution of a trace with Q=100.

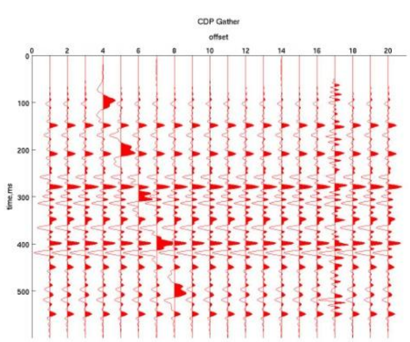

CDP gather with noise.

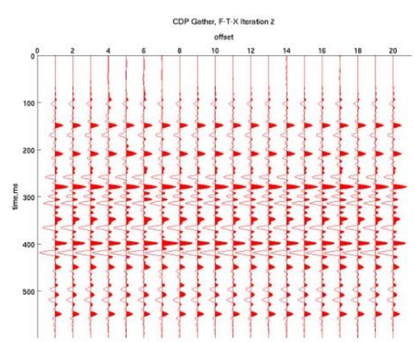

CDP gather after f-t-x noise attenuation.

Split-step two-way phase-shift time stepping for wavefield propagation

Ben D. Wards*, Gary F. Margrave and Michael P. Lamoureux

SUMMARY

The phase-shift time-stepping equation (PSTS) is a wavefield propagator that allows two-way in time propagation for the acoustic wave equation. PSTS is based an an exact solution to the constant velocity acoustic wave equation. It is adapted to a variable velocity wave equation by a windowed Fourier transform where in each window a constant velocity solution is computed. We consider a correction to the phase-shift time-stepping equation that corrects the wave propagators for variable velocity. The correction is based on a similar Taylor-series expansion used to derive the split-step correction for one-way depth steppers or to derive higher-order in time pseudospectral methods using the modified equation approach or Lax-Wendroff method. The computational properties of the split-step correction to PSTS equation are similar to higher-order in time pseudospectral methods.

Similar to one-way in depth wavefield propagators, two-way in time wavefield propagators are solutions that originated from solving the constant velocity acoustic wave equation. The constant velocity integral solutions are adapted to heterogenous medium by replacing the constant velocity in the solution with a variable velocity

$$U^{n+1}(\vec{x}) = -U^{n-1}(\vec{x}) + 2\mathcal{F}^{-1}_{\vec{k}\to\vec{x}}\left[\cos\left(2\pi v(\vec{x})|\vec{k}|\delta t\right)\mathcal{F}_{\vec{x}\to\vec{k}}\left[U^n(\vec{x})\right]\right], \qquad (1)$$

where $\mathcal{F}_{\vec{x}\to\vec{k}}$ if the forward Fourier transform with respect to the spacial coordinate $\vec{x}$ which corresponds to the Fourier variable $\vec{k}$ and the superscript *n* represents the discrete time and *U* is the amplitude of the wavefield.. These Fourier-like integrals, however, are too computationally complex to be calculated explicitly and must be approximated. Equation (1) should be compare with the generalized PSPI formulation of wavefield depth continuation algorithms. When the the function cosine is replaced by its power series expansion, the resulting time stepping scheme reduces to higher-order in time pseudospectral methods using the modified equation approach. For example the fourth-order in time pseudospectral approximation is

$$U^{n+1} = -U^{n-1} + 2U^n + \delta t^2 v^2 (\Delta U)^n + \frac{v^4\delta t^4}{12}\left(\Delta^2 U\right)^n. \qquad (2)$$

Instead of expanding the cosine about the velocity zero the cosine can be expanded about the reference velocity v_0 with a perturbation $\delta v = v(x) - v_0$ instead of v(x). The resulting wavefield propagator is

$$\begin{aligned} U^{n+1}(\vec{x}) \simeq &- U^{n-1}(\vec{x}) + 2\mathcal{F}^{-1}_{\vec{k}\to\vec{x}}\left[\cos(2\pi v_{ref}|\vec{k}|\delta t)\mathcal{F}_{\vec{x}\to\vec{k}}\left[U^n(\vec{x})\right]\right] \\ &- 2\pi\delta v(\vec{x})\Delta t\mathcal{F}^{-1}_{\vec{k}\to\vec{x}}\left[|\vec{k}|\sin\left(2\pi v(\vec{x})|\vec{k}|\delta t\right)\mathcal{F}_{\vec{x}\to\vec{k}}\left[U^n(\vec{x})\right]\right] + \ldots . \end{aligned} \qquad (3)$$

If the velocity variations are small relative to the velocity, then the above equation results in less dispersion and velocity errors than an equivalent order pseudospectral method.

Trace interpolation and elevation statics by conjugate gradients

Marcus R. Wilson* and Robert J. Ferguson

SUMMARY

We present a conjugate-gradient based inversion to correct for surface statics and irregular trace spacing. The algorithm returns a rough solution to the extrapolated wavefield with complexity $\mathcal{O}(n^{2.5})$, although convergence is much slower in the evanescent region. Some trace interpolation occurs with no smoothing operator being applied, but recovered wavefields do not coincide in norm with known source wavefields at low frequencies. We expect that accuracy of the solution can be improved through careful smoothing, or separate treatment of the wavelike and evanescent regions, and we can reduce runtime by passing a fast series expansion operator as input to the conjugate gradient method.

EXAMPLE

An image is phase shifted to the surface from 100 metres depth, 30% of traces are set to zero to model irregular spatial sampling, and least squares inversion is effected using conjugate gradients to recover the source wavefield using a simplified a priori velocity model. The conjugate gradient algorithm performs some trace interpolation when no smoothing operator is used, and effectively inverts the phase shift effect to refocus the image, although errors due to velocity uncertainty, and slow convergence in evanescent region are observed.

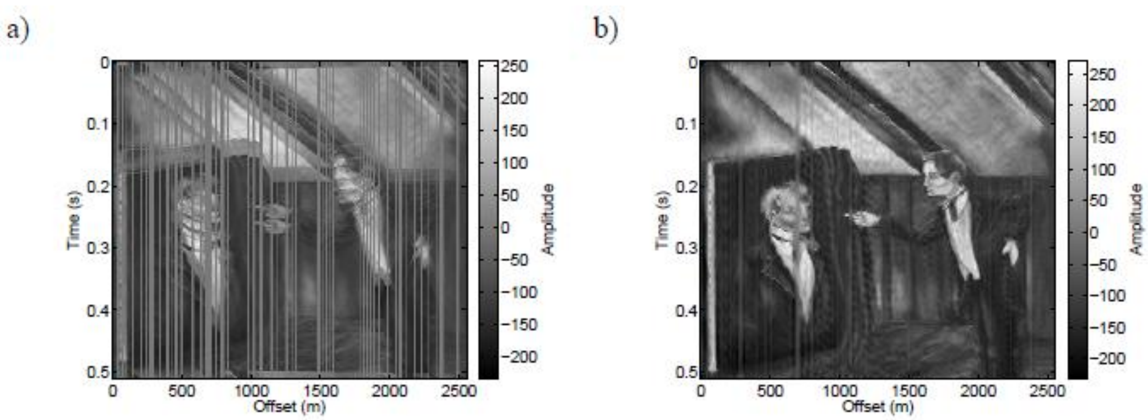

FIG. 1. a) Phase shifted image with 30% trace decimation and lateral velocity variation that is not well known b) Weighted least squares inversion using conjugate gradients: $\sqrt{n}$ iterations, using a simplified velocity model and no smoothing.

Microseismic hypocenter location using nonlinear optimization

Joe Wong*

SUMMARY

In microseismic hypocenter location, we observe the arrival times caused by hydraulic fracturing and know the geophone coordinates. Ray-tracing through a layered-earth model with known velocities produces calculated arrival times from a hypocenter to geophone arrays. By minimizing the misfit between observed and calculated arrival times via a modified Levenberg-Marquardt inversion scheme, hypocenter coordinates satisfying the observed data were found through nonlinear optimization.

In real-world microseismic surveys monitoring hydraulic fracturing, arrival times from a perforation shot in the treatment well are used to calibrate velocity values prior to hypocenter location. The shot location, the geophone coordinates, and layer depths are known, and the model velocities must be found. In synthetic simulations, we applied pattern search (PS) and the genetic algorithm (GA) to find velocities that minimized the misfit between observed and calculated perforation shot arrival times. In the simulations, PS performed better than Levenberg-Marquardt inversion and GA.

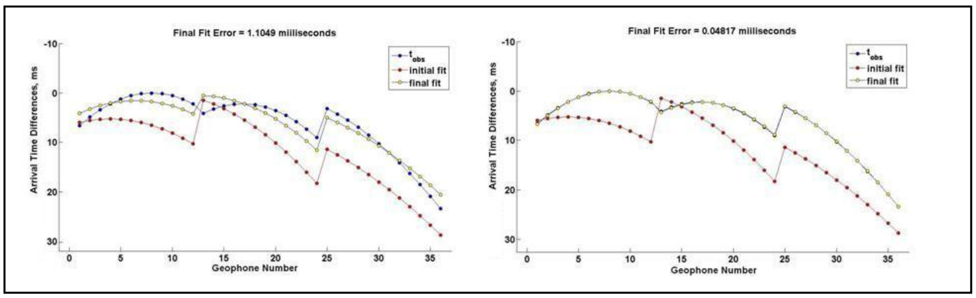

Fig. 1: Hypocenter location by modified Levenberg-Marquardt inversion of reduced arrival times from a surface array of geophones. Blue dots are the observed times. Red dots are calculated times for the initial guess of source coordinates; yellow dots are calculated times for relocated source coordinates after 17 iterations (left) and after 30 iterations (right). After 30 iterations, the source location from inversion is almost identical to the true source location, and the calculated times coincide with the observed times.

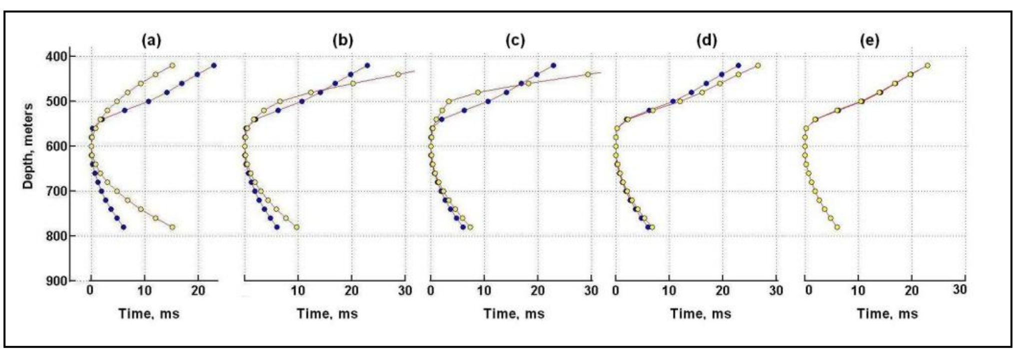

Fig. 2: Genetic algorithm inversion for velocity calibration using data from a vertical observation well. Blue dots are the reduced observed times from a calibration shot. Yellow dots are reduced calculated times for velocity values found after (a) 1 generation (starting values); (b) 10 generations; (c) 20 generations; (d) 30 generations; (e) 69 generations (final velocity values cause yellow and blue dots to coincide).

Physical modeling of a 3D marine seismic survey

Joe Wong, Rolf Maier, Eric Gallant, and Don Lawton

SUMMARY

SEG-Y writing capability has been added to the acquisition software used by the U of C Seismic Physical Modeling Facility. With SEG-Y file writing in place, we conducted a model survey simulating a 3D marine seismic survey, with model dimensions scaled up by 10^4. The target was a green silicone rubber sheet molded to have a crossed-anticline topography on its upper surface. The target was immersed in about 1200m of de-mineralized water. An array of sixteen receiving transducers between two transmitting transducers was used to do acquisition. About 50,000 traces were collected over an area measuring x=2600m by y=2500m on a grid with Δx=100m and Δy=50m. Gathers of seismograms were plotted using PROMAX for visual inspection of the data.

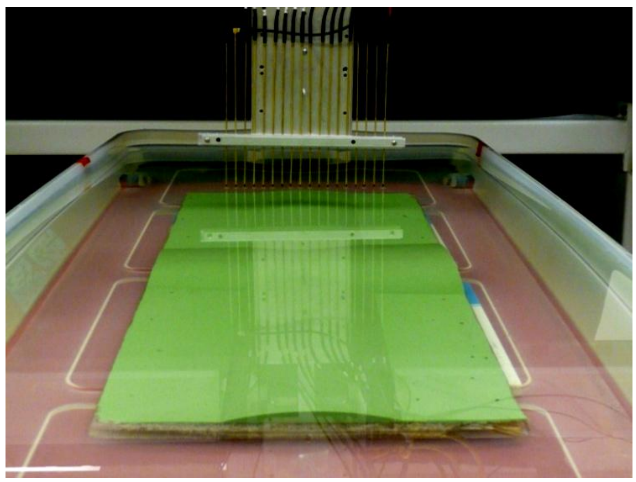

FIG. 1: Array of sixteen receiver piezopin transducers between two transmitter piezopin transducers, positioned over a molded silicone rubber target immersed in 120mm of de-mineralized water.

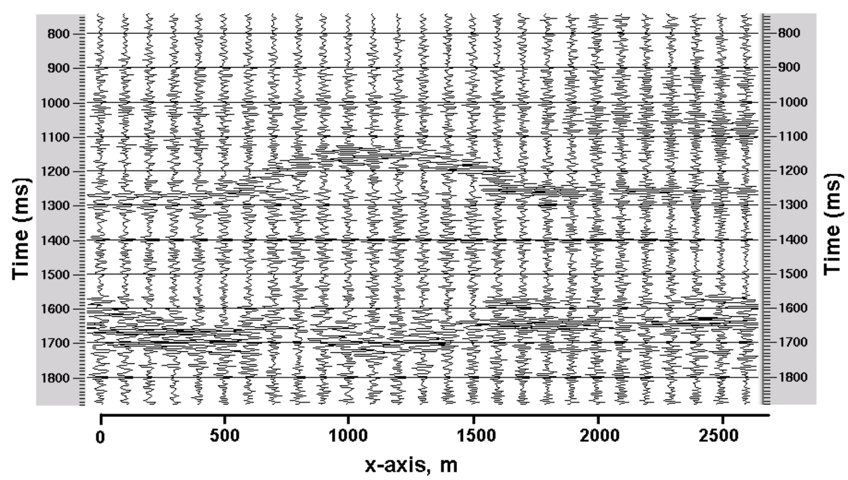

FIG. 2: Common offset (500m) gather. There are clear reflections from the top an bottom of the target.

Feasibility of solving least squares prestack Kirchhoff migration using multigrid methods

Abdolnaser Yousefzadeh and John C. Bancroft

SUMMARY

The feasibility of different approaches of using multigrid methods in solving the linear system of Kirchhoff Least-Squares Prestack Time Migration (LSPSTM) equation is investigated.

Numerical examples showed that LSPSTM problem is not solvable by the Jacobi or Gauss-Seidel iterations. The matrix $\boldsymbol{G'G}$ is not diagonally dominant. Consequently, the standard multigrid which uses Jacobi or Gauss-Seidel as iterative solvers is not applicable. Large memory size is another problem associated with this method.

Conjugate Gradient (CG) is an effective solver. Least Squares CG (LSCG) has the advantage of using operators instead of matrices. It is shown that the convergence rate of the CG is independent of the frequency content of the solution. Therefore, it does not converge more rapidly with high frequency contents than the low frequency. Figure 1 shows the CG convergence rate of a LSPSTM of a synthetic example with different dominant frequencies in the data.

To date, this study shows using the CG as an iterative solver for the multigrid may slightly reduces the number of iterations for the same rate of convergence in the Conjugate Gradient itself. However, it does not reduce the total computational cost.

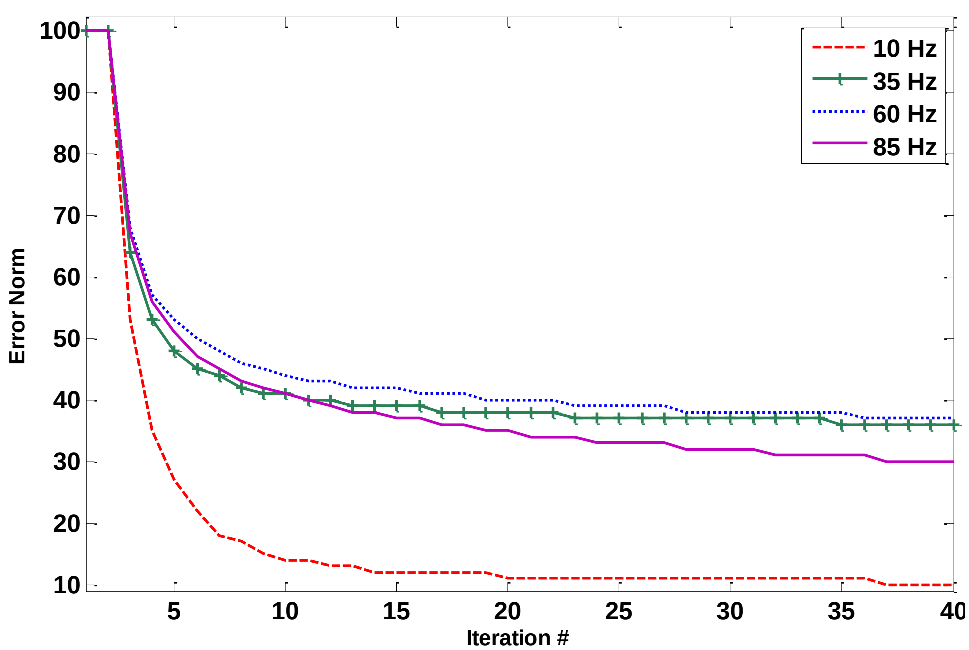

FIG. 1. Convergence of LSCG to solve damped LSPSTM for a synthetic data with wavelets with different dominant frequencies: 10, 35, 60 and 85 Hz.

Estimation of *Q* and phase velocity using the stress-strain relaxation spectrum

Dali Zhang, Michael P. Lamoureux, and Gary F. Margrave

SUMMARY

We present a numerical inversion method for estimation of *Q*-factor and phase velocity in linear, viscoelastic, isotropic media using reconstruction of relaxation spectrum from measured or computed complex velocity or complex modulus of the medium. Mathematically the problem is formulated as an inverse spectral problem for reconstruction of spectral measure in the analytic Stieltjes representation of the complex modulus using rational approximation in the frequency domain. A rational (Padé) approximation to the spectral measure is derived from a constrained least squares minimization problem with regularization. The recovered stress-strain relaxation spectrum is applied to numerical calculation of frequency dependent *Q*-factor and frequency dependent phase velocity for known analytical models of a standard linear viscoelastic solid (Zener) model as well as a nearly constant-*Q* model which has a continuous spectrum. Numerical results for these analytic models show good agreement between theoretical and predicted values and demonstrate the validity of the algorithm. The proposed method can be used for evaluating relaxation mechanisms in seismic wave¯eld simulation of viscoelastic media. The constructed lower order Padé approximation can be used for determination of the internal memory variables in TDFD numerical simulation of viscoelastic wave propagation.

RESULTS

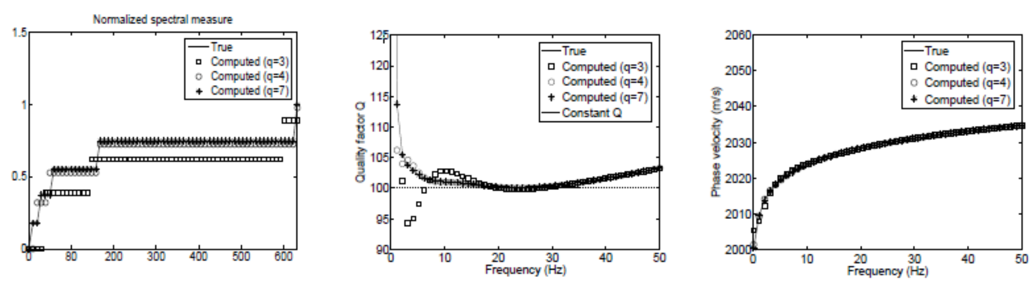

Figure 1: Result for the standard linear solid model with a discrete relaxation spectrum. Reconstruc-tion of the normalized spectral measure (left), *Q*-factors (middle) and phase velocities (right).

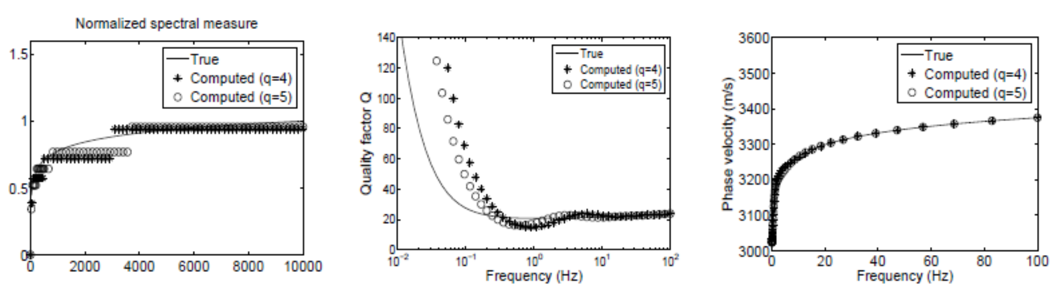

Figure 2: Recovery of the normalized spectral measure (left) and estimation of *Q*-factors (middle) and phase velocities (right) for model with a continuous relaxation spectrum using di®erent lower orders of [*p; q*]-Padé approximation.

Numerical modeling of shear-wave splitting and azimuthal velocity analysis in fractured media

Zimin Zhang*, Don C. Lawton, and Robert R. Stewart

SUMMARY

This report presents the processing and interpretation of seismic modeling data of the earth models for a fractured layer, based on well logs associated with potash mining. The purpose of the work is to study azimuthal seismic anisotropy, shear-wave splitting, and time-lapse seismic signals caused by vertically aligned cracks. The results show that seismic velocity anisotropy can be detected by both vertical and horizontal components of the HTI earth model; it is especially evident on radial component. Shear-wave splitting is evident and the crack orientation determined from the polarization of fast and slow shear waves is consistent with the input model. The time-shift and amplitude changes due to anisotropic layer are also apparent on both vertical and radial component data. The time-shift on radial data is up to 5ms and the amplitude change is up to 46%.

The modeled data correlate nicely with the well data. Considering the correlation results of well and surface seismic data in the previous study, this suggests that multi-component seismic data are interpretable in this potash area. This also suggests that by searching for seismic anisotropy, shear-wave splitting on the multi-component seismic data or by looking for changes in repeated seismic surveys, we may be able to detect/monitor cracks and crack orientation in HTI model.

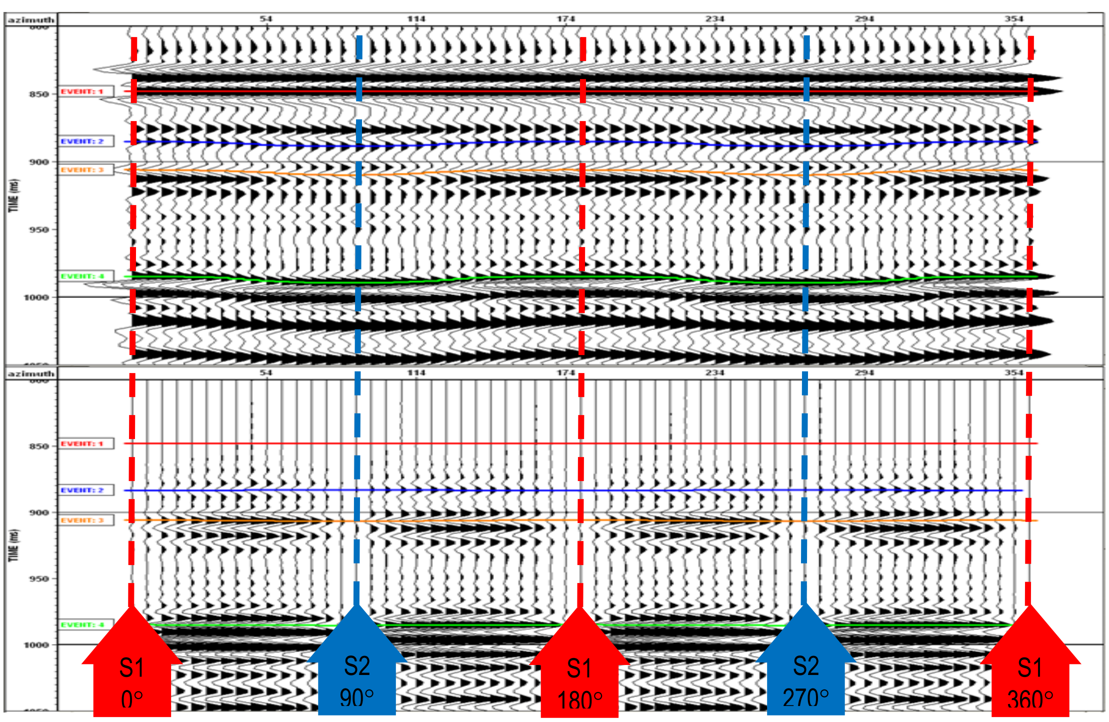

Figure 1. Radial (top) and transverse (bottom) components azimuth bin stack of HTI earth model. The red dashed lines show the fast shear-wave (S1) polarization direction and the blue dashed lines show the slow shear-wave (S2) polarization direction.